Karl Thomas Hjelmervik

Sonar false alarm rate suppression using classification methods based on acoustic modelling

Thesis for the degree of Philosophiae Doctor

Trondheim, May 2011

Norwegian University of Science and Technology
Faculty of Information Technology, Mathematics
and Electrical Engineering
Department of Electronics and Telecommunications

NTNU – Trondheim
Norwegian University of
Science and Technology

NTNU
Norwegian University of Science and Technology

Thesis for the degree of Philosophiae Doctor

Faculty of Information Technology, Mathematics and Electrical Engineering
Department of Electronics and Telecommunications

ISBN 978-82-471-2795-7 (printed ver.)
ISBN 978-82-471-2796-4 (electronic ver.)
ISSN 1503-8181

Doctoral theses at NTNU, 2011:128

Printed by NTNU-trykk

Sonar false alarm rate suppression using classification methods based on acoustic modelling

Karl Thomas Hjelmervik

March 10, 2011

Abstract

The use of high–resolution, active sonar systems in littoral environments often results in high false alarm rates. False alarm rate inflation (FARI) and non–Rayleigh reverberation (NRR) are two well–documented causes. FARI may occur when the reverberation in the normaliser window is non–stationary, while NRR may occur when the sonar footprint is too small for the central limit theorem to apply for the scatterer statistics. The main originator for false alarms in littoral environments are either the sea floor itself or objects located on the sea floor.

Automatic classification methods may be used to reduce the false alarm rate. Conventionally, advanced sonar processing or image processing techniques have been used directly on received data. Increased availability of environmental information allows for more sophisticated algorithms that employ acoustic modelling to extract more information from recorded data.

This thesis addresses two topics of interest. The first topic is on how acoustic modelling combined with environmental knowledge may be used to increase the ability of anti–submarine warfare sonars to classify a detected target. The second topic is on how environmental uncertainty may be reduced in order to improve the fidelity of the proposed classification algorithms.

Acknowledgements

I would first like to thank the Norwegian Defence Research Establishment (FFI) and the Norwegian University of Science and Technology (NTNU) for funding my research. A particular thanks to Elling Tveit and John Mikal Størdal at FFI and my supervisor professor Jens Martin Hovem at NTNU and Sintef for making this possible.

I would also like to thank my coauthors in the attached papers, and particularly Geir Helge Sandsmark, Petter Østenstad, and Jan Kristian Jensen. Geir Helge for sharing his impressive understanding of signal processing with me, and Petter and Jan Kristian for helping me understand oceanographic phenomena.

The ideas pursued in my PhD work are the results from many insightful discussions with colleagues at FFI and NTNU. I would therefore like to thank all contributors to these discussions, whereof many have also contributed by giving internal reviews to my papers before submission. In particular I would like to thank Jens Hovem, Henrik Berg, Stein Nilsen, and Dag Tollefsen.

My work would not be possible without high–quality data. I would therefore like to thank the partners in the New Array Technology (NAT) III project for allowing me to use collected sonar data from NAT III sea trials. I would also like to thank the crew on FFIs research vessel, H. U. Sverdrup for collecting high–resolution topographic and oceanographic data in the Norwegian trench.

Finally, and most importantly, I would like to thank my family for supporting me in my academic work; my parents, my three children, and particularly my wife, Karina, who has also contributed with reviews of my papers.

Summary

Littoral sonar operation is complicated by high false alarm rates, particularly for high–resolution sonar systems such as modern anti–submarine warfare sonars. Typically, high concentrations of false alarms are observed around wrecks, sea mounts, and along rocky ridges. Some of these false alarms result in generation of tracks exhibiting target–like behaviour. Improved classification algorithms are needed to reduce the false alarm rate.

This thesis presents seven papers describing methods that may increase the performance of modern sonars in anti–submarine warfare operations. All presented methods pursue at least one of two topics of interest. Topic A is on exploiting available environmental information to increase the classification ability of anti–submarine warfare sonars in littoral waters. Topic B is on limiting the environmental uncertainty during operation.

Four papers relate to topic A and introduce new methods for target classification. The two first papers present methods on how reverberation modelling may be used to predict what areas are prone to increased false alarm rates. The next two papers apply a ray tracing algorithm for determining the depth of a detected target. This algorithm requires a known environment and recorded arrival times and angles. The fourth paper also includes a focalisation method that tunes the environment in order to increase the accuracy of the target depth estimates. All these methods are sensitive to environmental uncertainty. Errors in environmental parameters, particularly the sound speed profile, may result in ambiguous or erroneous target classification. The remaining papers, all on topic B, seek to alleviate this problem. The fifth paper introduces a method that inverts sound speed profiles from data recorded on available sensors, such as measurements of sound speed close to the sonar depth. The sixth paper presents a method that classifies areas as acoustically stable or unstable on basis of modelled oceanographic data by employing empirical orthogonal function classification, clustering approaches, and acoustic modelling. The seventh paper investigates how the sonar – target geometry influences acoustic stability in face of environmental uncertainty.

Contents

Paper 1 **Sonar false alarm reduction using detailed bathymetry data and acoustic propagation modelling**

Paper 2 **Predicting sonar false alarm rate inflation using acoustic modeling and a high-Resolution terrain model**

Paper 3 **Target depth estimation using a ray backpropagation scheme on sonar data – simulations and experiments**

Paper 4 **Target depth estimation using a ray backpropagation scheme on mid-frequency, active sonar data**

Paper 5 **Inverting the water column sound speed**

Paper 6 **Finding acoustically stable areas through EOF classification**

Paper 7 **In ocean evaluation of low frequency active sonar systems**

1 Introduction

Sea trials in littoral environments show that high–resolution, active sonars generate particularly many false alarms in presence of ship wrecks and terrain features such as seamounts and underwater ridges [1–4]. Possible causes for high false alarm rates include false alarm rate inflation [5–8] and non–Rayleigh reverberation [1, 9–16]. False alarm rate inflation is induced by a non–stationary reverberation power level in the normaliser windows. Non–Rayleigh reverberation, also called clutter, appears when the sonar resolution is so high that the sonar footprint is too small for the central limit theorem to apply for the scatterer statistics. The false alarm rate depends on the sonar system, the choice of signal processing, and on the present environment [1, 6, 13, 15, 16]. In littoral environments the main originators of false alarms are either the sea floor itself or objects located on the sea floor [2–4].

Recently, much research has been made on predicting and controlling false alarm rates. This research includes fields such as normalisation [6, 7, 11, 17], detection [10], image processing [18–20], acoustic modelling [4, 21, 22], and alternative matched filtering techniques [3]. The research is partly motivated by the increased use of high resolution naval sonars in littoral environments. After the cold war the focus of anti–submarine warfare has shifted from open water scenarios to littoral scenarios. Concurrently the resolution of naval sonars has improved; higher bandwidths due to improved processing and sonar technology, and improved bearing resolution due to the introduction of active towed array systems in naval warfare.

This thesis presents false alarm rate reduction methods based on acoustic modelling. False alarms are suppressed by classifiying received sonar echoes as either false alarms or potential targets. The first four papers in this thesis present two different types of target classification methods. The first type of method predicts the occurence of false alarm rate inflation using reverberation modelling. The predictions are used to estimate a probability of a received echo being a false alarm. The second type of method uses a ray back-propagation scheme [23] to estimate the depth of a detected target. Since false alarms typically originate from the sea floor, target depth information is a useful classification clue. The fidelities of the proposed methods depend strongly on the accuracy of available environmental input, since the acoustic field is sensitive to environmental uncertainty [24–29]. For mid–frequency sonars (1–10 kHz) an uncertain sound speed profile is an important contributor to the uncertainty in acoustic field predictions. The last four papers

of this thesis explore how uncertainty in sound speed may be reduced to increase the accuracy of acoustic modelling and thereby improve both the results of the proposed classification methods and sonar performance modelling in general.

1.1 Motivation

The Norwegian navy is procuring modern anti–submarine warfare (ASW) frigates, Fridtjof Nansen–class frigates. The first frigate was delivered to the Norwegian navy in 2006. The frigates are equipped with advanced acoustic sensors for submarine detection; a hull–mounted sonar called Spherion MRS2000 and an active towed array sonar called CAPTAS. Both systems have high resolutions and similar systems have been shown to generate large amounts of false alarms in littoral environments [4, 22].

The Norwegian government funds a large number of programs intended to increase the knowledge of the environment in the Norwegian economic zone. In the underwater domain, these programs include oceanography (the Norwegian Meteorological Institute, Nansen Environmental and Remote Sensing Center, Institute of Marine Research), fishery (Institute of Marine Research), and sea floor mapping (Norwegian Mapping Authority, Geological Survey of Norway, Norwegian Defence Research Establishment). Sea floor mapping includes mapping of bottom depths and bottom properties. The ongoing project Mareano [30] gives public access to some of this information. The abundance of information on the subsurface environment may give Norway a considerable tactical advantage in ASW operations in Norwegian territory. However, knowing the environment is not enough, equally important is knowing how to take advantage of this knowledge. The Russian admiral Sergei Gorshkov said: "The major navies of the world are technological equals – that navy possessing a superior knowledge of the environment, and knowing how to take tactical advantage, will be victor." Gorshkov makes a point of not only knowing the environment, but also taking advantage of this knowledge. The latter is a key–point for the motivation of this thesis. The thesis includes seven papers that present methods and theories on how environmental knowledge may be extended and exploited with the overall goal to improve the classification performance of modern naval sonars.

1.2 Focus of the thesis

The main focus of the presented work is to improve the classification ability of active ASW sonars in littoral environments. The two main topics of this thesis are:

A *How to exploit available environmental information in order to increase the classification ability of ASW sonars*

B *How to deal with environmental uncertainty*

Topic A includes use of various sources of environmental information, refined processing algorithms, and acoustic modelling in order to extract additional information from recorded sonar data during operations. Topic B includes methods that reduce the impact environmental uncertainty has on the methods introduced in topic A.

1.3 History of naval sonars

The emergence of submarines in naval warfare introduced a need for new sensors capable of detecting submerged targets. Unlike electromagnetic signals, acoustic signals may propagate for hundreds of kilometers in water and still be detected above ambient noise. As early as 1490, Leonardo da Vinci showed that distant ships could be heard by extending a listening tube into the water by placing an ear to the dry end of the tube. During World War I the British developed the ASDIC, the first anti–submarine warfare (ASW) sonar. The first operational ASDIC, presented in 1919, was an active, hull–mounted sonar and operated on frequencies from 20 to 50 kHz.

In the inter–war period, low–frequency acoustic signals were observed to propagate longer distances than high–frequency signals due to frequency–dependent attenuation. Another important discovery, made in the late 1940s by the American scientist Ewing, was that submarines could be detected via other propagation paths than the direct path, e. g. bottom reflected path and in convergence zones. These two discoveries encouraged the development of high–powered, low–frequency, active sonar systems. New hull–mounted sonars were introduced with increased power and lower frequencies, culminating in the scanning sonar. The scanning sonar consisted of an array of

hydrophones capable of both transmission and reception. This allowed directionality in both transmission and reception.

Sonar development was clearly driven by the rapid development of the submarine. During the cold war, passive, towed array sonars were introduced as an alternative to active, hull–mounted sonars for long–range detection. However, as submarines became more quiet, passive sonar systems no longer obtained the necessary detection ranges, and as the speed of the submarines increased, longer detection ranges were required. In the 1980s and 1990s the low–frequency, active, towed array sonar was developed as an alternative to passive towed array sonars.

ASW in World War II consisted mainly of protecting high–value units, for instance transport vessels, from submarine attacks. Allied transport convoys were constantly attacked by German submarines, and ASW vessels were deployed to defend the convoys. During the Cold War, ASW was played out in the blue ocean with the intent of tracking large nuclear submarines at long distances. After the Cold War the focus of ASW has shifted from blue ocean scenarios to littoral scenarios. For instance protecting landing crafts during landing of military personell or equipment. In littoral environments modern sonar systems, such as low–frequency, active, towed array sonars are troubled with high false alarm rates. In addition, nuclear submarines are no longer the main subsurface threat. Affordable, small, silent submarines with low target strengths are considered the main threat in the future. Their maneouverability enables them to hide in shallow waters close to the coast line among rocks and sea mounts, making them almost impossible to detect and classify.

1.4 Organisation of the thesis

Chapter 2 contains the necessary background for understanding the attached papers. Important concepts and theory are described and presented. Chapter 3 briefly summarises the key points of each attached paper. Chapter 4 gives an overall conclusion of the work described in this thesis. The attached papers are included at the end of the thesis.

2 Background

This thesis covers a range of subjects within the fields of acoustics and signal processing such as sonar processing, acoustic modelling, empirical orthogonal functions, inversion, detection theory, and sensitivity analysis. The following sections provide the reader with definitions of concepts and a background for each of these subjects.

2.1 Sonar systems

This thesis treats two different types of sonar systems; anti–submarine warfare (ASW) sonars and echo sounder systems. Each system is described in the following sections.

2.1.1 Anti–submarine warfare sonars

This thesis includes data from two different types of active ASW sonars; hull–mounted sonars and towed array sonars. Active ASW sonars use underwater sound propagation to detect submerged targets. An acoustic signal is transmitted from a source, the signal echoes off targets present in the ocean before returning to the acoustic receiver. At the same time ambient noise and returns from other acoustic scatterers in the ocean are received. The sonar attempts to detect the target echo among reverberation and noise.

Towed array systems are horisontal arrays of hydrophones towed by a vessel. Active systems also include a towed source. The main advantages of such systems are that the array depth is adjustable and that their large size allows high horisontal angle resolution even for low frequencies. Adjustable depth allows the sonar operator to place the array at a depth that is advantageous for long–range acoustic propagation, e. g. in a sound channel. Long arrays allow beamforming with high resolution in angle, which is essential for resolving target location at long ranges and also improves noise suppression, see section 2.2.1. Linear arrays, arrays with a single hydrophone width, have left–right ambiguity. This means that the array is unable to discern which side of the array a detected target is present. In modern ASW towed array systems this problem is solved by using either two parallell linear arrays or triplet arrays [31].

As the name suggests, hull–mounted sonars are fixed to the hull of the vessel with an acoustically transparent sonar dome separating the transduc-

ers from the water. Due to the size–limitation of such systems, they are limited to mid– or higher frequencies. Modern hull–mounted systems are able to beamform both vertically and horisontally and have no left–right ambiguities. Vertical beamforming is used to concentrate transmitted power in vertical angles dominated by propagating modes, e. g. propagation paths with minimal bottom interaction. Horisontal beamforming improves the capability of the sonar for locating a target.

2.1.2 Echo sounders

Echo sounding is a technique for measuring bottom depth by transmitting an acoustic pulse vertically from a hull–mounted echo sounder and receiving the subsequent bottom reflections. The bottom depth, D, is estimated using the following expression:

$$D = \frac{T}{2\widehat{s}}, \tag{1}$$

where T is the time from transmission to reception, $\widehat{s}$ is the depth–averaged slowness. Slowness is defined as:

$$s = \frac{1}{c}, \tag{2}$$

where c is the sound speed. The sound speed must be measured frequently during operation in order to secure high accuracy in the measurements.

The coverage of an echo sounder system may be improved by using multi–beam systems. Multi–beam systems transmit an acoustic pulse in a wide sector and receive in beams with different vertical steering angles. For more information on beams, see section 2.2.1. Cross–path coverage may be gained by using ray tracing models to estimate cross–path bottom depths from arrivals at angles other than the vertical. The high–resolution topography information used in several of the attached papers was measured using a multi–beam echo sounder.

2.2 Sonar processing

The main focus of the thesis is on ASW sonar systems, the sonar processing described below is the processing used for detecting a submarine using a frequency modulated (FM) pulse. Other pulses, such as the continuous wave

pulse requires different processing, but since the FM pulse is the only pulse shape considered in the attached papers, theory on different pulses are not included here. The main intent of conventional active ASW sonar processing is to detect and locate targets whose acoustic returns are embedded in reverberation and noise. The following paragraphs give a brief introduction to the different signal processing techniques used in conventional sonar processing to detect and locate a target.

2.2.1 Beamforming

Beamforming is a commonly used technique to aid in detection and localisation of a target. Beamforming exploits the relative time delays of received arrivals on different hydrophones in the receiver array in order to determine the direction from which an echo arrives [32]. A conventional beamformer sums the received signal from all hydrophones after applying a phase shift that depends on hydrophone location. For linear arrays with K equally spaced hydrophones the beamformed signal, s_b, equals [33]:

$$s_b(j,\theta) \;=\; \sum_{k=0}^{K-1} s_h(j,k) \exp\left(2\pi i k \frac{d}{\lambda} \sin\theta\right),$$

where $s_h(j,k)$ is the received signal in hydrophone number k at sample number j, θ is the steering angle, d is the distance between hydrophones, and λ is the wavelength. On conventional sonars a set of beams with different steering angles are processed. The main advantages of beamforming are directivity and noise suppression [34]. Directivity allows determination of target direction. Noise sources are suppressed since the noise from only a limited angular space is received. An example of a beamformed data sequence is shown in Fig. 1. Interested readers are referred to Therrien [35] and Van Trees [36] for more thorough descriptions of beamforming.

2.2.2 Matched filter

Like beamforming, the matched filter is commonly used to improve detection and localisation of a target. Matched filtering [36], also called pulse compression, correlates the received signal with a known signal. The matched filtered

signal, $s_m(j,\theta)$, is then given by:

$$s_m(j,\theta) = \sum_{n=-\infty}^{\infty} h(j-n)s_b(n,\theta). \tag{3}$$

For active sonars, $h(j)$ is a time–reversed version of the transmitted signal. The advantages of matched filtering include a processing gain and increased range resolution. The processing gain, G, depends on the product of the frequency bandwidth, B, and the pulse length, T, of the signal used:

$$G \;=\; BT. \tag{4}$$

Note that increased pulse length also results in increased reverberation, and increased bandwidth in increased noise levels. An example of a matched filtered data sequence is shown in Fig. 1. Interested readers are referred to Therrien [35] and Van Trees [36] for more thorough descriptions of matched filtering.

2.2.3 Normalisation

After beamforming and matched filtering, the received signal is passed through a normaliser:

$$s_n(j,\theta) = \frac{s_m(j,\theta)}{n(j)},$$

where j is the analysed sample, $s_n(j,\theta)$ is the normalised signal, also frequently called the estimated signal–to–reverberation and noise ratio (SNR), and $n(j)$ is the estimated background. The background is typically estimated as follows:

$$n(j) = \frac{1}{C}\sum_{l=-L/2}^{L/2} c(l)s_m(j,\theta),$$

where L is the width of the normalisation filter. C is defined as:

$$C = \sum_{l=-L/2}^{L/2} c(l). \tag{5}$$

$c(l)$ varies for different normalisers. For the CA CFAR (cell averaging constant false alarm rate) normaliser [5] $c(l)$ is defined as:

$$c(l) = 0, |l| < K$$
$$c(l) = 1, l \geq K$$

where $K < \frac{L}{2}$. Samples where $c(l) = 0$ is commonly called the guard band [6]. The main intent of the normaliser is to remove trends from the received signal, such as the signal decay with range. The reader is referred to Richards [5] for thorough discussions on the subject of normalisation.

2.2.4 Detection

Target detection using active sonars is a binary decision problem, where the intent is to decide between two hypotheses:

1. a target echo is present in the received signal
2. a target echo is not present in the received signal

The decision is made by applying a threshold, T, to the normalised signal [36]:

$$s_n(j, \theta) \geq T \quad \Rightarrow \quad \text{choose hypothesis 1}$$
$$s_n(j, \theta) < T \quad \Rightarrow \quad \text{choose hypothesis 2}$$

Samples with a present target that results in a threshold–crossing are called detections. The normalised signal may fail to cross the threshold even with a target present. This is frequently called a miss. The probability of detection, P_d, is the probability that the signal crosses the threshold when a target echo is present. P_d depends on the threshold and the signal strength distribution. Due to spikes in reverberation and noise, the normalised signal may exceed the selected threshold even without a present target. Such threshold–crossings are undesired and are called false alarms. Probability of false alarm, P_{fa}, is the probability of undesired threshold–crossings. Assuming an exponentially distributed normalised signal and using a CA CFAR normaliser, then the probability of false alarm is given by [5]:

$$P_{fa} \quad = \quad \exp(-T).$$

The threshold is therefore uniquely determined from the desired probability of false alarm. Interested readers are referred to Van Trees exhaustive work on detection theory for further reading [36].

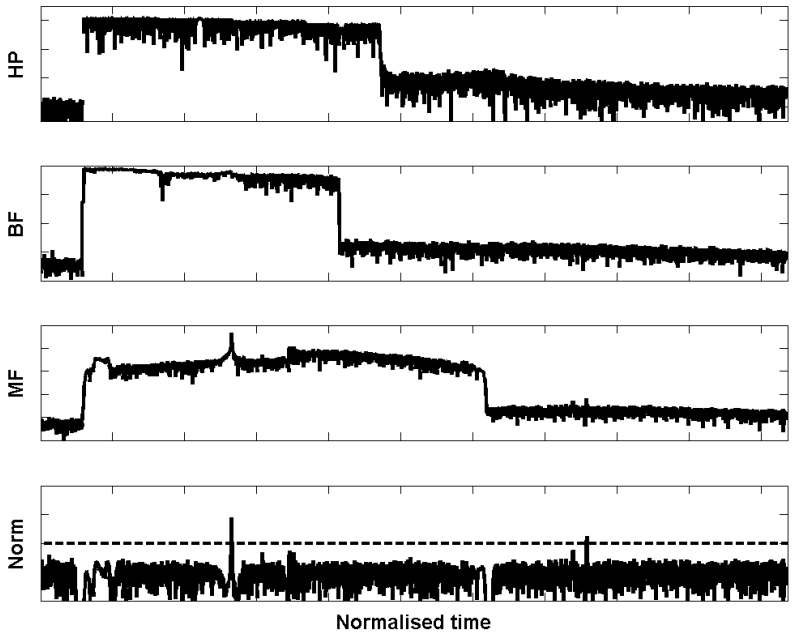

Figure 1: A data segment is processed. The magnitude of hydrophone data (HP), beamformed data (BF), matched filtered data (MF), and normalised data (Norm) are shown. All scales on the vertical axes are logarithmic.

2.2.5 Example

A sonar data segment is processed using the processing chain described in the previous sections. Fig. 1 shows processed data on each level. Only data from a single hydrophone is shown, but data from all hydrophones are used in the processing. Two threshold–crossings are detected. The first detection is obvious at all processing stages. The second detection is not discernable in the hydrophone and beamformed data and only barely discernable in the matched filtered data. This illustrates the importance of the normaliser as a trend–remover. Notice also how the matched filter effectively pinpoints the location of the first detection.

2.3 Raytracing and sonar performance modelling

Numerical models may be used to estimate sound propagation. Jensen *et al*. [37] give a thorough description of the most popular modelling methods available for estimating sound propagation in water. One such modelling method is the raytracer, which is a geometrical method that traces rays perpendicular to the wavefront of an acoustic wave. Ray theory was originally formalised to describe the propagation of light in optics and is an extension of Snells law, also called the law of refraction, which forces rays to refract towards lower sound speeds as they propagate through the medium. Raytracing is a high–frequency approximation that does not take diffraction into account. The work presented in this thesis involves sonar data with frequencies in the kHz domain where the high–frequency assumption holds. This makes raytracing the preferred acoustic model in this thesis.

The following sections give a brief description of raytracing and how it may be used to model reverberation and sonar performance. Two raytracers used in this thesis, PlaneRay and Lybin, are presented.

2.3.1 Basic ray concepts

The list below contains a description of basic ray concepts:

- Refraction is the bending of rays due to changing sound speed along the path of the ray.
- A turning point is where the ray grazing angle changes sign due to refraction.
- Travel time, at a specific raypoint, is the time it takes the ray to propagate from the source to the specific raypoint.
- Initial angle is the grazing angle of the ray at the source.
- Adjacent rays have adjacent initial angles.
- Ray tube is a volume bounded by three adjacent rays, or in the case of 2d raytracing, an area bounded by two adjacent rays.
- Ray intensity at a certain point depends on the area of the ray tube at that point as well as source power, Jensen *et al*. [37] give a detailed account on how ray intensity is estimated.

2.3.2 Ray categories

Rays are frequently categorised. The ray reflection and refraction history determines what category a ray belongs to. The list below describes the basic categories:

1. Direct path (DP): No reflections and refractions
2. Bottom bounce (BB): One bottom reflection
3. Surface bounce (SB): One surface reflection
4. Upward refracted (UR): One lower turning point (convex shape of the path)
5. Downward refracted (DR): One upper turning point (concave shape of the path)

Fig. 2 illustrates the different categories. Higher order categories include several combinations of reflections and refractions, e. g. BB–SB–BB, a category containing rays reflected off the bottom, then the surface, and finally the bottom again.

2.3.3 Eigenrays

Eigenrays are rays of different categories that propagate from a given source position to a specified target position, see Fig. 2. Jensen *et al*. [37] suggest different eigenray search methods. One of them, the interpolation method, traces a fan of rays from the source and registers the two adjacent rays of each category that pass each side of the target. The properties of the rays, such as initial angle, travel time, and intensity are then interpolated to find a single eigenray for each ray category.

2.3.4 Transmission loss modelling

Raytracers are frequently categorized as either coherent and incoherent [37]. This relates to how the raytracer estimates the acoustic pressure, $p(r, z, \theta)$, at a single point. The acoustic pressure is here represented in sylindrical coordinates where r is the range, z is the depth, and θ is the horisontal angle. Coherent raytracers sum the pressure contribution from each eigenray

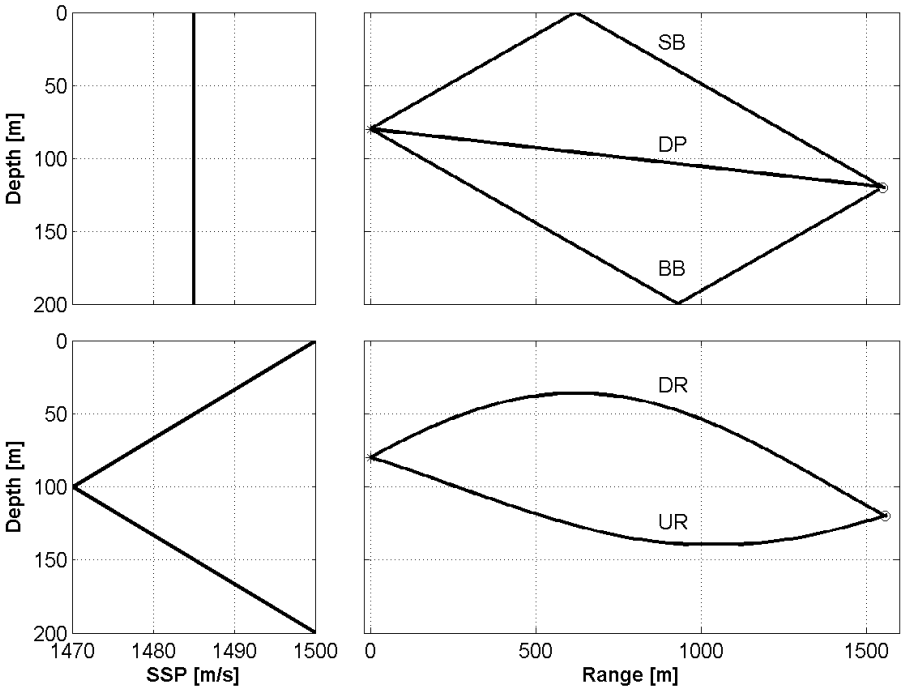

Figure 2: Eigenrays from a source (star) at 80 m depth to a receiver (circle) 1560 m distant at 120 m depth are shown. Three categories of eigenrays are shown in the upper right plot; bottom bounce (BB), surface bounce (SB), and direct path (DP). Two categories of eigenrays are shown in the lower right plot; upward (UR) and downward refracted (DR). The plots to the left show the sound speed profiles used to determine the paths. The rays were traced using PlaneRay.

crossing the relevant point coherently, that is, a complex summation that includes pressure phase and magnitude:

$$p^{(c)}(r,z,\theta) \;=\; \sum_{j=0}^{N-1} p_j(r,z,\theta), \tag{6}$$

where N is the number of eigenrays crossing (r,z,θ) and $p_j(r,z,\theta)$ is the complex pressure of eigenray number j. Incoherent raytracers sum the squared

pressure magnitude of each ray crossing the relevant point:

$$p^{(i)}(r,z,\theta) \;=\; \sqrt{\sum_{j=0}^{N-1} |p_j(r,z,\theta)|^2}. \tag{7}$$

The transmission loss, tl, is found using the following expression [37]:

$$tl(r,z,\theta) \;=\; \frac{I(r,z,\theta)}{I_0}. \tag{8}$$

The logarithmic expression is more frequently used in literature:

$$TL(r,z,\theta) \;=\; 10\log_{10} tl(r,z,\theta). \tag{9}$$

$I(r,z,\theta)$ is the intensity:

$$I(r,z,\theta) \;=\; \frac{p(r,z,\theta)^2}{2\rho(r,z,\theta)c(r,z,\theta)}, \tag{10}$$

where ρ is the density, c is the sound speed, and I_0 is the intensity at 1 m distance from a reference spherical, free source. The transmission loss is incoherent if the input pressure is estimated as shown in (7), and coherent if the pressure from (6) is input.

2.3.5 Reverberation modelling

The principle behind active sonars is to transmit an acoustic signal from a source and then receive returns on a receiver. Acoustic returns consist of both desired and undesired returns. Desired returns are echoes from targets, e. g. submarines in anti–submarine warfare. Undesired returns, also called scattering, consist of returns from acoustic scatterers in the ocean. The summed contribution of all these scatterers is called reverberation. Reverberation is typically divided into three categories [34]: surface reverberation, volume reverberation, and bottom reverberation. In littoral sonar operations, and particularly for variable depth sonars such as the active, low–frequency, towed array sonar, bottom reverberation typically limits the sonar conditions and causes increased false alarm rates and possibly sonar clutter, as discussed later. Bottom reverberation, $rl(r,\theta)$, from a scattering patch with area A, may be modelled using the following expression [39]:

$$rl(r,\theta) \;=\; \sum_{j=0}^{N-1}\sum_{k=0}^{N-1} tl_j(r,z_b,\theta)tl_k(r,z_b,\theta)A\sigma(\phi_j,\phi_k), \tag{11}$$

where $tl_j(r, z_b, \theta)$ is the linear transmission loss of a single eigenray from the source to the scattering patch, $tl_k(r, z_b, \theta)$ is the linear transmission loss of a single eigenray from the scattering patch to the receiver, and ϕ_j and ϕ_k are the grazing angles of the incoming and outgoing eigenrays at the scattering patch. $\sigma(\phi_j, \phi_k)$ is the scattering function [38]. A commonly used scattering function is Lamberts law:

$$\sigma(\phi_j, \phi_k) \quad = \quad \mu \sin \phi_j \sin \phi_k. \tag{12}$$

More realistic scattering functions, such as the perturbation model and the Kirchhoff model are described by Hovem [39].

2.3.6 Sonar performance modelling

Sonar performance may be modelled by using the logarithmic sonar equation [34]:

$$SE \quad = \quad SL - TL_f - TL_b - RNL + TS - DT, \tag{13}$$

where SE is the signal excess, TL_f is the transmission loss from the source to the target, TL_b is the transmission loss from the target to the receiver, RNL is the reverberation and noise level, TS is the target strength, and DT is the detection threshold. A thorough description of each parameter can be found in Urick [34]. Transmission loss and reverberation may be estimated using an acoustic model, e. g. a raytracer. The probability of detecting a target at a location where the modelled signal excess level is 0 dB, is 50 %. Receiver operating curves [34] may be used to determine the probability of detection for other signal excess levels. The probability of false alarm depends on the selected detection threshold, see section 2.2.4.

2.3.7 PlaneRay

PlaneRay [40] was developed and is maintained by professor Jens Hovem at Sintef and the Norwegian University of Science and Technology. PlaneRay is a coherent raytracer that uses the interpolation method for determining eigenrays. The raytracer was originally tailored for fast geoacoustic inversion. The idea is that since the water–column raytracing is independent of the bottom properties, PlaneRay is run a single time only during the inversion process. The losses due to bottom reflections are updated for each bottom interacting ray as the bottom properties change during the inversion.

In this thesis, PlaneRay is used for modelling travel times and initial angles of eigenrays. The eigenrays shown in Fig. 2 are estimated using PlaneRay. In the figure basic eigenrays are presented only, but PlaneRay is also capable of estimating more complex arrivals.

2.3.8 Lybin

Lybin [41] is the property of the Norwegian Navy and was developed by Svein Mjølsnes at the Norwegian Defence Logistic Organisation and is currently maintained by the Norwegian Defence Research Establishment. The model was originally developed for use on sonar vessels in the Norwegian Navy for sonar performance modelling.

In this thesis, Lybin is used for incoherent modelling of reverberation and sonar performance. Fig. 3 shows the graphical user interface of Lybin as well as plots of modelled rays, transmission loss, and reverberation. Lybin has very low computation time, less than 0.1 s for simple cases such as the one shown in Fig. 3.

2.4 Empirical orthogonal functions

Empirical orthogonal functions (EOF) or principal component analysis (PCA) is used for statistical analysis of spatial or temporal variability of physical fields. Preisendorfer and Mobley [42] give a detailed account of PCA techniques on oceanographic and meteorological data. Characterisation of oceanographic data by EOFs was introduced in the 1970s [42], and extended to represent sound speed profiles (SSP) by Tolstoy et al [43] in the early 1990s. The main advantage of characterising SSPs by EOFs is that the information from entire SSPs may be contained in a few scalar coefficients. For example, two EOFs and their coefficients give a sufficient representation of the Munk–profile [23].

EOFs for a set of SSPs may be derived by first interpolating the SSPs to a uniform grid of N depths and then organising them in a data matrix, C:

$$\mathbf{C} = \begin{bmatrix} \mathbf{c_1}^T \\ \mathbf{c_2}^T \\ \vdots \\ \mathbf{c_M}^T \end{bmatrix}, \tag{14}$$

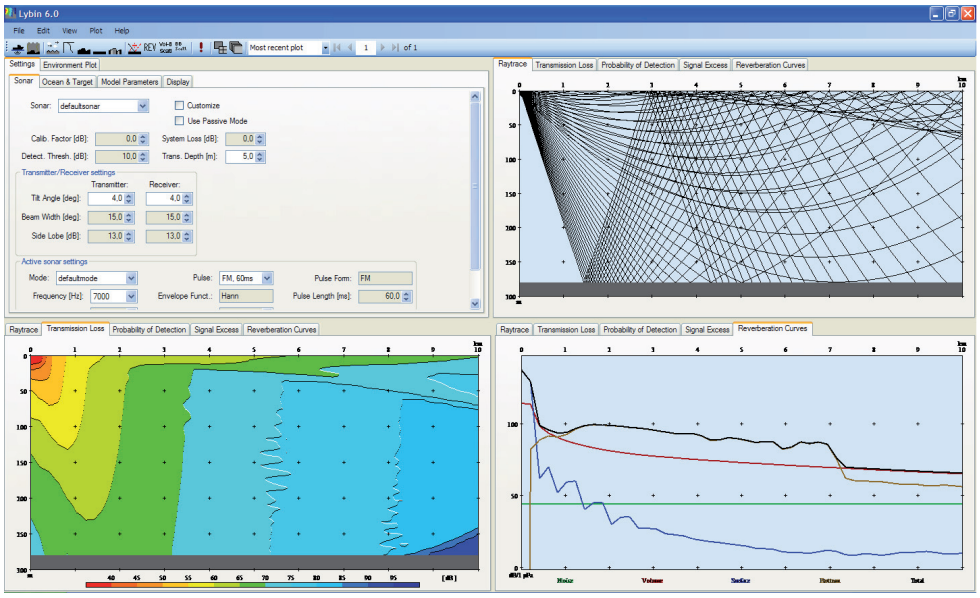

Figure 3: Graphical user interface of the acoustic model Lybin v6.0. The upper right plot shows the raytrace. The lower left plot shows modelled transmission loss levels. The lower right plot shows modelled noise and reverberation levels.

where $\mathbf{c_j}$ is an interpolated SSP. Let $\overline{\mathbf{c}}$ be the depth–averaged sound speed profile:

$$\overline{\mathbf{c}} \quad = \quad \frac{1}{M} \sum_{j=1}^{M} \mathbf{c_j}. \tag{15}$$

A single SSP may then be expanded in any set of orthonormal basis vectors [35]:

$$\mathbf{c_j} \quad = \quad \overline{\mathbf{c}} + \mathbf{U}^T \boldsymbol{\kappa}^{(j)}. \tag{16}$$

The elements of the coefficient vector $\boldsymbol{\kappa}^{(j)}$ may be determined as follows [35]:

$$\boldsymbol{\kappa}^{(j)} \quad = \quad \mathbf{U}\mathbf{x_j}, \tag{17}$$

where $\mathbf{U}$ is a matrix containing the transposed basis vectors, $\mathbf{u_k}^T$, on each row, and $\mathbf{x_j}$ is given by:

$$\mathbf{x_j} \quad = \quad \mathbf{c_j} - \overline{\mathbf{c}}. \tag{18}$$

The basis vectors are called EOFs. Since the EOFs are orthonormal, then:

$$\mathbf{u_k}^T\mathbf{u_l} = \begin{cases} 1, k = 1 \\ 0, k \neq 1 \end{cases} \tag{19}$$

The EOFs are found by solving the following eigenvalue problem:

$$\mathbf{R_x u_k} = \lambda_k \mathbf{u_k}, \tag{20}$$

where λ_k is the eigenvalue corresponding to the kth EOF and $\mathbf{R_x}$ is the covariance matrix [35]:

$$\mathbf{R_x} = \frac{1}{M} X^T X, \tag{21}$$

where the mean subtracted data matrix, X, is given by:

$$\mathbf{X} = \begin{bmatrix} \mathbf{x_1}^T \\ \mathbf{x_2}^T \\ \vdots \\ \mathbf{x_M}^T \end{bmatrix}. \tag{22}$$

The method is only meaningful if there is some correlation between the inputted SSPs. Poorly correlated data sets require more EOFs than well correlated data sets for proper representation of the data. The proportion of variances, Λ_l, is a useful indicator of this correlation and is frequently used for determining how many EOFs are required for a sufficient representation of the data set:

$$\Lambda_l = \sum_{k=0}^{l} \lambda_k \Bigg/ \sum_{k=0}^{N-1} \lambda_k. \tag{23}$$

Note that the eigenvalues are here sorted from largest at $k = 0$ to smallest at $k = N - 1$. Typically, a threshold T is selected, and the number of EOFs used is determined as follows:

$$\min_l \left(\Lambda_l \geq T\right). \tag{24}$$

New sound speed profiles with the same statistical properties as the original data set may be constructed using:

$$\mathbf{c} = \overline{\mathbf{c}} + \mathbf{U}^T \boldsymbol{\kappa}. \tag{25}$$

The elements, κ_k, of the coefficient vector are modelled as zero–mean random processes with variances given by λ_k [35]. The probability density function used to model the random process should be selected with care so as to retain the higher order moments as well as the mean and variance.

2.4.1 Example

In connection to the sea acceptance tests of the new Norwegian frigates, a set of 20 SSPs were measured in the Norwegian trench in September 2008, see Fig. 4 (a). Fig. 4 (b) shows the first four EOFs estimated from the measured SSPs. The corresponding eigenvalues are shown in Fig. 4 (c). Observe how quickly the eigenvalues fall off for increasing coefficient number. Using a threshold, T, of 0.9, see (24), then according to the proportion of variances shown in Fig. 4 (d) four EOFs are sufficient for representing the measured SSPs. A set of constructed SSPs using (25) are shown in Fig. 4 (e). Gaussian probability density functions are used to model the coefficients. Notice the maxima (at approximately 40 m) and minima (at approximately 60 m) in the constructed SSPs. These extreme values are not observed in the original data set and are probably unphysical. They are generated due to outliers in the first and third coefficient, see Fig. 4 (b). This is a good example of how non–physical artifacts are generated in statistically modelled SSPs when using a random generator that does not model the physics. Such artifacts may be avoided by replacing the Gaussian random generator by a more physical random generator, or by introducing some kind of reality filter. A simple and robust filter here is selecting a maximum and minimum allowed sound speed at all depths. Fig. 4 (f) shows a set of generated SSPs where $c \in [1480m/s, 1512m/s]$. The new set generated SSPs compare better visually with the original set of SSPs.

2.5 False alarm rates in high reverberant conditions

Sea trials in littoral environments with high reverberant conditions show that high–resolution sonars generate particularly many false alarms in presence of ship wrecks and terrain features such as seamounts and underwater ridges [1–4]. Possible causes for the high false alarm rates include false alarm rate inflation [5–8] and non–Rayleigh reverberation [1, 9–16].

False alarm rate inflation is a signal–processing–induced phenomenon that occurs when the reverberation power level is non–stationary in the normaliser

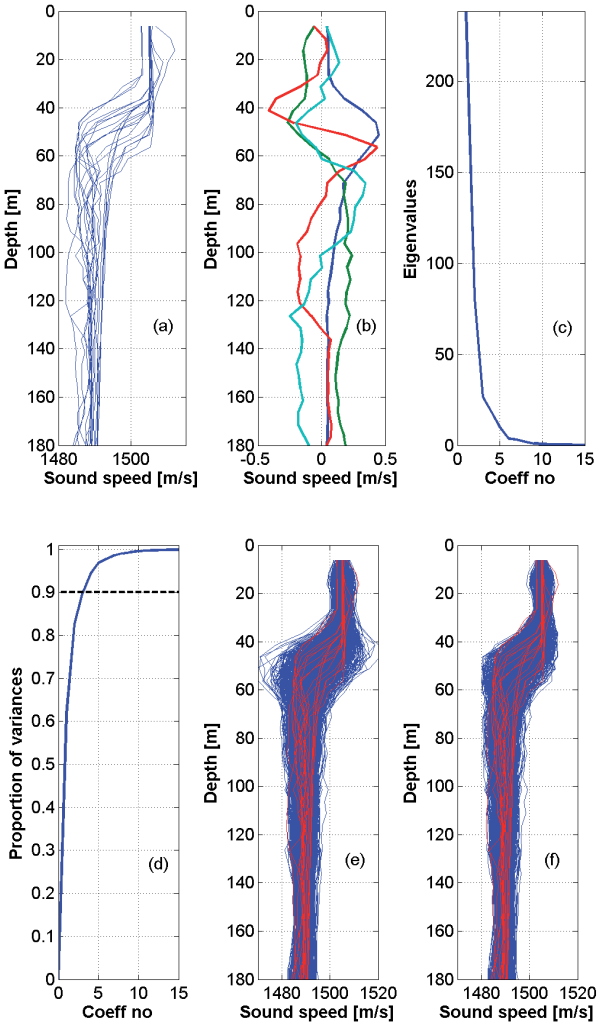

Figure 4: (a) 20 SSPs measured in the Norwegian Trench in September 2008. (b) First (blue), second (green), third (red), and fourth (cyan) EOF derived from the 20 SSP measurements. (c) Eigenvalues corresponding to the first 15 EOFs. (d) Proportion of variances plot for the first 15 EOFs. (e) Original SSPs (red) and constructed SSPs (blue) using (25) with coefficients modelled as random processes. (f) Original SSPs (red) and constructed SSPs (blue) using (25) with coefficients modelled as random processes, but with requirements on maximum and minimum sound speed.

window. E. g., the reverberation in the analysed sample originates from a sea mount, while most of the normaliser window falls to the side of the seamount, resulting in an underestimated background power estimate and therefore increased false alarm rate. This phenomenon is closely related to target masking [5], which occurs in the opposite situation when the seamount is located within the normalisation window resulting in an overestimation of the background level and therefore lost detections.

Non–Rayleigh reverberation is often referred to as sonar clutter. The Rayleigh probability density function is often assumed to model reverberation induced matched filter (MF) envelope well. The reverberation is non–Rayleigh when this assumption does not hold. Use of high–resolution sonars in littoral environments often result in non–Rayleigh distribution of MF data, typically with heavier tailed distributions [1, 9–11, 13–16]. This results in greater false alarm rates than anticipated when assuming Rayleigh reverberation.

Prediction and reduction of clutter and raised false alarm rates are the focus of many published studies. Studies cover different fields such as normalisation [6–8, 17], detection theory [44], image processing [18–20], acoustic modelling [4, 21, 22, 45], and other signal processing techniques [3]. Recently, several papers have been published on which environmental and sonar characteristics control clutter, such as sonar beamwidth [15] and multi–path environments [13, 16]. These papers give useful and insightful descriptions of the clutter phenomenon.

2.6 Acoustic inversion

Bucker [46] introduced matched field processing (MFP), a widely used technique for estimating the location of detected noise sources. Given a known environment, the acoustic fields received on an array of hydrophones from various target locations are modelled. The modelled acoustic field is then compared to the recorded acoustic field by using a cost function, and the target location is estimated by finding the location with optimal cost and therefore best comparison between model and recordings. Detailed descriptions of MFP cost functions and their advantages and disadvantages are found in [47]. Baggeroer *et al.* [48] give an excellent overview of the work done on MFP up until 1993.

The method has since been extended by including nuisance parameters in the search. Nuisance parameters may for instance be environmental param-

eters or the geometry of the receiver array. These parameters are uncertain and this uncertainty must be accounted for to secure good target location estimates. Focalisation [23] and marginalisation [49] are commonly used methods for including nuisance parameters in the inversion process. Focalisation selects a set of parameters that minimises the cost function, while marginalisation integrates the cost function over all environmental parameters before determining the optimal target location (or whatever other parameters are attempted inverted). Dosso and Wilmut [50] compare marginalisation to focalisation.

Bayesian inversion [51–53] is an extension to MFP. Unlike traditional MFP, Bayesian inversion outputs the posterior probability density function (PPD) for each parameter in the inversion process. The PPD may be used to determine standard deviations, mean estimates, and MAP-estimates for each inverted parameter. This additional information gives an understanding of the quality of inverted parameters.

In the above mentioned work, data from passive sonars were used. MFP has also successfully been extended to low–frequency, active sonars [54] showing promising results for target depth estimation. The main advantage of active sonars is that the propagation time from the sonar to the target is known. The propagation time may be used to estimate the range of the target.

Target location estimation using back propagation was introduced by Tappert [57], and later demonstrated for passive sonars using raytracing [23, 55, 56]. Vertical angles of incoming signals from a target are measured on a receiver array. Rays are traced from the sonar in the direction given by the measured angles. Locations where traced rays intersect are candidate target positions. Back propagation is related to the method called time–reversal [58]. Time–reversal or phase–conjugation is a method borrowed from the field of optics where the received field is retransmitted from the receiver and thereby, due to reciprocity, focused on the source. This method is popular in current underwater communication research. Instead of retransmitting the received field, the back propagation method inputs the environment and the received field into an acoustic model in order to find the target location. The method has recently also been used in air acoustics [59, 60]. To the authors knowledge back propagation has not before been demonstrated for active sonar data.

2.7 Acoustic sensitivity to environmental uncertainty

Validity of sonar performance models is generally limited by environmental uncertainty. James and Dowling [29] give an extensive overview of research on how environmental uncertainty influences acoustic field predictions. In littoral environments acoustic propagation is strongly influenced by bottom interaction [25] and the water–column sound speed [24–27]. The acoustic field in littoral environments is therefore very sensitive to uncertainty in the sound speed profile and bottom properties.

The acoustic sensitivity to environmental uncertainty is typically analysed by running an acoustic model repeatedly with Monte Carlo simulated environmental input and then analysing the output using some kind of sensitivity measure, for instance the coefficient of variation [28]:

$$\frac{\sigma(r, z, \phi)}{m(r, z, \phi)}, \tag{26}$$

where σ and m are the standard deviation and expectation of a suitable acoustic field parameter, *e. g.* pressure. Both are represented in sylindrical coordinates, (r, z, ϕ). The coefficient of variation represents the sensitivity of the acoustic field in a single position, and must therefore be spatially integrated in some way to examine the total sensitivity.

Monte Carlo methods require a large amount of calculations and are therefore time consuming. Other methods have been suggested. Dosso *et al.* [28] introduce a linearised measure of sensitivity. The underlying assumption is that for sufficiently small environmental perturbation the relationship between changes in the acoustic field is linearly dependent on changes in the environment. If this assumption holds, then the acoustic sensitivity to different environmental parameters may be analysed one parameter at a time, which is far more efficient than a full Monte Carlo approach. Finette [61] shows how environmental uncertainty may be included directly in an acoustic model by incorporating the uncertainty in sound speed in the narrow angle parabolic equation [37].

The uncertainty in sound speed may be reduced by frequent sound speed measurements, but this is costly and not always feasible. An alternative approach is to invert sound speed profiles (SSP) from recorded acoustic data in order to improve the acoustic modelling [23, 52, 56, 62, 63]. Inversion approaches may also be used to obtain other environmental information such as bottom properties. Generally speaking, if the acoustic field is sensitive to

uncertainty in an environmental parameter, then the parameter is eligible for inversion. Inversion techniques using data from naval sonars are frequently called through–the–sensor techniques. One such application is inverting bottom properties from recorded reverberation data [53]. The inverted bottom properties are then used in acoustic modelling in order to improve the results from sonar performance modelling for that system.

3 Description of attached papers

The following subsections give brief summaries of the contents of the papers. All papers are related to at least one of the two topics listed in section 1.2. The papers are listed below together with their status (published or unpublished), my role in writing them, and what topic is adressed:

1. **Sonar false alarm reduction using detailed bathymetry data and acoustic propagation modelling**
    - Published in the proceedings of Underwater Defense Technology Conference Exhibition 2005 in Amsterdam.
    - Main author
    - Adresses topic A
2. **Predicting sonar false alarm rate inflation using acoustic modelling and a high-resolution terrain model**
    - Published in IEEE Journal of Oceanic Engineering april 2010
    - Sole author
    - Adresses topic A
3. **Target depth estimation using a ray backpropagation scheme on sonar data – simulations and experiments**
    - Unpublished manuscript. Submitted to IEEE Journal of Oceanic Engineering
    - Sole author
    - Adresses topic A

4. **Target depth estimation using a ray backpropagation scheme on mid-frequency, active sonar data**

    - Published in proceedings of European Conference in Underwater Acoustics 2010.
    - Sole author
    - Adresses topic A and B

5. **Inverting the water–column sound speed**

    - Published in proceedings of European Conference in Underwater Acoustics 2010.
    - Sole author
    - Adresses topic B

6. **Finding acoustically stable areas through EOF classification**

    - Unpublished manuscript. Submitted to IEEE Journal of Oceanic Engineering.
    - coauthor
    - Adresses topic B

7. **In ocean evaluation of low frequency active sonar systems**

    - Published in proceedings of Acoustics08 in 2008.
    - Main author
    - Adresses topic B

3.1 Summary of the first paper: Sonar false alarm reduction using detailed bathymetry data and acoustic propagation modelling

Active low-frequency towed array sonar systems used in littoral waters experience high false alarm rate, mainly due to reflections from bottom features and steep slopes. This was confirmed by results from two sea trials (2001 and 2002) carried out in the NAT III (New Array Technology) project. The partners in NAT III were TNO-FEL (Netherlands Organisation for Applied

Scientific Research, Physics and Electronics Laboratory), TUS (Thales Underwater Systems) and FFI (Norwegian Defence Research Establishment).

The paper describes an automatic algorithm for classifying detections as false alarms due to raised reverberation levels. Given a high–resolution topography map, the acoustic model Lybin [41] is used to predict received reverberation levels on a specified active sonar. Zones of high probability of false alarms are introduced as geographical areas where normalised modelled reverberation exceeds a preset threshold. Echoes are automatically correlated to predicted zones of high probability of false alarms. Each echo is assigned a value called the percentile overlap. High percentile overlap values indicate that there is a high probability of that echo being generated due to raised reverberation levels.

The method is employed on a data set from the 2002 NAT III sea trial carried out in the Norwegian trench. Data from a small area (8 km by 7 km) with strong variations in the topography was focused on. 5% of the area was predicted as zones of high probability of false alarm, and 60% of the echoes accumulated over 20 pings in the selected area were located within zones of high probability of false alarms.

3.2 Summary of the second paper: Predicting sonar false alarm rate inflation using acoustic modelling and a high-resolution terrain model

This paper refines the method presented in the first paper, and gives a theoretical foundation for why high normalised modelled reverberation levels coincide with increased false alarm rates.

By combining a fast and accurate acoustic model with a high-resolution terrain model, occurence of false alarm rate inflation may be predicted. The described method outputs the modelled probability of false alarm, which is the probability that a false alarm is generated at a given location due to false alarm rate inflation.

Given high–resolution topography and a measured sound speed profile, the acoustic model Lybin [41] is used to model reverberation for a specified sonar. The modelled reverberation is then normalised using a normaliser window equivalent to the normaliser window used on recorded sonar data from the specified sonar. For a given model–resolution cell, the probability that a single sample in matched filtered and beam formed sonar data exceeds

the detector threshold is derived from the normalised modelled reverberation. This probability is the probability of false alarm due to false alarm rate inflation.

The presented method is used on a data set from the 2002 NAT III sea trial in the Norwegian trench. Modelled probability of false alarm is shown to compare well with spatial concentrations of recorded false alarms, but the modelling underestimates the probability of false alarm by approximately a factor of four. The cause of the underestimation is probably that the method does not completely predict the true probability of false alarm, since other causes of false alarms may also be present, e. g. clutter and noise spikes.

3.3 Summary of the third paper: Target depth estimation using a ray backpropagation scheme on sonar data – simulations and experiments

This paper presents a method that uses ray backpropagation, see section 2.6, on active sonar data in order to estimate the depth of a detected target. A narrow vertical beamwidth of the sonar is required, since accurate vertical arrival angle measurements are needed. The arrival time, vertical arrival angle, and measured environment are inputted in the acoustic raytracer PlaneRay [40]. Due to uncertainties in measured arrival angle a fan of rays are traced with initial vertical angles within two standard deviations of the measured vertical arrival angle. Each ray is assigned a probability determined from a Gaussian probability density distribution with an expectation given by the measured vertical angle. The probability of the target being located at a specific depth is determined by summing the probability contribution of all rays with end points at that depth. The target depth probability density function is determined, and a maximum a posteriori (MAP) estimate and an estimate for the standard deviation are extracted. This information may be used for classification, for instance by prioritising targets with target depth MAP estimates above the sea floor. The estimated standard deviation is a measure of how reliable the target depth estimate is.

The fidelity of the method is studied by simulating different environments with detected targets at different depths and ranges and with different signal–to–reverberation and noise ratios (SNR). The target depth estimates are shown to deteriorate for increasing ranges and decreasing SNRs. In simple scenarios and for sufficiently high SNR (23 dB), the method is shown

applicable for ranges up to 15 km.

The method is finally tested on recorded data for targets located on the sea floor and in the upper half of the water column. The method successfully estimates the target depth with an accuracy sufficient for classification purposes 82% of the time. Averaged over all measurements the target depths are estimated within 40 m of the true depth.

3.4 Summary of the fourth paper: Target depth estimation using a ray backpropagation scheme on mid-frequency, active sonar data

In this paper the method described in the third paper is developed further and given a stronger theoretical foundation. As in the third paper ray backpropagation is used, but is here combined with a Bayesian inversion approach [51] to estimate the a posteriori target depth probability density function. The introduction of Bayesian theory allows inclusion of a priori probabilities assigned to the environment. Tuning of the environment, by means of focalisation [23], is included in order to improve target depth estimation. Two environmental parameters are considered; sonar depth and sound speed profile. The former is included to take into account ship heave due to surface waves and ship motion. The latter is included by using empirical orthogonal functions (EOF) to represent sound speed profiles. Two EOFs are assumed sufficient for describing the sound speed variability. The sonar depth and EOF coefficients are varied in order to find the MAP estimate of the target depth. The computation time of this method far exceeds the computation time of the method described in the third paper, but the inclusion of focalisation improves the accuracy of the results.

3.5 Summary of the fifth paper: Inverting the water–column sound speed

This work presents an inversion method for estimating sound speed profiles by exploiting available sensor information. Sensor information considered includes sound speed measurements close to sonar equipment and echo sounder data used to estimate depth–averaged slowness. The depth–averaged slowness may be estimated from echo sounder data if the bottom depth is known.

Empirical orthogonal functions are determined from a set of known sound

speed profiles. The sound speed profiles used may be climatological data or, as used in this work, modelled sound speed profiles, e. g. from the MIPOM ocean model [64]. Sound speed profiles are generated by varying the weights of each EOF. Analytical and differentiable expressions, that include the EOF–coefficients as the only variables, are derived for each type of measurement (direct sound speed measurements and depth–averaged slowness). A conjugate gradient search is used in order to estimate a sound speed profile that matches well with measured values collected from the sensors.

A common problem during sonar operations is to determine how often to measure the sound speed profile. An algorithm for assessing the quality of the most recently measured sound speed profile is introduced. The sonar performance modelled using the most recent sound speed profile measurement is compared to the sonar performance modelled using an inverted sound speed profile. The hypothesis is that when the most recent measured sound speed profile results in a poor comparison, then a new sound speed profile should be measured. This is equivalent to a binary decision problem. The algorithm was applied on a simulated data set, and the probability of detection (the probability of deciding that a poor–quality measured sound speed profile is of poor quality) and probability of false alarm (the probability of deciding that a high–quality measurement is of poor quality) were shown to be 61% and 6%, respectively.

For a simulated data set, sonar performance predictions based on inverted sound speed profiles were shown to be comparable to performance modelled on basis of four-hourly sound speed measurements. This indicates that for simple sonar performance modelling, for instance for modelling the expected detection range during sonar operation, the presented inversion method may be used instead of measurements of the sound speed profile.

3.6 Summary of the sixth paper: Finding acoustically stable areas through EOF classification

Validity of sonar performance models is generally limited by environmental uncertainty [29], and particularly uncertainty in the sound speed profile (SSP) [24–27, 65]. Rapid environmental assessment (REA) missions, e. g. using gliders, and advanced ocean models may be used to reduce this uncertainty prior to sonar operation.

This paper presents a method on how EOFs may be used for locating

acoustically stable water masses in otherwise unstable waters. Acoustically stable water masses are defined as areas where modelled target signal excess has low sensitivity to expected oceanographic variability. A simple stability measure based on modelled signal excess is derived in order to measure the acoustic stability of an area.

A map of acoustically stable areas is the main output. This output is for instance useful for planning deployment of gliders during a REA mission. Large, geographically contiguous groups indicate acoustically stable areas where frequent SSP measurements are unnecessary, e. g. low concentration of gliders. Geographically mixed groups indicate the opposite. Other applications include determination of suitable locations for sonar tests that require stable sonar conditions and efficient optimization of sonar parameters in acoustically stable areas.

Modelled oceanography from the MI-POM ocean model [64] for an area close to the Western coast of Norway is used as an example. Surface salinity is a commonly used indicator for classifying water masses as either Atlantic water or coastal water. A simple comparison of the distribution of the first EOF coefficient and the surface salinity values shows that EOFs are also useful for classifying water masses. Based on the modelled sound speed profiles, the area is divided into acoustically stable subareas using the method described above. Both large contiguous groups and smaller, geographically mixed groups are generated. The locations of the geographically mixed groups match well with areas where mixing of coastal water masses and Atlantic water masses supposedly occurs, while the larger groups coincide well with homogeneous water masses.

3.7 Summary of the seventh paper: In ocean evaluation of low frequency active sonar systems

All though this paper does not directly address the topic B, as described in section 1.2, the relevance is strong enough for the work to be included here. Unlike the other papers, the work presented in this paper relates to a non–operational scenario, namely acceptance tests for naval sonars at sea.

Sonar performance measurements in the sea are always affected by uncontrollable and/or uncertain environmental conditions, such as sound speed variations, bottom topography, or the acoustic properties of the sea floor. This paper presents a method to determine a sonar – target geometry which

minimizes the uncertainty in target signal excess due to environmental variability.

An acoustic model is used to estimate signal excess for a large number of sound speed profiles measured in the relevant area. The results are compared while searching for a target range and depth where estimated signal excess is robust with respect to the expected variability of the sound speed profile in the actual area.

The achieved sensitivity of signal excess to environmental changes is demonstrated for different test geometries. Robustness in signal excess is shown to be highly dependent on target range and depth and sonar depth. Careful selection of the sonar – target geometry may reduce the uncertainty in modelled signal excess.

4 Conclusion

The thesis contains seven papers that address two relevant topics of research:

A *How to exploit available environmental information in order to increase the classification ability of anti–submarine warfare (ASW) sonars*

B *How to deal with environmental uncertainty*

The first topic is addressed by developing new classification algorithms. The first two papers present methods of predicting what areas are prone to high false alarm rates. The predictions are based on detailed environmental knowledge and acoustic modelling. The third and fourth papers present methods were vertical beamforming of sonar data is exploited in order to find the vertical arrival angle of target echoes. Ray backpropagation is then used to estimate target depth. Target depth is a very useful classification clue, and the method is proved sufficiently accurate for classification.

The achilles heel of the proposed classification algorithms is their need for accurate environmental information. Uncertainty in sound speed profile may result in ambiguous or erroneous results. The second topic deals with methods that reduces the uncertainty in the sound speed profile. The fourth and fifth papers present methods on how the sound speed profile may be extracted from data recorded during sonar operation. The last two papers present methods that analyse the acoustic stability of geographical areas. The assessment is based on a large set of sound speed profiles from the

analysed area. This data set can either be obtained from an ocean model or be densely measured sound speed profiles.

Papers six and seven introduce methods that are useful for determining acoustically stable areas for conducting sea trials in, for instance sonar tests. During the sea acceptance tests for the sonars on the new Norwegian F310–class frigates, these methods have been employed successfully. The oceanographic field was sampled densely using a moving vessel profiler. The method described in the sixth paper was then used to find acoustically stable areas within the measured area. On basis of the sound speed profiles measured in the selected area, the method in the seventh paper was then used to find the optimal sonar – target geometry for the acceptance tests. By optimal is here meant minimised uncertainty in the acoustic field.

4.1 Future work

Listed below are unresolved issues that are suggested for future work.

4.1.1 Normalisation optimiser

The second attached paper introduces a method where reverberation modelling is used to find areas susceptible to false alarm rate inflation. The occurence of false alarm rate inflation depends not only on the present environment, but also on the sonar parameters used and particularly the normaliser used. The developed method may be extended to automatically configure the normaliser in order to reduce false alarm rate inflation, e. g. by varying the normaliser window and guardband sizes.

4.1.2 Countering target masking

Another possible extension of the method introduced in the second paper is prediction of target masking. Target masking is often exploited tactically in order to hide from radars, for instance by placing military assets next to forests or other strong scatterers. Likewise, in naval warfare, submarines could hide in front of strong upslopes or seamounts to avoid detection. This tactic can be countered by predicting what areas are prone to target masking and then use one–sided normaliser windows to avoid the effects of target masking.

4.1.3 Automatic classification on basis of target depth estimation

The target depth estimator introduced in the third and fourth papers is suitable for implementation in combat management systems as a classification tool. The next step should be to test a prototype version live during sonar operation. An unresolved issue is how to best exploit multiple ping information. The two papers introduce different ways of coping with this problem. The method used in the fourth paper is most refined but also very slow. The computational cost could be reduced by implementing an improved search algorithm, such as simulated annealing. Another problem is that the assumption of independence between pings made in equation (13) in the fourth paper is in some cases questionable. The arrival time and angle measurements are probably independent, but the environmental input is not. If the assumption of independence is invalid then other means of exploiting multiple ping information must be made, such as the ones described in the third paper.

4.1.4 Sound speed profile inversion

The fifth paper presents a method for inverting the sound speed profile from echo sounder data and direct sound speed measurements. This method has been tested on a simulated scenario only and should therefore be tested on measurements for verification. The next step would be to make a prototype version live on a sonar vessel. The inverted sound speed profile can then be used either to check if the most recently measured sound speed profile is valid or to be used as input to sonar performance modelling. This could also be combined with the target depth estimator or normalisation optimiser to improve the results.

4.1.5 Spatio–temporal assessment of acoustic stability

The method for categorising the acoustic stability of geographical areas presented in the sixth paper may be extended to take into account temporal variablity. By analysing spatio–temporal variations, it should be possible to estimate how often sound speed measurements should be made to ensure a proper sampling of the environment during for instance sonar operation or rapid environmental assessment missions.

4.1.6 Acoustic sensitivity analyses for different sources of environmental uncertainty

The method described in the seventh paper has been successfully put to use during the sea acceptance tests for the Norwegian F310 frigates. However, the uncertainty in the sound speed profile is the only environmental uncertainty considered. The method may easily be extended to include other environmental parameters such as wind speed, bottom depths, and bottom properties. Furthermore, geometric uncertainties such as uncertainty in sonar depth and target location may also be included. Assuming locally linear acoustic sensitivity to each of these uncertain parameters, then stability plots that combine uncertainty in all these parameters simultaneously may easily be made. The contribution of each parameter may also be studied separately in order to determine what parameters the acoustic field is most sensitive to uncertainties in. This may shed light on how a test procedure may be improved to reduce the uncertainty of the test results.

Another possible extension is to find more objective ways of determining whether a certain situation is acoustically stable. The current method is subjective since it requires visual inspection of stability plots to determine the stability.

References

[1] N. P. Chotiros, H. Boehme, T. G. Goldsberry, S. P. Pitt, R. A. Lamb, A. L. Garcia, and R. A. Altenburg, *Acoustic backscattering at low grazing angles from the ocean bottom. Part II. Statistical characteristics of bottom backscatter at a shallow water site*, J. Acoust. Soc. Am., vol. 77, no 3, 1985.

[2] M. K. Prior, *A Scatterer Map for the Malta Plateau*, IEEE J. Oceanic Eng., Vol. 30, No 4, October 2005.

[3] M. K. Prior and A. Baldacci, *The physical causes of clutter and its supression via sub–band processing*, NURC–PR–2006–021, 2006.

[4] J. Wegge, E. M. Dombestein, A. L. Gjersøe, K. T. Hjelmervik, and E. Tveit, *Active Sonar Clutter Prediction*, Proceedings from Underwater Defence Technology Conference and Exhibition, Malmo 2003.

[5] M. A. Richards, *Fundamentals of Radar Signal Processing*, the McGraw-Hill Companies, 2005.

[6] H. Rohling, *Radar CFAR Thresholding in Clutter and Multiple Target Situations*, IEEE Trans. Aerosp. Electron. Syst., Vol. AES–19, No 4, July 1983.

[7] P. P. Gandhi and S. A. Kassam, *Analysis of CFAR Processors in Non-homogeneous Background*, IEEE Trans. Aerosp. Electron. Syst., Vol. 24, No 4, July 1988.

[8] D. A. Abraham, *Statistical normalization of Non-Rayleigh reverberation*, OCEANS '97, MTS/IEEE Conference Proceedings.

[9] A. P. Lyons and D. A. Abraham, *Statistical characterizations of high–frequency shallow–water seafloor backscatter*, J. Acoust. Soc. Am., vol. 106, no 3, 1999.

[10] D. A. Abraham and A. P. Lyons, *Novel physical interpretations of K–distributed reverberation*, IEEE J. Oceanic Eng., Vol. 27, No 4, April 2002.

[11] D. A. Abraham and A. P. Lyons, *Reverberation envelope statistics and their dependence on sonar bandwidth and scattering patch size*, IEEE J. Oceanic Eng., Vol. 29, No 1, April 2004.

[12] D. A. Abraham and A. P. Lyons, *Simulation of Non–Rayleigh Reverberation and Clutter*, IEEE J. Oceanic Eng., Vol. 29, No 2, April 2004.

[13] K. D. LePage, *Statistics of Broad–Band Bottom Reverberation Predictions in Shallow–Water Waveguides*, IEEE J. Oceanic Eng., Vol. 29, No 2, April 2004.

[14] B. R. la Cour, *Statistical Characterization of Active Sonar Reverberation Using Extreme Value Theory*, IEEE J. Oceanic Eng., Vol. 29, No 2, April 2004.

[15] D. A. Abraham, *The effect of Multipath on the Envelope Statistics of Bottom Clutter*, IEEE J. Oceanic Eng., Vol. 32, No 4, October 2007.

[16] D. A. Abraham, *Array Modeling of Active Sonar Clutter*, IEEE J. Oceanic Eng., Vol. 33, No 2, April 2008.

[17] T. J. Barnard and F. Khan, *Statistical Normalization of Spherically Invariant Non–Gaussian Clutter*, IEEE J. Oceanic Eng., Vol. 29, No 2, April 2004.

[18] F. B. Shin, D. H. Kil and R. F. Wayland, *Active Impulsive Echo Discrimination in Shallow Water by Mapping Target Physics–Derived Features to Classifiers*, IEEE J. Oceanic Eng., Vol. 22, No 1, January 1997.

[19] S. Dugelay and D. A. Abraham, *Reduction of low frequency active sonar clutter through image processing*, SACLANTCEN SR–272–UU, 1999.

[20] R. Laterveer, *Single ping clutter reduction: segmentation using Markov random fields*, SACLANTCEN SR–307, 1999.

[21] F.–P. A. Lam, F. P. A. Benders, P. Schippers, and S. P. Beerens, *Environment Adaption for LFAS and Corresponding 3D Modelling of Sonar Performance*, Proceedings from Underwater Defence Technology Conference and Exhibition, La Spezia 2002.

[22] K. T. Hjelmervik, A. L. Gjersøe, E. Tveit, and J. Wegge, *Sonar false alarm reduction using detailed bathymetry data and acoustic propagation modelling*, Proceedings from Underwater Defence Technology Conference and Exhibition, Amsterdam 2005.

[23] M. D. Collins and W. A. Kuperman, *Focalization: Environmental focusing and source localization*, J. Acoust. Soc. Am., vol. 90, no 3, 1991.

[24] S. E. Dosso, *Environmental uncertainty in ocean acoustic source localization*, Inverse Problems, vol. 19, no 2, 2003, pp. 419–431.

[25] K. LePage, *Modeling Propagation and Reverberation Sensitivity to Oceanographic and Seabed Variability*, IEEE J. Oceanic Eng., Vol. 31, No 2, April 2006.

[26] S. Finette, *A stochastic representation of environmental uncertainty and its coupling to acoustic wave propagation in ocean waveguides*, J. Acoust. Soc. Am., vol 120, no 5, 2006.

[27] K. LePage and B. E. McDonald, *Environmental Effects of Waveguide Uncertainty on Coherent Aspects of Propagation, Scattering, and Reverberation*, IEEE J. Oceanic Eng., Vol. 31, No 2, April 2006.

[28] S. E. Dosso, P. M. Giles, G. H. Brooke, D. F. McCammon, S. Pecknold, and P. C. Hines, *Linear and nonlinear measures of ocean acoustic environmental sensitivity*, J. Acoust. Soc. Am., vol. 121, no 1, 2007.

[29] K. R. James and D. R. Dowling, *A method for approximating acoustic–field–amplitude uncertainty caused by environmental uncertainties*, J. Acoust. Soc. Am., vol 124, no 3, 2008.

[30] http://www.mareano.no/english/index.html

[31] J. Groen, S. P. Beerens, and Y. Doisy, *Adaptive Port–Starboard Beamforming of Triplet Sonar Arrays*, IEEE J. Oceanic Eng., Vol. 30, No 2, April 2005.

[32] H. Hobæk, *Akustisk avbildning og arrayteknologi*, Fysisk institutt, Universitetet i Bergen, 1995.

[33] x. Lurton, *An Introduction to Underwater Acoustics - Principles and Applications*, Springer Verlag, 2002.

[34] R. J. Urick, *principles of underwater sound*, 3rd ed., Peninsula Publishing, 1983.

[35] C. W. Therrien, *Discrete Random Signals and Statistical Signal Processing*, Prentice Hall, 1992.

[36] H. L. Van Trees, *Optimum array processing (Detection, Estimation, and Modulation Theory, Part I-IV)*, Wiley, 2002.

[37] F. B. Jensen, W. A. Kuperman, M. B. Porter, and H. Schmidt, *Computational ocean acoustics*, 2nd printing, Springer Verlag, 2000.

[38] K. V. Mackenzie, *Long–Range Shallow–water Bottom Reverberation*, J. Acoust. Soc. Am., vol. 34, no 1, 1962.

[39] J. M. Hovem, *The physics of sound in underwater environments*, to be published by Peninsula Publishing, ca 2010.

[40] J. M. Hovem, *An acoustic underwater propagation model based on ray tracing and plane wave reflection coefficients*, Theoretical and Computational Acoustics 2007, Edited by Michael Taroudakis and Panagiotis

Papadakis, Published by the University of Crete, Greece, 2008. pp. 273-289 (ISBN: 978-960-89785-4-2).

[41] K. T. Hjelmervik, E. M. Dombestein, S. Mjølsnes, T. S. Såstad and J. Wegge, *The acoustic raytrace model Lybin – Description and application*, Proceedings from Underwater Defence Technology Conference and Exhibition, Glasgow 2008.

[42] R. W. Preisendorfer and C. D. Mobley, *Principal Component Analysis in Meteorology and Oceanography*, Elsevier science publishers, 1988.

[43] A. Tolstoy, *Acoustic tomography via matched field processing*, J. Acoust. Soc. Am., vol. 89, no 3, 1991

[44] D. A. Abraham and P. K. Willett, *Active Sonar Detection in Shallow Water Using the Page Test*, IEEE J. Oceanic Eng., Vol. 27, No 1, January 2002.

[45] K. T. Hjelmervik, A. L. Gjersøe, S. Alsterberg, *Sonar simulation module for land–based sonar operator training*, Proceedings from Underwater Defence Technology Conference and Exhibition, Hamburg 2006.

[46] H. P. Bucker, *Use of Calculated Sound Fields and Matched-Field Detection to Locate Sound Sources in Shallow Water*, J. Acoust. Soc. Am., vol. 59, no 2, 1976.

[47] A. Tolstoy, *Matched Field Processing for Underwater Acoustics*, World Scientific, Singapore, 1993.

[48] A. B. Baggeroer, W. A. Kuperman, and P. N. Mikhalevsky, *An overview of matched field methods in ocean acoustics*, IEEE J. Ocean. Eng. 18, pp. 401424, 1993.

[49] A. M. Richardson and L. W. Nolte, *A posteriori probability source localization in an uncertain sound speed, deep ocean*, J. Acoust. Soc. Am., vol. 89, no 5, 1991.

[50] S. E. Dosso and M. J. Wilmut, *Comparison of focalization and marginalization for Bayesian tracking in an uncertain ocean environment*, J. Acoust. Soc. Am., vol. 125, no 2, 2008.

[51] P. Gerstoft and C. F. Mecklenbruker, *Ocean acoustic inversion with estimation of a posteriori probability distributions*, J. Acoust. Soc. Am., vol. 104, no 2, 1998.

[52] D. Tollefsen and S. E. Dosso, *Three–dimensional source tracking in an uncertain environment*, J. Acoust. Soc. Am., vol 125, no 5, 2009.

[53] S. E. Dosso, P. L. Nielsen, and C. H. Harrison, *Bayesian inversion of reverberation and propagation data for geoacoustic and scattering parameters*, J. Acoust. Soc. Am., vol. 125, no 5, 2009.

[54] G. Hickman and J. L. Krolik, *Matched–field depth estimation for active sonar*, J. Acoust. Soc. Am., vol. 115, no 2, 2004.

[55] P. Voltz and I.-T. Lu, *A time-domain backpropagating ray technique for source localization*, J. Acoust. Soc. Am., vol. 95, no 2, 1994.

[56] I.-T. Lu, *Simultaneous characterization of source, array and environment using a ray travel-time inversion approach*, J. of Comput. Acoust., vol. 5, no 2, 1997.

[57] F. D. Tappert, L. Nghiem-Phu, and S. C. Daubin, *Source Localisation Using the PE Method*, J. Acoust. Soc. Am., vol. 78, 1985 (abstract only).

[58] M. Fink, *Time reversal of ultrasonic fields I. Basic principles*, IEEE Trans. Ultrason. Ferroelectr. Freq. Control, vol 39, no 5, pp. 555566, 1992.

[59] D. Mennitt and M. Johnson, *Multiple–array passive acoustic source localization in urban environments*, J. Acoust. Soc. Am., vol. 127, no 5, 2010.

[60] D. G. Albert, L. Liu, and M. L. Moran, *Time reversal processing for source location in an urban environment*, J. Acoust. Soc. Am., vol. 118, no 2, 2005.

[61] S. Finette, *Embedding uncertainty into ocean acoustic propagation models*, J. Acoust. Soc. Am., vol. 117, no 3, 2005.

[62] L. T. Fialkowski, M. D. Collins, and J. S. Perkins, *Source localization in noisy and uncertain environments*, J. Acoust. Soc. Am., vol 101, no 6, 1997.

[63] E. Svensson, *Inverting acoustic communication signals for the sound speed profile*, J. Acoust. Soc. Am., vol 120, no 3, pp 1347 - 1355, 2006.

[64] H. A. Engedahl, *Implementation of the princeton ocean model (pom/ecom3d) at the norwegian meteorological institute*, Norwegian Meteorological Institute, Oslo, Norway, Research Report 5, 1995.

[65] S. E. Dosso, M. G. Morley, P. M. Giles, G. H. Brooke, D. F. McCammon, S. Pecknold, and P. C. Hines, *Spatial field shifts in ocean acoustic environmental sensitivity analysis*, J. Acoust. Soc. Am., vol. 122, no 5, 2007.

Paper 1

Sonar false alarm reduction using detailed bathymetry data and acoustic propagation modelling

Sonar false alarm reduction using detailed bathymetry data and acoustic propagation modelling

Karl Thomas Hjelmervik[1], kth@ffi.no
Amund L. Gjersøe[1], alg@ffi.no
Jon Wegge[1], jwe@ffi.no
Elling Tveit[1], etv@ffi.no

1 Abstract

Active low-frequency towed array sonar systems used in littoral waters experience high false alarm rate, mainly due to reflections from bottom features and steep slopes. This was confirmed by results from two sea trials (2001 and 2002) carried out in the NAT III (New Array Technology) project. The partners in NAT III were TNO-FEL (Netherlands Organisation for Applied Scientific Research, Physics and Electronics Laboratory), TUS (Thales Underwater Systems) and FFI (Norwegian Defence Research Establishment).
This paper describes a method of reducing the false alarm rate using an acoustic model. Predicted *zones of high probability of false alarms* are introduced as geographical areas where the normalised modelled reverberation exceeds a preset threshold. A method of automatically correlating recorded monostatic echoes with the predicted zones is presented. A *probability of false alarm* is linked to the echoes for tracking purposes, resulting in lower track probability in *zones of high probability of false alarms.*

2 Introduction

This paper is based on work in the NAT III programme. NAT III, was a co-operation between TNO-FEL, TUS and FFI. The purpose of the programme was to assess the advantages of bistatic operations with low frequency active sonars, LFAS. An LFAS system was tested in Norwegian waters in two sea trials in 2001 and 2002. In particular, the system's performance in shallow and coastal waters was evaluated. The programme was closed in November 2004. The data presented in this paper is from the 2002 sea trial.

The main advantages of LFAS systems are the high beam resolution and the good performance at long distances. A problem in fjords and in shallow, coastal waters is the amount of echoes[2] generated from each transmission[3]. Submarines are not the only reflectors, but terrain features causes cluttering of echoes. These false echoes behave similarly to submarine echoes, and they are in great numbers. An ideal tracker[4] is easily jammed if fed by many echoes, and is not able to process the data in real-time. Approaches to deal with this problem can roughly be divided into two categories; simplifying the tracker or reducing the amount of echoes. The method suggested in this paper is of the latter sort. The idea is to use knowledge on the

[1] Scientist at the Norwegian Defence Research Establishment.
[2] Echoes are received reflections of the transmitted pulse from reflectors in the sonified medium.
[3] A transmission is the acoustic energy transmitted by the sonar.
[4] A tracker is an algorithm that creates a path of a hypothetical target using series of echoes from different transmissions.

environment in combination with an acoustic propagation model in order to predict what areas are most likely to generate false echoes. This information can be used to either remove recorded echoes within these areas or reduce the track probability of tracks generated in them. Either solution would reduce the computational cost of the tracking process, allowing more advanced and accurate trackers to be used.

The method described is based on the work presented by Jon Wegge at the Underwater Defence Technology conference in Malmo 2003, see ref [1].

3 Low frequency active towed array sonars in Norwegian waters

Norwegian waters offer a wide range of environmental challenges due to the complexity in the oceanography and variations in the sea floor terrain. The north Atlantic Gulf steam interacts with coastal streams and fresh water from the land. The terrain varies between archipelago, deep fjords, shelves, and deep ocean conditions. In addition the waters are rich in terms of biology, not only introducing high false alarm likelihood, but also imposing restrictions on the use of LFAS.

Detailed hydrographic mapping enables us to better model the sonar performance. This again makes us more capable of predicting the likely locations of echoes from bottom reverberation, in addition to the range and path of acoustic energy.

Sonar processing in the past did not add detailed information neither from the terrain nor from any acoustic model. It was basically left to the operator to interpret the sonar response. However, with new sonars, the false alarms increase in number as a result of the increased range and bandwidth, but the alarms may be more accurately localized as a result of a narrower beam width. Thus there is a need for a more effective false alarm reduction filter, a method that is closer to reality as a result of the more accurate echo localization and detailed terrain information.

4 Method of correlating echoes with terrain

This section describes the method used to automatically correlate echoes with modelled zones of high reverberation. The first subsection presents the acoustic raytrace model, LYBIN. The second subsection defines *zones of high probability of false alarm*, and describes the method of predicting them. The third section describes how recorded echoes are correlated with *zones of high probability of false alarm.*

4.1 Acoustic model and reverberation modelling

The acoustic propagation model used is LYBIN. LYBIN is an incoherent ray trace model developed by Svein Mjølsnes at NDLO/Sea (Norwegian Defence Logistic Organisation). It models the transmission loss and reverberation in a single vertical cross section and uses the sonar equations, see ref [2], to compute the signal excess and probability of detection of a hypothetical target within the cross section. Input is the sonar parameters[5], a depth dependent sound speed profile, wind speed[6], bottom

[5] Such as sonar position, source level, frequency band, pulse length, beam widths and side lobe levels.

parameters[7] and range dependent bottom depths. Recent developments of LYBIN have made it range dependent in wind speed, sound speed and in bottom parameters as well.

A single LYBIN run computes the reverberation in a single direction from the sonar. LYBIN must therefore be run once for every direction of interest. The general problem requires a full, 360^0 coverage. In the examples shown in this paper a resolution in direction of two degrees has been used, that is LYBIN is run 360 times for every ping, and the direction of each LYBIN run is separated by 1^0. This method of using a 2d acoustic propagation model in a 3d problem, is in literature referred to as the *n*2d* method. The range resolution used is 45m. The depth resolution varies. 50 depth cells are used and the maximum depth depends on the current bottom profile.

4.2 Predicted zones of high probability of false alarms

Predicted *zones of high probability of false alarms* are areas where the acoustic model predicts local maxima in the reverberation.. The reverberation is computed using LYBIN and the *n*2d* method. The reverberation is then normalized in range using:

$$Norm(rev_i) = \frac{rev_i - \overline{rev_i}}{std(rev_i)} \qquad \text{Equation 1}$$

rev_i is the modelled reverberation in range cell *i.* $Norm(rev_i)$ is the normalized reverberation in range cell *i.* $\overline{rev_i}$ is the average reverberation in two split-windows to each side of range cell *i*. The windows have widths of 15 cells (675m), and five cells separate them (225m). $std(rev_i)$ is the estimated standard deviation using the same windows as in the averaging.

After normalization the data is thresholded to find the local maxima. In the example shown in this paper, the threshold is 8dB. (This threshold must not be confused with the threshold commonly used in detectors to extract echoes, see next section.) Note that the model resolution in range, the width of the normalization windows and the threshold value are interconnected. Peaks in the modelled reverberation are typically reduced when the model resolution decreases. The reason is that the reflected energy from bathymetric features is smeared out over large range cells. The size and separation of the normalization windows also directly influence the peaks in the normalized reverberation. Finally, the preset threshold determines which of these peaks result in *modelled detections.* Figure 1 illustrates the procedure for a single direction. This is done for all *n* directions, resulting in a set of discreet positions where the modelled and normalized reverberation exceeds a threshold.

---

[6] The wind speed is used to compute the surface back scatter, bubble attenuation close to the surface, ambient noise level and also surface forward scattering.

[7] LYBIN uses a single-valued parameter between 0 and 10 to classify all bottom types for both bottom backscatter and loss computations.

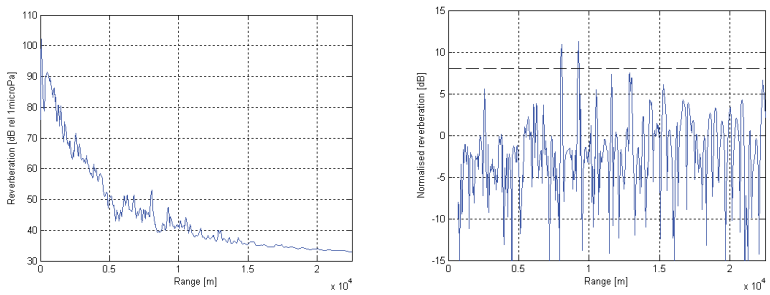

Figure 1: Left plot is modelled reverberation in dB rel 1□Pa. The right plot is the same data after normalization. The black dashed line in the right-hand plot is the threshold value.

Each range cell in a single LYBIN run represents an area, henceforth called area cells, which is equal to:

$$A = r\Delta r\ \Delta\theta\ A \qquad \text{Equation 2}$$

r is the range. Δr is the size of a range cell and equals the maximum model range R divided by the number of range cells. $\Delta\theta$ is the bearing resolution, that is the difference in angle between neighbouring LYBIN runs. The size of the area is proportional to range, which means that larger ranges results in higher uncertainty, and less ability to recognize bathymetric features. Keep in mind that a single bottom profile is used for each direction. This means that a prominent bathymetric feature within an area could be missed by the bottom profile, and therefore not modelled correctly. Higher resolution in bearing solves this problem, but bear in mind that the computational effort is inversely proportional to the bearing resolution, when using the *n*2d* method.

We realize that the exact position and extent of a clutter is uncertain. To make the method more robust to localisation errors, we extend all predicted areas to including neighbouring cells and we also merge areas that at very close. An imaging technique called dilation is used. Figure 2 illustrates the procedure. The areas are here called modelled detections, or just detections in the figure. The red squares represent detections. Yellow squares represent neighbouring cells. Cyan squares represent common neighbours of two or more modelled detections. A *zone of high probability of false alarms* is an area consisting of red, yellow and cyan cells in contact, directly or indirectly. In the example there are five zones, each of them are numbered and bounded by a red box.

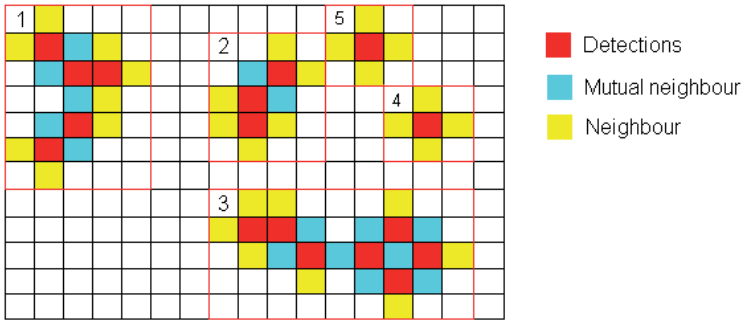

Figure 2: Illustration of dilation. The axis represents Cartesian resolution cells. The red squares represents modelled detections. Yellow squares represent neighbouring cells. Cyan squares represent common neighbours of two or more modelled detections

4.3 Correlating recorded echoes with zones of high probability of false alarms

The correlation of recorded echoes with modelled *zones of high probability of false alarms* is simple and straightforward. Each recorded echo's area of uncertainty is geographically compared to the location of zones. If they overlap, then the echo is defined as linked to that zone with a *percentile overlap* equal to the ratio of the overlapping area and the total uncertainty area of the echo. Figure 3 illustrates the concept. The intension of the percentile overlap (PO) is to use it in the tracking process. High PO of an echo should lower the probability of a track using it.

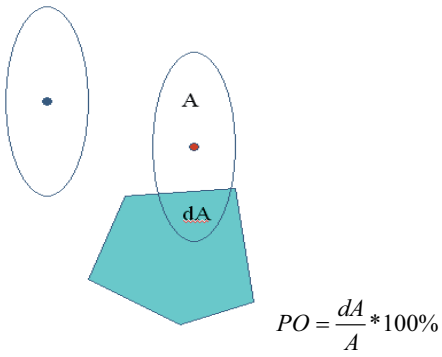

Figure 3: Illustration of correlation of recorded echoes (red and blue dots) with predicted *zones high probability of false alarms* (cyan areas).

Correlation percentage of a single transmission is a statistical parameter that shows how many echoes that are linked to a zone, compared to the total number of echoes for that transmission.

5 Results from correlation of recorded echoes and zones of high probability of false alarm

An area of 8km by 7km in Norwegian waters is used to illustrate the method. The area has strongly varying depth, ranging from 0m to 600m. Such varying bathymetry typically results in huge amounts of echoes. For the transmissions presented here, the average number of recorded echoes within the area is 2500. No methods of echo-reduction were applied.

Figure 4 shows echoes and zones of high probability of false alarm for four consecutive pings in a 8km by 7km area in littoral waters. The red echoes are linked to a zone, while the blue echoes are not. Clusters of echoes are bounded by ellipses and numbered. Most of these clusters consist of red echoes, especially the large clusters. A cluster with mainly red echoes is assumed predicted by the model. The correlation between clusters of echoes and zones of high probability of false alarm is good. The model does not easily predict lone echoes, but they seldom generate long living tracks anyway. In ping 17 it seems that there is a shift in angle of all echoes relative the sonar, reducing the correlation. This is most likely due to an error in the array heading, such errors influence positioning of echoes directly.

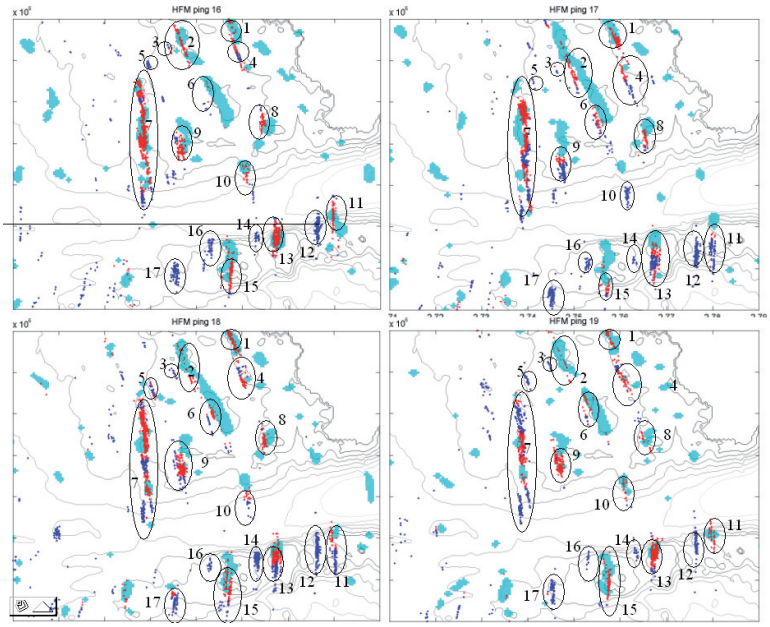

Figure 4: Echoes and zones of high probability of false alarm for four consecutive pings in example 1. The black line coming in from the left side in the upper-left plot represents the direction towards the sonar.

Clusters 12, 14, 16 and 17 are not predicted. Common for these clusters, are that they are generated in deeper terrain than the predicted clusters. Other studies on the same data set indicate that the sound speed profile used in the modelling has a too strong

sound speed channel. This results in entrapment of too much acoustic energy within the channel. See Figure 5. The peak labelled **1** is the probable cause for cluster 12, while the peak labelled **2** is the cause for cluster 11. A weaker sound channel would result in more acoustic energy propagating into the depths, and therefore deeper zones of high probability of false alarm.

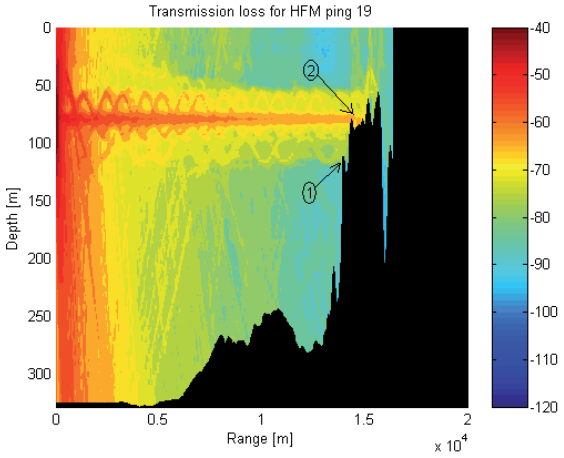

Figure 5: Transmission loss plot towards cluster 12 in ping 19.

Figure 6 shows statistics of how well the echoes and zones of high probability of false alarm are correlated for twenty pings. The average amount of echoes per ping is 2500 for the area studied. For most pings the correlation percentage exceeds 50%. There seems to be a shift in angle of all echoes in pings 2, 17 and 20, due to an error in the array heading. This is easily seen for ping 17 by studying Figure 4.

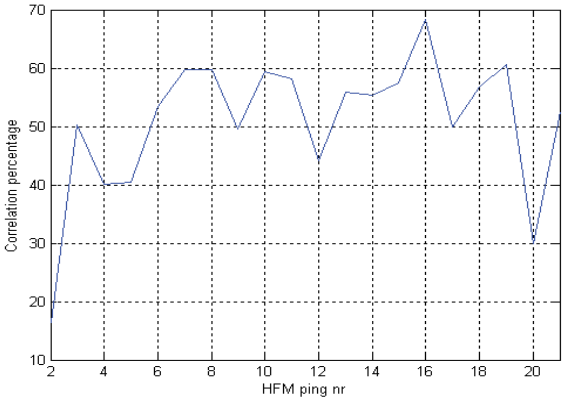

Figure 6: Correlation percentage in example 1 for 20 pings. Correlation percentage is the percentage of echoes that are linked to a zone of high probability of false alarm.

6 Thoughts on using the results in a recursive tracking algorithm

A popular and cost-effective algorithm for target tracking in a cluttered environment is the Interacting Multiple Model combined with the Probabilistic Data Association Filter (IMMPDAF) [3]. This filter manages to initiate, maintain and terminate tracks, and yields the probability that there is a target in track. As the algorithm is presented in [3] it ignores the information about the amplitude or the signal to noise ratio (SNR) of the echo. An improvement of the IMMPDAF to include means to benefit from the amplitude information (IMMFDAFAI) is presented in [4]. This made the data association better by weighing the echoes within the validation gate by their SNR, combined with the traditional weighing of echoes due to their position deviation compared to the predicted position. Further it also included using additional models when a track entered the maintenance mode. This allowed for better tracking under the manoeuvring of targets.
Our intention is to decrease the *probability of detection* (P_D) when our Percentile Overlap (PO, see Figure 3) is increasing. Our PO must not be confused with the *probability of false alarm* (P_F) [5]. How PO is related to P_D and SNR is not defined, but some pragmatically statements for the tracking algorithm can be defined:

a) Echoes with PO > $\boldsymbol{\tau}$ can not initiate tracks
b) Tracks in initiation mode (age < 10 pings) [4] can not use echoes with PO > $\boldsymbol{\tau}$
c) The amplitude (a) of echoes (M) with PO ≥ 0 within the validation gate [3] will be weighted (w) based on a function of PO and a: $w_i = \boldsymbol{f}(PO_i\, a_i)$, $i \in M$.

Here $\boldsymbol{\tau} \in [0,1]$ is a fixed threshold for PO to allow tracking in areas with heavy density of bottom reverberation.
The computational cost of the algorithm will be reduced by the statements a) and b). With statement c), the weight of the echo with a high PO will be decreased, and thus have a reduced influence on the data association of new measurements.

In some cases, the echoes from bottom reflection gain a higher SNR than the submarine close to the area. This is due to the differences in depths and size of the reflecting areas of the bottom feature and the submarine. When using the target tracker with amplitude information feature, we will suppress the echo from the submarine in favour of the stronger echo from the bottom feature, and possibly lead the tracker off the target. This opens for an investigation on the possibility of estimating the amplitude of a target, when tracking a target with some defined variation in amplitude. For estimation one have to expand the system models to include the SNR as a state variable. For computational cost effectiveness, this can be combined with the use of Percentile Overlap. Doing so, this can be used to define an additional maintenance mode for tracks near areas with high probability of false alarms due to reverberation.
The Percentile Overlap is expected to be an effective input variable to tracking algorithms to reduce false target tracks based on bottom reverberation, and to reduce computational cost of the tracking algorithms.

7 Conclusions

The method presented predicts that 5% of an 8km x 7km area are zones with high probability of false alarms. Comparison with real sonar echoes for that area shows that an average of 60% of the echoes falls within these zones. Each echo within a zone is assigned a *Percentile Overlap*. The Percentile Overlap can be used to reduce computation cost of tracking algorithms. It can also reduce the probability of tracks initiated based on echoes from bottom features, and possibly help the algorithm track targets through areas with dense clutter from bottom reverberation.

The method is sensitive to errors in array heading and environmental information. Errors in array heading cause a shifting of angle of all echoes. If the echoes are misplaced, then the model has no real chance in linking them to zones of high probability of false alarm. Errors in the sound speed profile cause the sound to propagate along wrong paths, typically displacing the zones of high probability of false alarm to either shallower or deeper areas. Finally, the method demands a high-resolution bottom depth grid in order to model the bottom reverberation with any success.

8 References

[1] Jon Wegge et al (2003): Active Sonar Clutter Prediction, UDT – Europe 2003.

[2] A. D. Waite (2002): “SONAR for Practicing Engineers”, 3rd ed., John Wiley and Sons Ltd

[3] Bar-Shalom, Chang and Blom (1990): "*Automatic track formation in clutter with a recursive algorithm*" In Bar-Shalom *"Multitarget-Multisensor Tracking - Advanced Applications"*Artech House, 1990

[4] Lerro and Bar-Shalom (1993): *"Interacting Multiple Model Tracking with Target Amplitude Feature"*, IEEE Transactions on aerospace and electronic systems, Vol. 29, No. 2, April 1993

[5] McDonough and Whalen (1995): *"Detection of Signals in Noise SE"* Academic Press, 1995

Paper 2

Predicting Sonar False Alarm Rate Inflation Using Acoustic Modeling and a High-Resolution Terrain Model

Is not included due to copyright

Paper 3

Target depth estimation using a ray backpropagation scheme on mid-frequency, active sonar data

Is not included due to copyright

Paper 4

Target depth estimation using a ray backpropagation scheme on mid-frequency, active sonar data

Target depth estimation using a ray backpropagation scheme on mid-frequency, active sonar data

Karl Thomas Hjelmervik [1]

[1]the Norwegian Defence Research Establishment and the Norwegian University of Science and Technology, **karl–thomas.hjelmervik@ffi.no**

Classification is one of the main challenges in anti–submarine warfare using active sonars in littoral waters. Sea mounts and rocky ridges may result in large numbers of false alarms, some exhibiting submarine–like behaviour. High false alarm rates result in complex tactical pictures. Efficient classification tools for reducing the amounts of false alarms are needed.

Conventional active sonar processing outputs a target's range and bearing. The presented method gives an estimate of the target depth on basis of data from a mid–frequency, active sonar. The vertical arrival angle is determined by beamforming received sonar data vertically. Ray backpropagation is combined with Bayesian inversion to estimate the a posteriori target depth probability density function. Empirical orthogonal functions (EOF) are used to represent the sound speed profile. EOF coefficients and sonar depth are included in the inversion in order to improve the target depth estimate.

The method is tested on recorded data from two targets; one located at 300 m depth and one at an unknown depth in the upper 81 m of the water–column. Target depth is estimated to 285 m depth and 45 m, respectively, which is sufficient for classification purposes in anti–submarine warfare.

1 Introduction

One of the main challenges in anti–submarine warfare using active sonars in littoral waters is classification. Varying topography and rocky outcrops result in a large number of false alarms [1–4], some of which exhibit very submarine–like behaviour [2]. High number of false alarms results in a complex tactical picture. Efficient classification tools for reducing the amounts of false alarms are therefore needed. This work presents a method that estimates target depth. Knowledge of target depth is a powerful classification clue which allows separation of false targets located on the sea floor, such as wrecks, sea mounts, and large boulders, from true targets.

Matched–field processing (MFP) is a widely used technique for estimating target location, and is mostly used for passive sonars [5, 6]. MFP has also successfully been extended to low–frequency, active sonars [7] showing promising results for target depth estimation. Bayesian inversion is an extension of MFP that also outputs the probability density function for the model parameters [8]. Collins and Kuperman [9] introduced focalisation as a means for improving target depth estimates by including environmental parameters, e. g. sound speed profiles, in the inversion process. An alternative method for target localisation is ray backpropagation [9–11]. This method has been demonstrated for low–frequency, passive sonar systems [9, 11]. Ray backpropagation is a method where acoustic rays are traced in a direction defined by the angle of arrival measured on the sonar. In the passive sonar case, multiple arrivals are needed. Locations where rays representing the different arrivals intersect are candidate target locations.

This paper presents a method that estimates the a posteriori target depth probability density function of a detected target. Vertical arrival angles and arrival times are measured using a mid–frequency, active sonar. Bayesian inversion and ray backpropagation are used to estimate probable target depths. Focalisation is employed by including sonar depth and the sound speed profile in the inversion process. Empirical orthogonal function (EOF) coefficients represent the sound speed profiles [9] in the inversion.

The method is applied on a data set containing detections of two different targets. The first target is a pipeline located on the sea floor at 300 m depth. The second target is an echo repeater located at an unknown depth less than 81 m.

2 Method

Let an unknown target be detected using standard active sonar processing; beamforming, matched filtering, and detection [12]. The measured vertical arrival angle is defined as the vertical steering angle maximising the signal–to–noise ratio (SNR) of the target echo. The vertical arrival angle, ϕ, and arrival time, t, are considered as Gaussian distributed random processes with standard deviations [13] given by:

$$\sigma_\phi = \frac{\phi_{BW}}{\sqrt{s}} \quad (1)$$

$$\sigma_t = \frac{1}{B\sqrt{s}} \quad (2)$$

s is the signal–to–noise ratio of the target echo. ϕ_{BW} is the vertical beamwidth of the sonar. B is the sonar bandwidth.

Let the model parameter vector, $\mathbf{m}$, contain relevant information on the environment as well as arrival time and vertical arrival angle. Target depth may then be modelled from

$\mathbf{m}$ by a raytracer [14]:

$$d(\mathbf{m}) = g(\mathbf{m}) \quad (3)$$

g is an operator describing the raytracer. $d(\mathbf{m})$ is the modelled target depth.

Let the elements in $\mathbf{m}$ be samples from independent random processes, and let the joint probability density distribution for the model parameters be given by $P(\mathbf{m})$, then:

$$P_m(\mathbf{m}) = P_{m1}(m_1)P_{m2}(m_2)\dots P_{mL}(m_L) \quad (4)$$

$P(m_j)$ is the probability density distribution for the jth parameter, m_j.

Bayes law states that:

$$P_{zd}(z|d(\mathbf{m}))P_d(d(\mathbf{m})) = P_{dz}(d(\mathbf{m})|z)P_z(z) \quad (5)$$

z is the true target depth, and $d(\mathbf{m})$ is the modelled target depth given by (3). The a posteriori probability density distribution (PPD) for target depth, $P_{zd}(z|d(\mathbf{m}))$, is given by:

$$P_{zd}(z|d(\mathbf{m})) = \frac{P_{dz}(d(\mathbf{m})|z)P_z(z)}{P_d(d(\mathbf{m}))} \quad (6)$$

Assuming $P_z(z)$ is uniform, then $P_d(d(\mathbf{m}))$ may be estimated by:

$$P_d(d(\mathbf{m})) = P_z(z)\int_{-\infty}^{\infty} P_{dz}(d(\mathbf{m})|z)dz \quad (7)$$

Combining (6-7) gives:

$$P_{zd}(z|d(\mathbf{m})) = \frac{P_{dz}(d(\mathbf{m})|z)}{\int_{-\infty}^{\infty} P_{dz}(d(\mathbf{m})|z)dz} \quad (8)$$

$P_{dz}(d(\mathbf{m})|z)$ is estimated by modelling the target depth for all combinations of model parameters, and assigning a probability to modelled target depth equal to the combined probability of all model parameters, $P_m(\mathbf{m})$. If multiple model parameter combinations result in the same depth, then the corresponding probabilities are summed. Let the water column be divided into K intervals, each of Δz width and centred at z_k. $P_{dz}(d(\mathbf{m})|z_k)$ may then be approximated as a step function with K intervals where the step heights are given by:

$$P_{dz}(d(\mathbf{m})|z_k) \approx \frac{1}{\Delta z}\int_{\mathbf{m}} \mathrm{H}\left(\frac{\Delta z}{2} - |z_k - d(\mathbf{m})|\right) P_m(\mathbf{m})\partial\mathbf{m} \quad (9)$$

H is the unit–step–function, which equals unity for non–negative arguments and zero otherwise. An expression for the PPD can then be found by combining (8–9). Fig. 1 illustrates how the PPD is derived.

Target depth mean– and MAP–estimates [15] are given by:

$$z_{mean} = \sum_{k=0}^{K-1} z_k P_{zd}(z_k|d(\mathbf{m}))\Delta z \quad (10)$$

$$z_{MAP} = \max_{z_k}\left(P_{zd}(z_k|d(\mathbf{m}))\right) \quad (11)$$

and the associated variance is given by:

$$\sigma_z^2 = \sum_{k=0}^{K-1}(z_k - z_{mean})^2 P_{zd}(z_k|d(\mathbf{m}))\Delta z \quad (12)$$

Mean–estimates, for targets located close to the sea floor, are generally pulled away from the sea floor due to reflectivity of the sea floor. This makes the mean–estimate a poor choice for separating real targets from false alarms generated at the sea floor. The MAP–estimate has no obvious weaknesses in that regard, and is therefore used here.

The PPD is so far derived for single–ping information only. Assuming stationary target depth and independent measurements of arrival time and arrival angle, then the theory may be extended to apply for multi–ping information as follows:

$$P(z_k|\mathbf{d}(\mathbf{M})) = \frac{\prod_{j=0}^{N-1} P_{dz}(d(\mathbf{m_j})|z_k)}{\int_{-\infty}^{\infty}\prod_{j=0}^{N-1} P_{dz}(d(\mathbf{m_j})|z_k)dz} \quad (13)$$

$\mathbf{m_j}$ is the model parameter vector that applies for ping number j. $\mathbf{M}$ is the model parameter matrix containing the model parameter vectors for all pings. The elements of the vector $\mathbf{d}(\mathbf{M})$ are target depths estimated by inputting $\mathbf{m_j}$ in (3). $P_{dz}(d(\mathbf{m_j})|z_k)$ is determined from (9). The MAP–estimate then becomes:

$$z_{MAP} = \max_{z_k}\left(P_{zd}(z_k|\mathbf{d}(\mathbf{M}))\right) \quad (14)$$

The theory may also be extended to limit the stationarity requirement for some or all model parameters. For instance, requiring that the sound speed profile remains the same for all pings, but allowing a non–stationary arrival time and arrival angle due to sonar and target movement. This extension is not within the scope of this work and therefore not included here.

3 Experimental data

A sea trial was conducted in the Norwegian trench at approximately 60° North and 4° East. The area is virtually flat with a sea floor depth of 300 m. The sound speed profiles were measured six times during the trial, see Fig. 2.

The vessel was equipped with a hull-mounted sonar, at 5 m depth, working on frequencies below 10 kHz. The sonar transmitted hyperbolic FM pulses with 2 kHz bandwidth and 1 s pulse length. The vertical beamwidth was 15°.

Several oil pipelines located on the seafloor, at approximately 300 m depth, crisscross the area of the sea trial. The sonar detected and maintained tracks on several pipelines. Measured arrival times and vertical arrival angles for one such track are shown in Fig. 3. This track was maintained for 16 pings.

An echo repeater was located in the area. The echo repeater was attached to a buoy and left to drift. The length of the cable from the buoy to the echo repeater was 81 m. The true

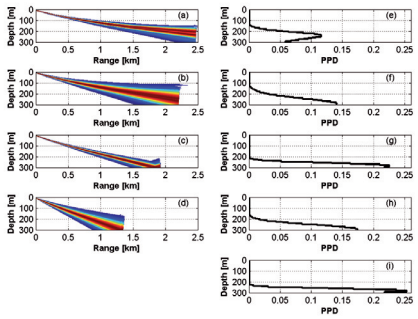

Figure 1: (a-d) show ray paths for four different pings. Each ray represents a single realisation of the random model input vector given by $\mathbf{m_j}$. The colour of the ray represents the a priori probability of the model given by $P_m(\mathbf{m_j})$. The a priori probabilities of all rays with end points within a single depth interval, centered at z_k, are summed to find the probability, $P_{dz}(d(\mathbf{m})|z_k)$, that the modelled target depth lies in that depth interval. (e-h) show the PPD estimated using (8). (i) shows the PPD based on all four measurements and is essentially the normalised product of (e-h), see (13).

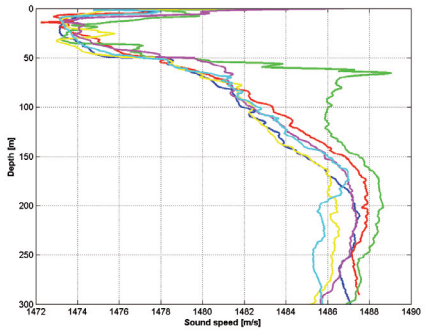

Figure 2: Measured sound speed profiles in the Norwegian trench at the time of the sea trial.

depth of the echo repeater is unknown, but is clearly less than 81 m. The sonar detected and maintained a track on the echo repeater for 87 pings. Measured arrival times and vertical arrival angles for this track are shown in Fig. 3.

4 Results and discussion

The described method is tested on data measured during the sea trial described in section 3. A raytracer called PlaneRay [17] is used. The model parameter vector, $\mathbf{m}$, includes

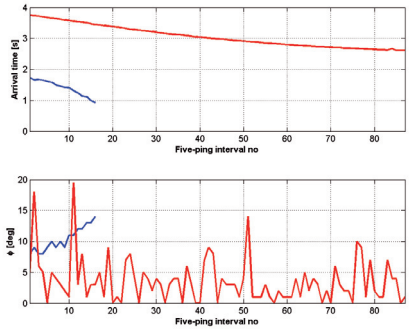

Figure 3: Measured arrival time (upper plot) and vertical optimal arrival angle (lower plot) as a function of ping number for the track on the pipeline (blue) and the echo repeater (red).

sound speed profile, sonar depth, arrival time, and vertical arrival angle. Each of these parameters are considered as Gaussian distributed random parameters.

On a flat sea surface, the sonar depth is 5 m below the sea surface. However, due to ship heave, the sonar depth is considered uniformly distributed between 2 m and 8 m.

The vertical arrival angle is considered Gaussian distributed with a standard deviation given by (1). Angles within two standard deviations of the measured arrival angles are considered. The uncertainty in arrival time is so low that errors of several standard deviations in size have no significant impact on the results. The arrival time is therefore considered as a deterministic constant.

The sound speed profile is represented by empirical orthogonal functions (EOF). EOFs are derived from the measured sound speed profiles shown in Fig. 2. Details on how this is done can be found in [16]. The proportion of variances [16] for the two first EOFs are 85 %, which is assumed sufficient to describe the sound speed profiles. Sound speed profiles are generated as follows:

$$\mathbf{c}(\boldsymbol{\kappa}) \quad = \quad \overline{\mathbf{c}} + \mathbf{U}^T \boldsymbol{\kappa} \tag{15}$$

$\overline{\mathbf{c}}$ is a vector containing the expected sound speed profile estimated by averaging the measured sound speed profiles. $\mathbf{U}$ is a matrix containing EOFs as rows. $\boldsymbol{\kappa}$ is a vector containing EOF coefficients. The EOF coefficients are zero–mean, Gaussian–distributed random processes and are included in the model parameter vector. The standard deviations of the coefficients are given by the square root of the corresponding eigenvalues [15]. Coefficient values within two standard deviations of 0 are considered.

Target depth PPDs based on the two tracks presented in section 3 are estimated using the described method. Ten depth–intervals are used in (9), each 30 m wide. Fig. 4 shows the target depth PPDs for the detected pipeline for all 16 pings.

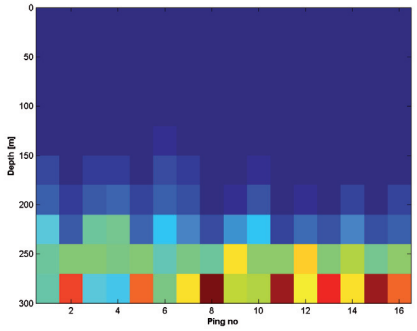

Figure 4: The target depth PPD for the pipeline is plotted for each ping number. The function is estimated using (8) on the data set presented in Fig. 3.

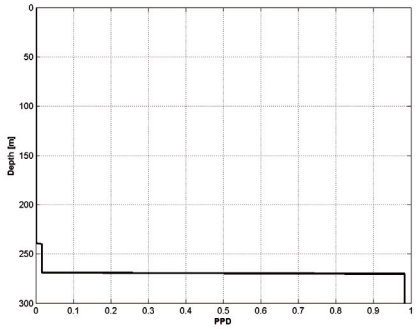

Figure 5: The target depth PPD for the pipeline estimated using (13) is plotted. This is essentially the product of all PPDs shown in Fig. 4.

The method estimates the target depth to be close to the bottom for all pings. Fig. 5 shows the PPD accumulated over all pings. The MAP–estimate for the target depth is 284 m, and the estimated standard deviation is 10 m. The true depth of the target is 300 m.

Fig. 6 shows the target depth PPDs for the echo repeater. The method estimates the target depth to be within the upper 60 m of the water–column for most pings. For a few pings, the PPD is almost uniform. These are pings where the SNR is low, resulting in high vertical angle standard deviations (1). Due to their high estimated target depth standard deviation, these pings have little influence on the PPD estimated from all pings shown in Fig. 7. The MAP–estimate for the target depth is 45 m, and the estimated standard deviation is 9 m. The true target depth is unknown, but below 81 m.

The accuracy of the target depth estimates is considered sufficient for classification purposes, since the main goal is to separate targets in the upper water–column from targets located on the sea floor.

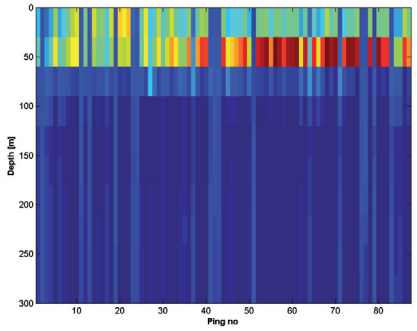

Figure 6: The target depth PPD for the echo repeater is plotted for each ping number. The function is estimated using (8) on the data set presented in Fig. 3.

5 Conclusion

A method capable of estimating the depth of a submerged target using mid–frequency, active sonar data is demonstrated. Ray backpropagation and Bayesian inversion are combined. The methods input is the present environment and recorded arrival times and vertical arrival angles.

The method is applied on a data set containing acoustic returns from a pipeline located on the sea floor at 300 m depth and an echo repeater located at an unknown depth less than 81 m. The a posteriori target depth probability density function was derived using Bayesian inversion and ray backpropagation. The sound speed profile was represented by empirical orthogonal functions (EOF), and the resulting EOF coefficients were included in the inversion. Sonar depth was also varied in the inversion process. The maximum a posteriori (MAP) estimate of the depth of the pipeline was 285 m and the standard deviation was 10 m. The MAP estimate of the depth of the echo repeater was 45 m with a standard deviation of 9 m.

Knowing the depth of a target is a powerful tool for classification of submarines and mine–like objects in the ocean. Filtering tracks on account of target depth may reduce the false alarm rate in littoral areas significantly.

Acknowledgment

Thanks to colleagues at FFI and the Norwegian University of Science and Technology (NTNU) for contributing their expert advise and guidance. Particular thanks to my supervi-

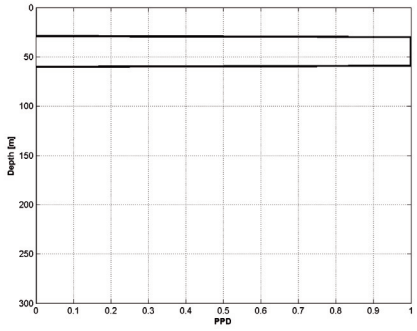

Figure 7: The target depth PPD for the echo repeater estimated using (13) is plotted. This is essentially the product of all PPDs shown in Fig. 6.

sor, professor Jens M. Hovem at NTNU, and my colleagues Geir Helge Sandsmark and Henrik Berg at FFI for aiding me in developing the presented method.

References

[1] M. K. Prior and A. Baldacci, *The physical causes of clutter and its supression via sub–band processing*, NURC–PR–2006–021, 2006.

[2] J. Wegge, E. M. Dombestein, A. L. Gjersøe, K. T. Hjelmervik, and E. Tveit, *Active Sonar Clutter Prediction*, Proceedings from Underwater Defence Technology Conference and Exhibition, Malmo 2003.

[3] K. T. Hjelmervik, A. L. Gjersøe, E. Tveit, and J. Wegge, *Sonar false alarm reduction using detailed bathymetry data and acoustic propagation modelling*, Proceedings from Underwater Defence Technology Conference and Exhibition, Amsterdam 2005.

[4] M. K. Prior, *A Scatterer Map for the Malta Plateau*, IEEE Journal of Oceanic Engineering, Vol. 30, No 4, October 2005.

[5] H. P. Bucker, *Use of calculated sound fields and matched field detection to locate sound sources in shallow waters*, Journal of the Acoustic Society of America, vol. 59, no 2, 1976.

[6] A. B. Baggeroer, W. A. Kuperman, and P. N. Mikhaelevsky, *Use of calculated sound fields and matched field detection to locate sound sources in shallow waters*, IEEE Journal of Oceanic Engineering, vol. 18, no 4, 1993.

[7] G. Hickman and J. L. Krolik, *Matched–field depth estimation for active sonar*, Journal of the Acoustic Society of America, vol. 115, no 2, 2004.

[8] P. Gerstoft and C. F. Mecklenbruker, *Ocean acoustic inversion with estimation of a posteriori probability distribuions*, Journal of the Acoustic Society of America, vol. 104, no 2, 1998.

[9] M. D. Collins and W. A. Kuperman, *Focalization: Environmental focusing and source localization*, Journal of the Acoustic Society of America, vol. 90, no 3, 1991.

[10] P. Voltz and I.-T. Lu, *A time-domain backpropagating ray technique for source localization*, Journal of the Acoustic Society of America, vol. 95, no 2, 1994.

[11] I.-T. Lu, *Simultaneous characterization of source, array and environment using a ray travel-time inversion approach*, Journal of Computational Acoustics, vol. 5, no 2, 1997.

[12] H. L. Van Trees, *Optimum array processing (Detection, Estimation, and Modulation Theory, Part IV)*, Wiley, 2002.

[13] A. Farina and E. Hanle, *Position Accuracy in Netted Monostatic and Bistatic Radar*, IEEE transactions on aerospace and electronic systems, vol. AES–19, no 4, July 1983.

[14] F. B. Jensen, W. A. Kuperman, M. B. Porter, and H. Schmidt, *Computational ocean acoustics*, 2nd printing, Springer Verlag, 2000.

[15] C. W. Therrien, *Discrete Random Signals and Statistical Signal Processing*, Prentice Hall, 1992.

[16] K. T. Hjelmervik, *Inverting the water column sound speed*, Prodeedings from European Conference in Underwater Acoustics 2010.

[17] J. M. Hovem et al, *An acoustic underwater propagation model based on ray tracing and plane wave reflection coefficients*, Theoretical and Computational Acoustics 2007, Edited by Michael Taroudakis and Panagiotis Papadakis, Published by the University of Crete, Greece, 2008. pp. 273-289 (ISBN: 978-960-89785-4-2).

Paper 5

Inverting the water column sound speed

Inverting the water column sound speed

Karl Thomas Hjelmervik[1]

[1]the Norwegian Defence Research Establishment and the Norwegian University of Science and Technology, **karl–thomas.hjelmervik@ffi.no**

Sonar performance models are commonly used in anti–submarine warfare operations. The validity of sonar performance models are generally limited by available environmental information, such as the present sound speed profile. However, frequent sound speed measurements are costly and slows down the operation.

This work presents an inversion method for estimating sound speed profiles by exploiting available sensor information. Sensor information considered includes sound speed measurements close to sonar equipment, and echo sounder data used to estimate depth–averaged slowness. Predicted oceanographic data and a bottom model are required. The inversion method derives empirical orthogonal functions (EOF) for modelled sound speed profiles. EOF coefficients are varied using conjugate gradient searches, in order to estimate a sound speed profile that matches well with measured values collected from the sensors.

The method is applied on simulated data. The inverted sound speed profiles are shown to resemble the simulated truth data well, and that sonar performance modelling based on inverted sound speed profiles is comparable to performance modelled on basis of four-hourly sound speed measurements. Furthermore, inverted sound speed profiles are shown useful for quality assessment of sound speed measurements.

1 Introduction

Validity of sonar performance models is generally limited by environmental uncertainty. James and Dowling [1] give an overview of research on how environmental uncertainty influences acoustic field predictions. Modelled acoustic fields are sensitive to uncertain water–column sound speed [2–5]. Frequent sound speed measurements reduce the uncertainty, but may be costly and is not always feasible. An alternative approach is to invert the sound speed profile (SSP) from recorded acoustic data. Collins and Kuperman introduced focalisation [6] as a means of improving source localisation by including the SSP in matched–field processing. Empirical orthogonal functions (EOFs) [7] were used to characterise the SSPs. The EOF coefficients were used as additional parameters in the inversion process. Inverting SSPs from acoustic data in order to improve acoustic modelling, has since been used in matched–field processing [8, 9] as well as other methods [10, 11].

This work presents an inversion method that estimates a local SSP from available sensor information using inversion. Sensor information considered are sound speed measured close to sonar equipment, and echo sounder data. Echo sounder data are used to estimate depth–averaged slowness. The measurements are performed in the immediate vicinity of the sensors and have high–update rates, and are therefore considered local in space and time.

The inversion method is applied on a simulated data set. In the simulations, a set of SSPs collected during a sea trial in the Norwegian trench using a moving vessel profiler [12], are simulated as truth data. Measurements are simulated by extracting data at the measurement depth from the truth data. Predicted SSPs from the MI-POM ocean model [13] are used to determine a set of EOFs. EOF coefficients are varied using conjugate gradient searches [15] in order to generate an SSP matching the simulated measurements. Inverted SSPs are compared to truth data. Modelled sonar performance using inverted SSPs is compared to modelled sonar performance using sound speed measurements. The acoustic model Lybin [14] is used to model the sonar performance. A method of assessing the quality of sound speed measurements using inverted sound speed profiles is also presented and discussed.

2 Method

The proposed method employs an inversion approach to estimate the SSP from a limited set of sound speed measurements. The inverted SSP is generated using EOFs. EOF coefficients are varied in order to minimise the difference between measurements and the inverted SSP. For easier implementation, slowness, s, is used instead of sound speed, c:

$$s = \frac{1}{c} \tag{1}$$

Section 2.1 shows how EOFs are generated from a set of SSPs. Costfunctions for minimisation and a minimisation method are presented in sections 2.2 and 2.3. A function for comparing modelled sonar performance for two different input SSPs is described in section 2.4.

2.1 Determining the empirical orthogonal functions for a set of measured slowness profiles

Consider a set of M measured slowness profiles each containing N equally gridded depth samples. Let $\mathbf{s_m}$ be an N–dimensional vector containing the slowness values from the mth profile. Let the slowness data matrix, $\mathbf{S}$, be given by:

$$\mathbf{S} = \begin{bmatrix} \mathbf{s_0}^T \\ \mathbf{s_1}^T \\ \vdots \\ \mathbf{s_{M-1}}^T \end{bmatrix} \tag{2}$$

The mean slowness, $\bar{\mathbf{s}}$, is given by:

$$\bar{\mathbf{s}} = \frac{1}{M}\mathbf{S}^T\mathbf{v} \tag{3}$$

$\mathbf{v}$ is an M–dimensional vector consisting of ones only. Let the scaled slowness, $\mathbf{x}$, be given by:

$$\mathbf{x} = \mathbf{s} - \bar{\mathbf{s}} \tag{4}$$

The scaled slowness data matrix is defined as:

$$\mathbf{X} = \begin{bmatrix} \mathbf{x_0}^T \\ \mathbf{x_1}^T \\ \vdots \\ \mathbf{x_{M-1}}^T \end{bmatrix} \tag{5}$$

$\mathbf{x_m}$ may be expanded in any set of N orthonormal eigenvectors $\mathbf{u_n}$ with coefficient vector κ_m, section 4.6.1 [7]:

$$\mathbf{x_m} = \mathbf{U}^T\kappa_m \tag{6}$$

$\mathbf{U}$ is the eigenmatrix given by:

$$\mathbf{U} = \begin{bmatrix} \mathbf{u_0}^T \\ \mathbf{u_1}^T \\ \vdots \\ \mathbf{u_{N-1}}^T \end{bmatrix} \tag{7}$$

The eigenvectors are found by solving the eigenvalue problem [7]:

$$\mathbf{R_x u_n} = \lambda_n \mathbf{u_n} \tag{8}$$

In literature $\mathbf{u_n}$ are often referred to as empirical orthogonal functions (EOF). $\mathbf{R_x}$ is the covariance matrix of the scaled slowness data matrix [7]:

$$\mathbf{R_x} = \frac{1}{M}\mathbf{X}^T\mathbf{X} \tag{9}$$

λ_n is the eigenvalue corresponding to eigenvector $\mathbf{u_n}$. The eigenvalues equal the variances of the corresponding coefficients κ_n [7]:

$$\mathrm{Var}(\kappa_n) = \lambda_n \tag{10}$$

New slowness profiles of the same class as the slowness profiles in the original data set may be generated by using (4) and (6). For an arbitrary coefficient vector κ, a new profile, $\hat{\mathbf{x}}$, may be generated using the following equation:

$$\hat{\mathbf{x}} = \mathbf{U}^T\kappa \tag{11}$$

Random slowness profiles may be generated by modelling the coefficient vector as a zero–mean random vector with variances given by the corresponding eigenvalues.

Let λ_n be ordered such that for increasing n, λ_n decreases. Higher orders of n often represent noise [7]. The vectors in (11) may therefore be truncated with insignificant loss of information on the slowness profile. A commonly used approach is to cut–off when the proportion of variances, Γ_l, exceeds a selected threshold. The proportion of variances is defined as:

$$\Gamma_l = \frac{\sum_{n=0}^{l}\lambda_n}{\sum_{n=0}^{N-1}\lambda_n} \tag{12}$$

The chosen threshold depends on the specific application, but a commonly used threshold is 95%.

2.2 Minimisation problem

Let the eigenmatrix, $\mathbf{U}$, and eigenvalue vector, λ, be estimated from a set of M slowness profiles, as described in the previous section. Let $\mathbf{d}$ be an JxK matrix containing K independent measurements made on J different sensors (e. g. depth–averaged slowness from an echo sounder or single–depth slowness values from sound speed sensors). If $J = N$, the coefficients, κ, may be found analytically. If $J < N$, then the system of equations is indeterminate and may not be solved directly. However, the problem may be solved by inversion, where a set of coefficients is sought that results in a generated slowness profile, $\widehat{\mathbf{s}}(\kappa)$, best matching the measured slowness values. Let $\widehat{\mathbf{d}}(\kappa)$ be a vector containing values derived from $\widehat{\mathbf{s}}(\kappa)$ that corresponds to the measurements $\mathbf{d}$.

$\mathbf{d}$ and $\widehat{\mathbf{d}}(\kappa)$ are related by Bayes theorem [16]:

$$P(\widehat{\mathbf{d}}(\kappa)|\mathbf{d})P(\mathbf{d}) = P(\mathbf{d}|\widehat{\mathbf{d}}(\kappa))P(\widehat{\mathbf{d}}(\kappa)) \tag{13}$$

The measurements, $\mathbf{d}$, are regarded as fixed values, $P(\mathbf{d})$ is therefore constant. κ is a random vector with independent elements and variance λ. The prior coefficient probability is then given by:

$$P(\kappa) = \prod_{n=0}^{N-1} P(\kappa_n) \tag{14}$$

κ is assumed Gaussian distributed. The probability density function relating to $P(\kappa_n)$ is then given by:

$$f_{\kappa_n}(\kappa_n) = \frac{1}{\sqrt{2\pi\lambda_n}}\exp\left(-\frac{\kappa_n^2}{2\lambda_n}\right) \tag{15}$$

Assuming a one–to–one relationship between κ and $\widehat{\mathbf{d}}(\kappa)$ and since κ is the only random input to $\widehat{\mathbf{d}}(\kappa)$, then:

$$P(\widehat{\mathbf{d}}(\kappa)) = P(\kappa) \quad (16)$$

$P(\mathbf{d}|\widehat{\mathbf{d}}(\kappa))$ is interpreted as the likelihood function, and the elements of $\widehat{\mathbf{d}}(\kappa)$ are assumed independent and Gaussian distributed. The likelihood function is then given by:

$$L(\kappa) = \prod_{j=0}^{J-1} L_j(\kappa) \quad (17)$$

where,

$$L_j(\kappa) = \frac{1}{\sqrt{2\pi}\sigma_{d_j}} \exp\left(-\sum_{k=0}^{K-1} \frac{\left(d_{jk} - \widehat{d}_j(\kappa)\right)^2}{2\sigma_{d_j}^2} \right) \quad (18)$$

d_{jk} are the elements of $\mathbf{d}$. σ_{d_j} is the estimated standard deviation of the jth sensor. $\widehat{d}_j(\kappa)$ are the elements of $\widehat{\mathbf{d}}(\kappa)$. The marginal probability density function that relates to the probability $P(\mathbf{d})$ may be determined by integrating the likelihood–function over all κ:

$$f_d(\mathbf{d}) = \int_{-\infty}^{\infty} L(\kappa) d\kappa \quad (19)$$

Combining (13–19) gives the posterior probability density (PPD) for the EOF coefficients:

$$f_{\widehat{d}}(\widehat{\mathbf{d}}(\kappa)|\mathbf{d}) = \prod_{j=0}^{J-1} L_j(\kappa) \prod_{n=0}^{N-1} f_{\kappa_n}(\kappa_n) \Big/ \int_{-\infty}^{\infty} L(\kappa) d\kappa \quad (20)$$

The MAP–estimates of the coefficients are found at the maximum value of the PPD. The PPD maximum value is found by maximising the exponents in (15) and (18), which is equivalent to the following minimisation problem:

$$\min_{\kappa \in \mathbf{R}^{\mathbf{N}}} \left(F(\kappa)\right) = \min_{\kappa \in \mathbf{R}^{\mathbf{N}}} \left(\sum_{j=0}^{J-1} \sum_{k=0}^{K-1} \frac{\left(d_{jk} - \widehat{d}_j(\kappa)\right)^2}{\sigma_{d_j}^2} + \sum_{n=0}^{N-1} \frac{\kappa_n^2}{\lambda_n} \right) \quad (21)$$

$F(\kappa)$ is the costfunction of the inversion problem, and the coefficient vector that minimises $F(\kappa)$ yields the optimal inverted slowness profile. According to Dosso *et al*. [16] the standard deviations, σ_{d_j}, may be estimated from the following expression:

$$\sigma_{d_j}^2 = \frac{1}{K} \sum_{k=0}^{K-1} \left(d_{jk} - \tilde{d}_j(\kappa)\right)^2 \quad (22)$$

where $\tilde{d}_j(\kappa)$ is estimated by solving the following minimisation problem:

$$\min_{\kappa \in \mathbf{R}^{\mathbf{N}}} \left(F(\kappa)\right) = \min_{\kappa \in \mathbf{R}^{\mathbf{N}}} \left(\sum_{j=0}^{J-1} \sum_{k=0}^{K-1} \left(d_{jk} - \tilde{d}_j(\kappa)\right)^2 + \sum_{n=0}^{N-1} \frac{\kappa_n^2}{\lambda_n} \right) \quad (23)$$

2.3 Example costfunction

A costfunction that applies for two types of slowness measurements is determined. The first type of measurements are slowness values, s_{jk}, derived from direct sound speed measurements at given measurement depths. j corresponds to measurement depth, and k to measurement number. The second type of measurement is depth–averaged slowness, m_{sk}, which may be measured by an echo sounder. Depth–averaged slowness is given by:

$$m_{sk} = \frac{T_k}{2(D - z_s)} \quad (24)$$

where z_s is the depth of the echo sounder. T_k is the kth measurement of the time it takes a transmitted acoustic pulse to reach the bottom and back again. D is the bottom depth. The depth–averaged slowness may be estimated from a generated slowness profile:

$$\widehat{m}_s(\kappa) = \frac{1}{N - n_s} \sum_{j=n_s}^{N-1} \widehat{s}_j(\kappa) \quad (25)$$

where n_s is the element number corresponding to z_s. The following costfunction then applies:

$$F(\kappa) = \sum_{j=0}^{N-1} \sum_{k=0}^{K-1} \frac{a_j}{\sigma_{s_j}^2} \left(s_{jk} - \widehat{s}_j(\kappa)\right)^2 + \frac{1}{\sigma_{m_s}^2} \sum_{k=0}^{K-1} \left(m_{sk} - \widehat{m}_s(\kappa)\right)^2 + \sum_{n=0}^{N-1} \frac{\kappa_n^2}{\lambda_n} \quad (26)$$

The standard deviations, σ_{s_j} and σ_{m_s}, are estimated using (22). The vector $\mathbf{a}$ with elements a_j, has the same length as $\mathbf{u_k}$, and is defined as 1 in elements corresponding to the measurement depths and 0 otherwise. Inserting (4) yields:

$$F(\kappa) = \sum_{j=0}^{N-1} \sum_{k=0}^{K-1} \frac{a_j}{\sigma_{x_j}^2} \left(x_{jk} - \widehat{x}_j(\kappa)\right)^2 + \frac{1}{\sigma_{m_x}^2} \sum_{k=0}^{K-1} \left(m_{xk} - \widehat{m}_x(\kappa)\right)^2 + \sum_{n=0}^{N-1} \frac{\kappa_n^2}{\lambda_n} \quad (27)$$

where x_{jk} and m_{xk} are scaled versions of the measured slownesses and depth–averaged slownesses, respectively. The costfunction may be split in three:

$$F(\kappa) = F_x(\kappa) + F_m(\kappa) + F_\kappa(\kappa) \quad (28)$$

where,

$$F_x(\kappa) = \sum_{j=0}^{N-1} \sum_{k=0}^{K-1} \frac{a_j}{\sigma_{x_j}^2} \left(x_{jk} - \widehat{x}_j(\kappa)\right)^2 \quad (29)$$

$$F_m(\kappa) = \frac{1}{\sigma_{m_x}^2} \sum_{k=0}^{K-1} \left(m_{xk} - \widehat{m}_x(\kappa)\right)^2 \quad (30)$$

$$F_\kappa(\kappa) = \sum_{n=0}^{N-1} \frac{\kappa_n^2}{\lambda_n} \quad (31)$$

Inserting (11) and (25):

$$F_x(\boldsymbol{\kappa}) = \sum_{j=0}^{N-1}\sum_{k=0}^{K-1}\frac{a_j}{\sigma^2_{x_j}}\left(x_{jk}-\sum_{n=0}^{N-1}U_{jn}\kappa_n\right)^2 \quad (32)$$

$$F_m(\boldsymbol{\kappa}) = \frac{1}{\sigma^2_{m_x}}\sum_{k=0}^{K-1}\left(m_{xk}-\sum_{j=n_s}^{N-1}\sum_{n=0}^{N-1}\frac{U_{jn}\kappa_n}{N-n_s}\right)^2 \quad (33)$$

Equations (31–33) are all differentiable with respect to κ_n:

$$\frac{\partial F_x(\boldsymbol{\kappa})}{\partial \kappa_n} = -2\sum_{j=0}^{N-1}\sum_{k=0}^{K-1}\frac{a_j U_{jn}}{\sigma^2_{x_{jk}}}\left(x_j-\sum_{n=0}^{N-1}U_{jn}\kappa_n\right)$$

$$\frac{\partial F_m(\boldsymbol{\kappa})}{\partial \kappa_n} = -\frac{2}{N-n_s}\left(\sum_{j=n_s}^{N-1}\frac{U_{jn}}{\sigma^2_{m_x}}\right)\sum_{k=0}^{K-1}\left(m_{xk}-\sum_{j=n_s}^{N-1}\sum_{n=0}^{N-1}\frac{U_{jn}\kappa_n}{N-n_s}\right)$$

$$\frac{\partial F_\kappa(\boldsymbol{\kappa})}{\partial \kappa_n} = 2\sum_{n=0}^{N-1}\frac{\kappa_n}{\lambda_n}$$

The costfunction differentiated with respect to κ_n then becomes:

$$\frac{\partial F(\boldsymbol{\kappa})}{\partial \kappa_n} = \frac{\partial F_x(\boldsymbol{\kappa})}{\partial \kappa_n}+\frac{\partial F_m(\boldsymbol{\kappa})}{\partial \kappa_n}+\frac{\partial F_\kappa(\boldsymbol{\kappa})}{\partial \kappa_n} \quad (34)$$

Since the costfunction and its derivatives are analytically known, the minimisation problem in (26) may be solved using a conjugate gradient method [15]. The computational cost may be strongly reduced by first truncating the coefficient vector with insignificant loss of accuracy, as discussed in section 2.1.

2.4 Comparing modelled sonar performance

In anti–submarine warfare operations sonar performance modelling is mainly used for determining whether the submarine is detected or not. Let the detection matrix, **D**, be given by:

$$\mathbf{D}(\mathbf{m}) = \mathrm{H}\big(\mathbf{SE}(\mathbf{m})\big) \quad (35)$$

The modelled signal excess [17], **SE**, is a matrix containing logarithmic signal excess values for all model depth– and range–cells. The depths and ranges are typically bounded by the sonar range, surface, and bottom depth. **m** is the model input, such as environment and sonar parameters. $H(x)$ is the Heaviside–function, which is defined as 1 for $x \geq 0$ and 0 otherwise. The detection matrix shows at what depths and ranges the sonar is expected to detect a submarine.

Let the model inputs $\mathbf{m_i}$ and $\mathbf{m_j}$ contain different SSPs, but be otherwise identical. Let the SSPs be given by $\mathbf{c_i}$ and $\mathbf{c_j}$. Let the compare function, $G(\mathbf{c_i},\mathbf{c_j})$, be defined as:

$$G(\mathbf{c_i},\mathbf{c_j}) = \frac{1}{N_r N_z}\sum_{m=0}^{N_r-1}\sum_{n=0}^{N_z-1}\delta\big(D_{mn}(\mathbf{m_i})-D_{mn}(\mathbf{m_j})\big) \quad (36)$$

N_r and N_z are the number of model range and depth cells, respectively. $\delta(l)$ is the Kronecker–delta function and defined as 1 when $l = 0$ and 0 otherwise. D_{mn} are the elements of

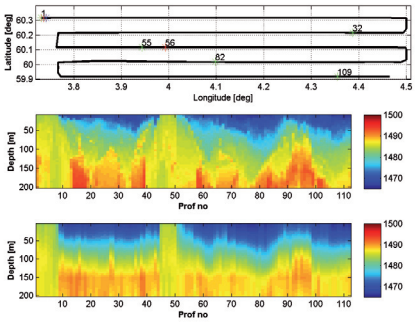

Figure 1: Path of the vessel (upper plot). Measured SSPs (centre plot). Inverted SSPs (bottom plot). The numbers (time indexes) and stars along the path of the vessel indicate the positions where the sound speed is measured in the first three scenarios described in section 5.2.

D. The compare function is used to evaluate how well the modelled sonar performance matches for two different input SSPs. A value of 1 indicates that the detection functions are identical, while 0 indicates a complete misfit.

3 Environment

In January 2010 the Norwegian Defence Research Establishment (FFI) conducted a sea trial in the Norwegian trench. FFI's research vessel, HU Sverdrup II, measured pressure, conductivity, and temperature as a function of depth down to approximately 200 m depth using an ODIM MVP200, a moving vessel profiler (MVP) [12]. SSPs are estimated from the measurements using the UNESCO formula [18]. Estimated SSPs (centre plot) and the path of the vessel (upper plot) are shown in Fig. 1.

An oceanographic model is available for the area the sea trial was conducted in. The model covers a 16 500 square kilometer area at the Western coast of Norway. The ocean model Westcoast-200m is a version of Princeton Ocean Model (POM) called MI-POM [13]. Fig. 2 shows SSPs extracted from the model for the area and time the sea trial was conducted in.

4 Simulated example

Consider a simulated sea trial where a sonar vessel follows the path shown in the upper plot in Fig. 1. Let the vessel's position be given by $\mathbf{x_l}$ at time t_l. The SSPs shown in the centre plot in Fig. 1 simulate the true SSPs, $\tilde{c}_j^{(l)}$, at position $\mathbf{x_l}$ at time t_l. The true SSPs are assumed constant and range–independent at times close to t_l and positions close to $\mathbf{x_l}$. j is the depth numerator. The depth is divided into 5 m intervals from 0 m to 200 m.

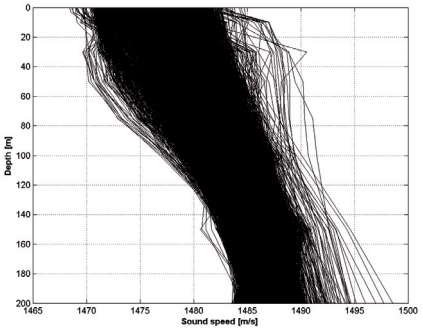

Figure 2: Modelled SSPs from the MI-POM ocean model [13].

The simulated vessel is equipped with an echo sounder, a towed transmitter, and a towed receiver array. The echo sounder and the towed array are both equipped with sensors measuring the sound speed directly with standard deviation, σ_c, of 0.2 $\frac{m}{s}$, e. g. an AQSV–1500 [22]. The echo sounder is mounted on the hull of the vessel at 5 m depth, corresponding to $j = 1$. The towed receiver array and transmitter are kept at 100 m depth, corresponding to $j = 20$. For each t_l, 30 direct sound speed measurements and echo sounder pings are simulated. The sound speed measurements are simulated by adding noise to the simulated true sound speed at the corresponding position and measurement depth:

$$c_{1k}^{(l)} = \tilde{c}_1^{(l)} + g \tag{37}$$

$$c_{20k}^{(l)} = \tilde{c}_{20}^{(l)} + g \tag{38}$$

k is the measurement number. The noise is modelled as zero–mean, Gaussian distributed noise with standard deviation given by σ_c

Let the expected bottom depth be 200 m with a standard deviation of 0.5 m. Measured depth–averaged slowness is simulated by computing mean slowness from simulated true SSP at that position and adding a zero–mean, Gaussian distributed noise, h, with standard deviation given by σ_m:

$$m_{sk}^{(l)} = \sum_{j=n_s}^{N-1} \frac{1}{\tilde{c}_j^{(l)}} + h \tag{39}$$

n_s is the depth–sample corresponding to the echo sounder depth. $N-1$ is the depth–sample number corresponding to bottom depth. The standard deviation, σ_m, is $2 \cdot 10^{-6}$ $\frac{s}{m}$, which corresponds to 0.5 m standard deviation in the bottom model.

EOFs are derived from the SSPs in the oceanographic model, shown in Fig. 2. The four first coefficients are used in the inversion, resulting in a proportion of variances of 0.98. A single inverted SSP, $\hat{\mathbf{c}}^{(\mathbf{l})}$, is determined for each t_l by solving (21). The MATLAB function MINIMIZE.M created by Carl Edward Rasmussen [19, 20] is used. It utilizes conjugate gradients and approximate linesearches. All inverted SSPs are shown in the lower plot in Fig. 1. The sound speed is generally underestimated in the lower 100 m, while the upper half of the SSPs are visually quite convincing. This is as expected since the two direct sound speed measurements made are in the upper half of the water–column; 5 m and 100 m depths.

5 Applications

Two applications using inverted SSPs are discussed on basis of the simulated data in the previous section: Quality assessment of measured SSPs and sonar performance modelling using inverted SSPs.

5.1 Quality assessment of measured sound speed profiles

This section shows how inverted SSPs may be used to assess the quality of measured SSPs. Let the vessel in the simulated example in section 4 make a single SSP measurement, given by $\mathbf{c}^{(\mathbf{m})}$, at time t_m during the sea trial. The SSP measurement is simulated as follows:

$$\mathbf{c}^{(\mathbf{m})} = \tilde{\mathbf{c}}^{(\mathbf{m})} \tag{40}$$

Let all true SSPs have an equal probability of being the one measured. At time t_l the quality, Q_{lm}, of the measured SSP is given by:

$$Q_{lm} = G(\tilde{\mathbf{c}}^{(\mathbf{l})}, \mathbf{c}^{(\mathbf{m})}) \tag{41}$$

where G is defined in (36). In a real sea trial this is an unknown quantity since the true SSP is unknown. However, Q_{lm} may be modelled by using the inverted SSP at time t_l instead of the true SSP:

$$\hat{Q}_{lm} = G(\hat{\mathbf{c}}^{(\mathbf{l})}, \mathbf{c}^{(\mathbf{m})}) \tag{42}$$

Fig. 3 shows $\hat{Q}_{lm}$ plotted versus Q_{lm} for all combinations of l and m. Notice that the main bulk of instances result in values close to 1.

The quality assessment of the measured SSP may be formulated as a binary hypothesis test. For each time t_l there are two outcomes of the test:

1. The measured SSP is high–quality
2. The measured SSP is low–quality

This is a binary decision problem [21], where the goal is to detect and report low–quality SSPs. Quality is determined by applying a threshold, T_0, on Q_{lm}:

$$Q_{lm} \geq T_0 \Rightarrow \text{high–quality SSP}$$
$$Q_{lm} < T_0 \Rightarrow \text{low–quality SSP}$$

T_0 is here chosen to be 50%, but should be sufficiently high to meet any requirements on the quality of the sonar performance modelling. Since Q_{lm} is unknown, this metric may not be used in the assessment. Instead the known quantity $\hat{Q}_{lm}$ may be used:

$$\begin{aligned} \hat{Q}_{lm} \geq T &\quad \Rightarrow \quad \text{high–quality SSP predicted} \\ \hat{Q}_{lm} < T &\quad \Rightarrow \quad \text{low–quality SSP predicted} \end{aligned}$$

The threshold T is here chosen to be 0.5 as indicated in Fig. 3. The test may result in four different outcomes:

1. The measured SSP is high–quality
   a) high–quality predicted
   b) low–quality predicted
2. The measured SSP is low–quality
   a) high–quality predicted
   b) low–quality predicted

Alternatives 1a and 2b are correct decisions, and correspond to the upper right and lower left quadrants in Fig. 3, respectively. 1b is a false alarm and 2a is a failed detection, corresponding to the lower right and upper left quadrants of Fig. 3, respectively.

Let probability of detection, P_d, be the probability that a low–quality profile is chosen to be low–quality by the test, and probability of false alarm, P_{fa} be the probability that a high–quality profile is chosen to be low–quality. P_d and P_{fa} may be estimated from the simulated data set as follows:

$$P_d(T) = \frac{\sum_l \sum_m \mathrm{H}(T - \hat{Q}_{lm})\mathrm{H}(T_0 - Q_{lm})}{\sum_l \sum_m \mathrm{H}(T_0 - Q_{lm})}$$

$$P_{fa}(T) = \frac{\sum_l \sum_m \mathrm{H}(T - \hat{Q}_{lm})\mathrm{H}(Q_{lm} - T_0)}{\sum_l \sum_m \mathrm{H}(Q_{lm} - T_0)}$$

where $\mathrm{H}(x)$ is the Heaviside function. By varying T from 0 to 1 in 0.1 steps receiver operating characteristic (ROC) curves [21] are estimated and shown in Fig. 4. The proposed detector algorithm performs significantly better than random decision. For $T = 0.5$ and $T_0 = 0.5$ there is a 61% probability of detecting a low–quality SSP and 6% probability of false alarm. The false alarm rate may be suppressed further by for instance requiring two consecutive detections before reporting a SSP as low–quality, all though this would decrease the probability of detecting a low–quality SSP as well.

5.2 Sonar performance modelling

In this section the quality of modelled sonar performance using inverted SSPs is compared to the quality of modelled sonar performance using SSP measurements of varying frequency.

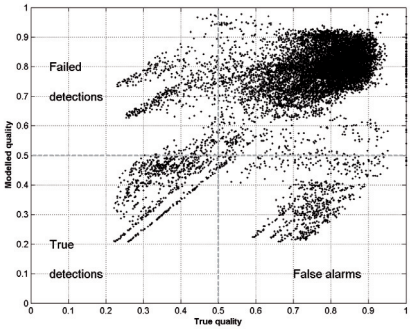

Figure 3: The modelled quality, $\widehat{Q}_{lm}$, of the measured SSP vs the true quality, $\hat{Q}_{lm}$ for all l and m. Low–quality SSPs are to the left of the vertical dashed line, and high–quality to the right. Detections are below the horisontal dashed line. The lower left quadrant contains detected low–quality SSPs. The upper left quadrant contains undetected low–quality SSPS. The upper right quadrant contains undetected high–quality SSPs. The lower right quadrant contains detected high–quality SSPs, so called false alarms.

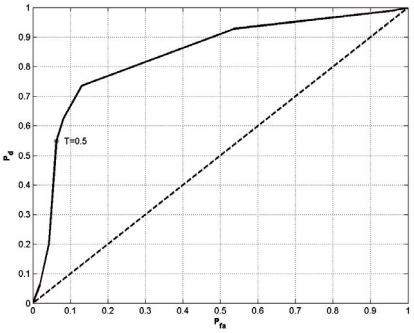

Figure 4: The solid line is the ROC–curve for the proposed detector when $T_0 = 0.5$ and T ranges from 0 to 1. The dashed line indicates the ROC–curve for a uniform, random choice of quality.

Four simulated scenarios based in the simulated sea trial described in section 4 are considered. In the first scenario the SSP is measured at the start of the run. In the second scenario two SSPs are measured, one at the start and one in the middle of the run. In the third scenario one measurement is made along every East-West going lag. Assuming a vessel speed of 4 $\frac{m}{s}$ this corresponds to one measurement every four hours. The positions of the measurements are indicated in Fig. 1. In order to simulate the limited accuracy of the measurements, zero–mean, Gaussian distributed ran-

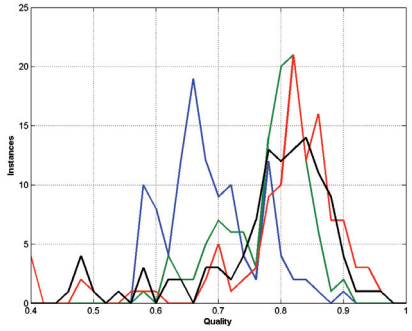

Figure 5: Distributions of estimated SSP qualities for the first (blue), second (red), third (green), and fourth (black) scenario.

dom noise with standard deviation of 0.25 $\frac{m}{s}$ is added to the measured sound speed at each depth. This error corresponds to the expected error on a Sippican XSV–01 [23], which is an expendable sound velocity profiler. The resulting SSP is then smoothed in a 5 m rectangular window. In the final scenario the inversion algorithm described in section 2 is used to estimate the SSP.

The quality of each SSP in each scenario is found by comparing the profiles to the true SSPs using the method described in section 2.4:

$$\begin{aligned} Q_1^{(l)} &= G\left(\mathbf{c}^{(\mathbf{l})}, \mathbf{c_1}\right) \\ Q_2^{(l)} &= G\left(\mathbf{c}^{(\mathbf{l})}, \mathbf{c}_\mathbf{2}^{(\mathbf{l})}\right) \\ Q_3^{(l)} &= G\left(\mathbf{c}^{(\mathbf{l})}, \mathbf{c}_\mathbf{3}^{(\mathbf{l})}\right) \\ Q_4^{(l)} &= G\left(\mathbf{c}^{(\mathbf{l})}, \hat{\mathbf{c}}^{(\mathbf{l})}\right) \end{aligned}$$

$\mathbf{c_1}$ equals the measurement in the first scenario, as described above. $\mathbf{c}_\mathbf{2}^{(\mathbf{l})}$ and $\mathbf{c}_\mathbf{3}^{(\mathbf{l})}$ equal the most recent measurements in the second and third scenarios, respectively. The results of the comparison are presented in Fig. 5. The averaged quality over all timesteps are 0.73 in the first scenario, 0.77 in the second, and 0.79 in the third scenario. When using the inverted SSPs, the averaged quality is 0.78. For simple sonar performance modelling, where the main goal is to determine the maximum detection range of a sonar, the inverted SSPs have a quality that is comparable to four–hourly sound speed measurements.

6 Conclusion

A new method for inverting water–column sound speed profiles is presented. The inversion is based on sound speed and echo sounder measurements made from the sonar platform. The high update–rates of these sensors ensure a local sound speed profile.

Sound speed profiles were inverted using a simulated data set. The inverted sound speed profiles resembled the true sound speed profiles. However the method must be tested on recorded data for final validation.

An algorithm for detecting poor–quality sound speed profiles was developed and tested on the simulated data set. Inverted sound speed profiles were used to assess the quality of measured sound speed profiles. By sound speed profile quality is here meant how well the modelled sonar performance using that particular sound speed profile compare to the modelled sonar performance using the true sound speed profile. The algorithm was shown to have a probability of detection of 61% and a probability of false alarm of 6% for the simulated test case.

The inverted sound speed profiles were also shown to result in modelled sonar performance comparable to four–hourly measured sound speed profiles for the simulated test case.

The inversion method gives some operational advantages during an actual anti–submarine warfare operation. The sound speed profile may be inverted for any vessel speed, unlike the traditional expendable sound velocity profiler which has an upper speed limit, e. g. $8\frac{m}{s}$ for a Sippican XSV–01 [23]. Secondly, the update rate of the inverted sound speed profile is higher than any other sound speed profiler known to the author. The measurement frequency depends on the bottom depth, due to the echo sounder, while the computation time of the method is a few seconds on a standard desktop computer.

Acknowledgment

Thanks to colleagues at FFI and the Norwegian University of Science and Technology (NTNU) for contributing their expert advise and guidance, especially my supervisor, professor Jens M. Hovem, and my colleague at FFI, Stein Nilsen. Also, thanks to the crew on H. U. Sverdrup for collecting the oceanographic and topographic data essential to this work.

References

[1] K. R. James and D. R. Dowling, *A method for approximating acoustic–field–amplitude uncertainty caused by environmental uncertainties*, Journal of the Acoustic Society of America, vol. 124, no 3, 2008.

[2] S. E. Dosso, *Environmental uncertainty in ocean acoustic source localization*, Inverse Problems, vol. 19, no 2, 2003, pp. 419–431.

[3] K. LePage, *Modeling Propagation and Reverberation Sensitivity to Oceanographic and Seabed Variability*, IEEE Journal of Oceanic Engineering, vol. 31, no 2, April 2006.

[4] S. Finette, *A stochastic representation of environmental uncertainty and its coupling to acoustic wave propaga-*

tion in ocean waveguides, Journal of the Acoustic Society of America, vol 120, no 5, 2006.

[5] K. LePage and B. E. McDonald, *Environmental Effects of Waveguide Uncertainty on Coherent Aspects of Propagation, Scattering, and Reverberation*, IEEE Journal of Oceanic Engineering, vol. 31, no 2, April 2006.

[6] M. D. Collins and W. A. Kuperman, *Focalization: Environmental focusing and source localization*, Journal of the Acoustic Society of America, vol. 90, no 3, 1991.

[7] C. W. Therrien, *Discrete Random Signals and Statistical Signal Processing*, Prentice Hall, 1992.

[8] L. T. Fialkowski, M. D. Collins, and J. S. Perkins, *Source localization in noisy and uncertain environments*, Journal of the Acoustic Society of America, vol. 101, no 6, 1997.

[9] D. Tollefsen and S. E. Dosso, *Three–dimensional source tracking in an uncertain environment*, Journal of the Acoustic Society of America, vol. 125, no 5, 2009.

[10] I.-T. Lu, *Simultaneous characterization of source, array and environment using a ray travel-time inversion approach*, Journal of Computational Acoustics, vol. 5, no 2, 1997.

[11] E. Svensson, *Inverting acoustic communication signals for the sound speed profile*, Journal of the Acoustic Society of America, vol. 120, no 3, pp 1347 - 1355, 2006.

[12] http://www.brooke-ocean.com/mvp200.html

[13] H. A. Engedahl, *Implementation of the princeton ocean model (pom/ecom3d) at the norwegian meteorological institute*, Norwegian Meteorological Institute, Oslo, Norway, Research Report 5, 1995.

[14] K. T. Hjelmervik, E. M. Dombestein, S. Mjølsnes, T. S. Såstad and J. Wegge, *The acoustic raytrace model Lybin – Description and application*, Proceedings from Underwater Defence Technology Conference and Exhibition, Glasgow 2008.

[15] W. H. Press, B. P. Flannery, S. A. Teukolsky and W. T. Vetterling, *NUMERICAL RECIPES, the Art of Scientific Computing (FORTRAN version)*, Cambridge university press, 1989.

[16] S. E. Dosso, P. L. Nielsen, and C. H. Harrison, *Bayesian inversion of reverberation and propagation data for geoacoustic and scattering parameters*, Journal of the Acoustic Society of America, vol. 125, no 5, 2009.

[17] R. J. Urick, *principles of underwater sound*, 3rd ed., Peninsula Publishing, 1983.

[18] P. Fofonoff and R. C. Jr Millard, *Algorithms for computation of fundamental properties of seawater*, Algorithms for computation of fundamental properties of seawater, 1983. Unesco Tech. Pap. in Mar. Sci., No 44, 53 pp.

[19] C. E. Rasmussen, *minimize.m*, http://www.kyb.tuebingen.mpg.de/bs/people/carl/code/minimize/

[20] C. E. Rasmussen, *Evaluation of Gaussian Processes and other Methods for Non-Linear Regression*, PhD thesis, Max Planck Institute for Biological Cybernetics, 1996.

[21] H. L. Van Trees, *Optimum array processing (Detection, Estimation, and Modulation Theory, Part IV)*, Wiley, 2002.

[22] http://www.aquamatic.dk/AQSV1.htm

[23] http://www.sippican.com

Paper 6

Finding acoustically stable areas through EOF classification

Finding acoustically stable areas through EOF classification

Jan Kristian Jensen, Karl Thomas Hjelmervik, and Petter Østenstad

Manuscript received ???; revised ???. J. K. Jensen, K. T. Hjelmervik (karl-thomas.hjelmervik@ffi.no), and P. Østenstad are with the Norwegian Defence Research Establishment. J. K. Jensen is also with the University of Bergen. K. T. Hjelmervik is also with the Norwegian University of Science and Technology,

Abstract

Validity of sonar performance models is generally limited by environmental uncertainty, and particularly uncertainty in the sound speed profile (SSP). Rapid environmental assessment (REA) missions, e. g. using gliders, and advanced ocean models may be used to reduce this uncertainty prior to sonar operation in hostile waters.

The presented work shows how data from ocean models may be used for planning of REA–missions. The area of operation is divided into oceanographically stable subareas using empirical orthogonal functions and different methods of clustering analyses on SSPs from the ocean model. The acoustic stability of each subarea is assessed using sonar performance modelling. Acoustically unstable areas are divided into smaller subareas. Acoustically stable groups are represented by a single SSP.

A map of acoustically stable areas in the area of operation is the main output. Large, geographically contiguous groups indicate acoustically stable areas where frequent SSP measurements are unnecessary, e. g. low concentration of gliders. Small and non–contiguous groups indicate the opposite. Other applications include determination of suitable locations for sonar tests that require stable sonar conditions, and efficient optimization of sonar operation in acoustically stable areas.

I. Introduction

Validity of sonar performance models is generally limited by environmental uncertainty. James and Dowling [1] give an extensive overview of research on how environmental uncertainty influences acoustic field predictions. Modelled acoustic fields are sensitive to uncertainty in sound speed profile (SSP) [2]–[7]. During sonar operations, sonar performance models are used for prediction of sonar ranges and for determining optimal placement of sonar assets during multi–platform sonar operations. A consequence of uncertainty in predicted sonar range is that more sonar assets are required during a sonar operation to obtain the required probability of success. This uncertainty can be reduced by increasing the knowledge of the environment, for instance by using ocean models or conducting rapid environmental assessment (REA) missions in the area of operation, e. g. glider operations.

Davis [8] introduced empirical orthogonal functions (EOF) to characterise oceanographic data. EOF has since been extensively used to describe and characterise water masses and spatial and temporal variations of the ocean

$e.\ g.$ [9]. EOFs are also frequently used in acoustic inversion and tomography $e.\ g.$ [10], [11]. The main advantage of characterising sound speed profiles by EOFs is that information from the entire SSP may be contained in a few scalar coefficients. For example, two coefficients are sufficient to characterise the Munk–profile [11].

Clustering analysis is a multivariate statistical technique for grouping data points with similar characteristics into clusters. In oceanography, it has most commonly been used to label and identify water masses according to measurements of depth, temperature and salinity [12]–[14]. In this study we take the leading coefficients from the EOF analysis of SSP as input to our cluster analysis. This is a method frequently used on echo sounder data for sea bottom classification $e.\ g.$ [15]. The EOF analysis reduces the dimensionality of the considered data set before the cluster analysis classifies the data set into several different categories. This has the desired effect of clustering SSPs with similar acoustic properties. A sonar performance model is then used to assess the acoustic sensitivity to oceanographic variations within those groups. This proves to be a useful tool for quick classification of acoustically stable versus unstable groups of SSPs. The main output of the method is a map of acoustically stable areas, where an acoustically stable area contains SSPs from the same group. Such maps are useful planning aids during REA missions and sonar operations since they indicate the presence of stable and unstable regions. Stable regions are typically dominated by large, geographically contiguous stable areas. Frequent SSP measurements are unnecessary in such regions, e. g. low concentration of gliders. Unstable regions typically consists of many small and non–contiguous stable areas. In such areas frequent SSP measurements are required. The information is also useful for determining a suitable area for conducting sonar tests that require stable acoustic conditions. Finally, a single SSP is assumed sufficient to model a representative sonar performance for an acoustically stable area. Optimal sonar parameters for sonar operation in each area may then be obtained with low computation cost, since the sonar performance is modelled for a single SSP only. Examples of how optimal sonar performance is determined using acoustic modelling can be found in literature, $e.\ g.$ [16].

The method is tested on SSPs from MI-POM [17], a high resolution numerical ocean model covering 16.000 square kilometers adjacent to the Norwegian West coast. Using this high resolution model as a basis for our calculations gives us a gridded data set where oceanographic dynamical features are realistically resolved. From an acoustic point of view, the main interest lies in the horizontal and vertical gradients of sound speed that is associated with the interface between low temperature, low salinity coastal water masses and comparatively warmer and more saline water masses of Atlantic origin. EOFs are determined for the modelled SSPs, and the geographical distribution of the first EOF coefficient is shown to correlate well with the distribution of upper layer salinity. The full method is applied on the data set and a map of acoustically stable areas is presented.

II. Method

The presented method divides a large set of SSPs into several smaller groups of profiles that are acoustically stable. A group is considered acoustically stable if variations in modelled signal excess [18], using the sound speed profiles of that group, are lower than a chosen threshold (section II-C). Groups not acoustically stable are split into smaller groups using a subdivision algorithm (section II-B). The subdivision is based on properties of the

coefficients in an EOF representation of the SSPs (section II-A). The end product is a map showing the geographic extent of the acoustically stable groups.

The overall method is as follows:

1) A group/subgroup of SSPs are input
    a) The acoustic fitness of the inputted group/subgroup is determined
        i) Groups/Subgroups with acoustic fitness exceeding the threshold T are accepted and not further processed.
        ii) Group/Subgroups with acoustic fitness lower than the threshold T are passed on to step 2).
2) A subdivision algorithm splits the group/subgroup into two or more subgroups
    a) Subgroups with less than K SSPs are removed
    b) Subgroups with more than K SSPs are returned to step 1)

For step 2) two different subdivision algorithms are used: Clustering of coefficients (CC), described in section II-B1, and ordering of coefficient magnitudes (OCM), described in section II-B2.

A. Empirical orthogonal functions

Consider a set of M SSPs each containing N depth samples. Let $c_m(z_n)$ be the sound speed at depth z_n in the m'th profile. The mean sound speed, $\overline{c}$, as a function of depth, is given by:

$$\overline{c}(z_n) \quad = \quad \frac{1}{M}\sum_{m=0}^{M-1} c_m(z_n) \tag{1}$$

Let $x_m[n]$ be defined as:

$$x_m[n] = c_m(z_n) - \overline{c}(z_n) \tag{2}$$

$x_m[n]$ may be expanded in any set of N orthonormal basis functions $u_k[n]$ with coefficients κ_k, [19] chapter 4.6.1:

$$x_m[n] \quad = \quad \sum_{k=1}^{N-1} \kappa_k^{(m)} u_k[n] \tag{3}$$

For real values of $x_m[n]$ the coefficients for expanding $x_m[n]$ are given by:

$$\kappa_k^{(m)} \quad = \quad \sum_{n=0}^{N-1} u_k[n] x_m[n] \tag{4}$$

The basis functions are determined by solving the eigenvalue problem given by:

$$\mathbf{R_x u_k} \quad = \quad \lambda_k \mathbf{u_k} \tag{5}$$

where $\mathbf{u_k}$ are eigenvectors and contain the function values of the discrete orthonormal basis functions $u_k[n]$. In literature $u_k[n]$ are often referred to as empirical orthogonal functions (EOF), λ_k are the corresponding eigenvalues and equal the variance of the corresponding coefficients κ_k [19]. $\mathbf{R_x}$ is the covariance matrix of the data matrix:

$$\mathbf{R_x} \quad = \quad \frac{1}{M}\mathbf{X}^T\mathbf{X} \tag{6}$$

where,

$$\mathbf{X} = \begin{bmatrix} \mathbf{x_1}^T \\ \mathbf{x_2}^T \\ \vdots \\ \mathbf{x_M}^T \end{bmatrix} \tag{7}$$

New SSPs, $c_i[z_n]$ may be generated by combining (2) and (3):

$$c_i[z_n] = \overline{c}[z_n] + \sum_{k=1}^{N-1} \kappa_k u_k[n] \tag{8}$$

The coefficients, κ_k, should be modelled as zero-mean random processes with variance λ_k.

Higher orders of k often represent noise in the measurements. The series in (8) may therefore be truncated without risking loss of information on the SSP. A frequently used approach to select the cut–off is to determine where the proportion of variances exceeds a set threshold. The proportion of variances is defined as:

$$\Lambda_l = \frac{\sum_{k=0}^{l} \lambda_k}{\sum_{k=0}^{N-1} \lambda_k} \tag{9}$$

l is the cut–off. The selected threshold depends on the applications, but a commonly used threshold is 95%.

B. Subdivision algorithms

1) Clustering of EOF coefficients (CC): Cluster analysis is assigning data points with similar characteristics to the same group of data, called cluster [20]. A common implementation, called hierarchical clustering, is to start with each data point contained within its own unique cluster, one point per cluster. Some function gives an objective measure of the similarity – or distance – between cluster pairs, and the most similar (closest) cluster pair is joined. The process is repeated until some metric of success is achieved (e.g. [21]) or when the process is subjectively judged to give the most meaningful representation of the data distribution. Among the vast multitude of possible functions, the Euclidean distance function is a straight forward choice with intuitive parallels to conventional geometry. Also, some choices must be made about defining distances between clusters with more than one member, such as closest neighbor, average midpoint, weighted average and so on.

In oceanography, cluster analysis has proven successful for identifying water masses according to the data points of temperature, salinity and depth [13], [14]. In this study we perform cluster analysis on the leading EOF coefficients for SSPs calculated in section II-A. SSP's with similar vertical structure will have similar coefficients and be close together in coefficient space — and will be assigned to the same cluster. This method is strikingly similar to the bottom type classification of acoustic survey data by Milligan and others [22], but we have not been able to find literature where this is done for SSP's or other oceanographic parameters.

The cluster analysis is merely a tool for the overall algorithm presented in II. Conceptually, we describe the overall method as starting with one large cluster which then is tested by the acoustic fitness function II-C. If approved, all is good; if it fails, then that cluster is split in two and the test is repeated for each of the new clusters.

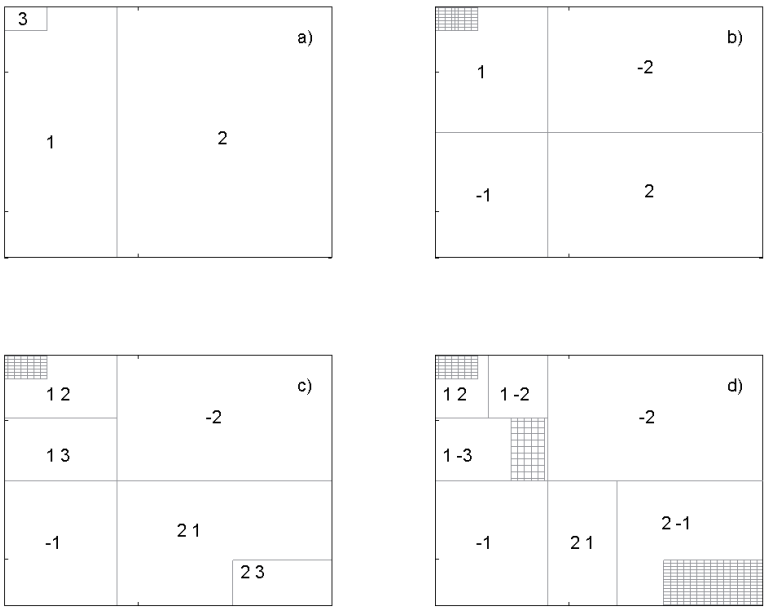

Fig. 1. a) The area is divided into subgroups based on the absoulute value of the strongest coefficients to the SSPs, in this case the first and second coefficient are the strongest, noted 1 and 2. b) Groups found in a) is split based on the sign of the strongest coefficient. Subgroups containing fewer than K SSPs are removed and the acoustic stability of each remaining group is determined. c) Step a) is repeated for the unstable areas in b) using the second strongest coefficient. d) Step b) is repeated for the new areas found in c).

2) Ordering of EOF coefficient magnitude (OCM): Ordering of EOF coefficient magnitude is a method introduced here for dividing a large group of SSPs into several smaller subgroups with similar statistical properties. The main advantage of this method compared to previously described clustering method is its ability to process very large data sets. The full method, as described in section II, using the OCM subdivision algorithm, is illustrated with an example in Fig. 1.

The coefficient with the highest absolute value is found for each SSP and is henceforth called the strongest coefficient. The SSPs are divided into subgroups represented by their strongest coefficient. In this case, for all SSPs, the first or second coefficient is strongest and the areas containing each subgroup are represented by 1 and 2 in the plot (Fig 1 a). b) Each of the subgroups are split in two by taking the sign of the coefficient into account, which results in one subgroup with a positive strongest coefficient, and a subgroup with a negative strongest coefficient. Subgroups containing fewer than K SSPs are removed, in this case the area with coefficient number 3 (both

positive and negative) as the strongest coefficient (Fig 1 b). The acoustic stability of each subgroup is tested. Stable subgroups are kept. Unstable subgroups are divided again by repeating the steps above on the second strongest coefficient (Fig 1 c) Two of the subgroups (1 and 2) in Fig 1 b) were found unstable and divided into smaller subgroups. For the SSPs in subgroup 1, the second and third coefficients are the second strongest coefficients. For subgroup 2 the first and third coefficients are second strongest, see Fig 1 c). These areas are again divided based on the sign of the second strongest coefficient. Note that subgroups 2 3 and 1 3 are removed as they contain less than K SSPs. In Fig 1 d) the remaining areas are checked if they are acoustic stable. This process continues until all subgroups are found stable or too small.

C. Acoustic fitness function

Assume cylindrical symmetry and let the random function $SE(r, z, \mathbf{c})$ represent the true signal excess of a target located in (r, z), where the vector $\mathbf{c}$ contains the depth–dependent SSP. The SSP is assumed range–independent. Let $\mathbf{c}$ be the only random parameter influencing $SE(r, z, \mathbf{c})$.

Given N SSPs, $\mathbf{c_n}$, where $n = 1, 2, 3, ..., N$, in an area, let $\mathbf{c}$ for that area be uniformly distributed over the N SSPs, meaning all SSPs have an equal probability of being the true SSP in the given area. $SE(r, z, \mathbf{c_n})$ is the modelled signal excess in dB using the nth SSP as input. $s(r, z, \mathbf{c_n})$ is the linear signal excess:

$$SE(r, z, \mathbf{c_n}) \quad = \quad 10 \log_{10} s(r, z, \mathbf{c_n}) \tag{10}$$

The expected signal excess in the area is estimated as the mean modelled, linear signal excess:

$$m_s(r, z) \quad = \quad \frac{1}{N} \sum_{n=0}^{N-1} s(r, z, \mathbf{c_n}) \tag{11}$$

Let $P_{SE}(r, z, \mathbf{c_n}, T_{\Delta SE})$ be the probability that the mean signal excess lies within $T_{\Delta SE}$ of the true signal excess at an arbitrary target location given by (r, z):

$$P_{SE}(r, z, \mathbf{c}, T_{\Delta SE}) \quad = \quad Pr\left\{|10 \log_{10} m_s(r, z) - SE(r, z, \mathbf{c})| \leq T_{\Delta SE}\right\} \tag{12}$$

The true SSP, $\mathbf{c}$, is unknown, but since all SSPs have an equal probability of being the true SSP, then (12) may be estimated as follows:

$$P_{SE}(r, z, T_{\Delta SE}) \quad \approx \quad \frac{1}{N} \sum_{n=0}^{N-1} H\left(\left| 10 \log_{10} \left(\frac{m_s(r, z)}{s(r, z, \mathbf{c_n})} \right) \right| - T_{\Delta SE} \right) \tag{13}$$

where $H(x)$ is the Heaviside function and outputs 0 for arguments lower than 0, and 1 otherwise.

$\widehat{P}(T_{\Delta SE})$ is the probability that the modelled signal excess lies within $T_{\Delta SE}$ of the true signal excess at the target location. An a priori probability density distribution of the target location, $g(r, z, \phi)$, is required. If unknown, a uniform distribution is used. $P(T_{\Delta SE})$ is then given by:

$$\widehat{P}(T_{\Delta SE}) \quad = \quad \int_0^{2\pi} \int_0^H \int_0^R P_{SE}(r, z, T_{\Delta SE}) g(r, z, \phi) r \mathrm{d}r \mathrm{d}z \mathrm{d}\phi \tag{14}$$

H is the bottom depth and R is the sonar range.

The depths and ranges considered should be limited to regions with sufficient acoustic energy. This is implemented by adding the following constraint:

$$10\log_{10} m_s(r,z) \quad > \quad T_{SE} \tag{15}$$

This constraint is added to (14) yielding the acoustic fitness function (AFF):

$$P(T_{\Delta SE}) \quad = \quad \int_0^{2\pi}\int_{-\infty}^{\infty}\int_{-\infty}^{\infty} P_{SE}(r,z,T_{\Delta SE})g(r,z,\phi)H(10\log_{10} m_s(r,z) - T_{SE})r\mathrm{d}r\mathrm{d}z\mathrm{d}\phi \tag{16}$$

AFF is used to determine the acoustic stability of a group of SSPs, as described in step 1 in section II.

A potential problem for large, acoustically stable groups, is that the group may contain several disparate sets of SSPs that would be best represented as different acoustically stable groups. This may occur because the number of SSPs in the largest of these sets is large enough to satisfy the requirement on $P(T_{\Delta SE})$, masking the presence of smaller but distictly different sets of SSPs. Therefore we have added an additional requirement on acoustically stable groups: if the number of SSPs with negative argument in the Heaviside function in (13) exceeds a selected number, for instance 10% of the number of SSPs in the original data set, then the group is considered acoustically unstable.

The proposed fitness function is a robust means of assessing acoustic stability. Note that signal excess is estimated from incoherent transmission loss, acoustic phase is therefore completely ignored. The chosen fitness is useful for the application considered; sonar performance modelling. Other applications may require different fitness functions that may also include phase information, but this is not considered within the scope of this work.

III. Data sets

The SSPs used in this study are based on three dimensional forecasts of temperature and salinity for 12 UTC, March 7th, 2007 from the high resolution numerical ocean model Westcoast 200m. This ocean model is a version of Princeton Ocean Model (POM) called MI-POM [17], [23], run operationally by the Norwegian Meteorological Institute (met.no). The model domain covers an area of approximately 16.500 km^2, from 59.30 N 4 E to 61 N 5.75 E with a horizontal resolution of 200 m, see Fig. 2. The data are downsampled to a horizontal resolution of approximately 1 km, which we here refer to as the full data set. SSPs from surface to 200 m depth at nine depth levels are used and shown in Fig. 3. Most data from fjords and inlets are removed and locations where model depth is less than 200 m are excluded. The data set then totals 10033 profiles, from which 3 additional subsets are extracted: One subsampled to 2873 profiles in a semi–regular grid (blue outline in figure 2) and two smaller area subsets with resolutions identical to the full data set. Subset 1 is bounded by the coordinates 60.00–60.17 N, 4.00–4.51 E (720 profiles) and subset 2 is bounded by 60.47-60.92 N, 3.98-4.48 E (175 profiles), shown in Fig. 2.

IV. Experimental results

The two following subsections present results from an oceanographic analysis and results from the method described in section II. The oceanographic analysis compares surface salinity contours to geographic distributions of EOF coefficients. EOF coefficients for each SSP in the full data set and each subset are derived using (4). Fig.

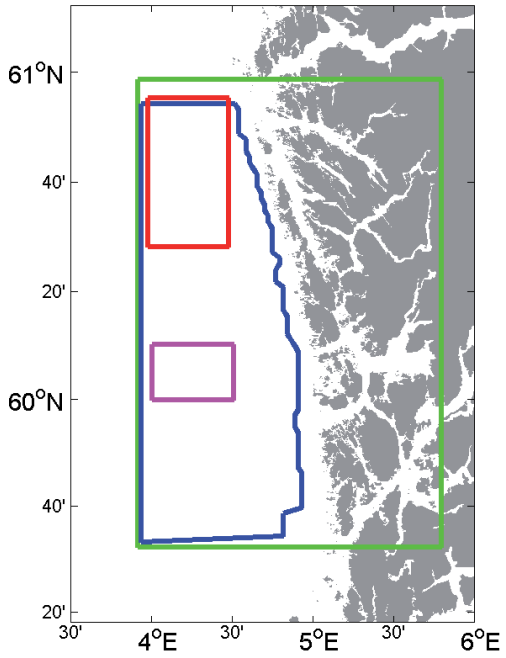

Fig. 2. Green rectangle: Full model area. Blue outline: Extent of the model data used when excluding data with model depth less than 200 m and data in fjords and inlets. Magenta rectangle: Subset 1. Red rectangle: Subset 2.

4 shows the proportion of variances. The proportion of variances exceeds 95 % when using three coefficients for the full area data sets (full and reduced resolution), and five and four coefficients, respectively, for subset 1 and 2. The subdivision algorithms, CC and OCM use five and four coefficients, respectively.

A. Investigation of the acoustic fitness function

The proposed method divides a large group of SSPs into acoustically stable sub–groups using EOF and cluster analysis on the SSPs. For this to be meaningful acoustic stability must in some way correlate with SSP variability. This correlation is demonstrated in Fig. 5, where the AFF proposed in section II-C is shown to decrease for increasing sound speed variability.

The number of SSPs needed to ensure a tolerable accuracy in the AFF is studied in Fig. 6. The estimated standard deviation of $P(T_{\Delta SE})$ drops for increasing number of SSPs used to estimate $P(T_{\Delta SE})$. Sufficiently high K in step 2, see II, should be selected in order to ensure the desired accuracy in $P(T_{\Delta SE})$.

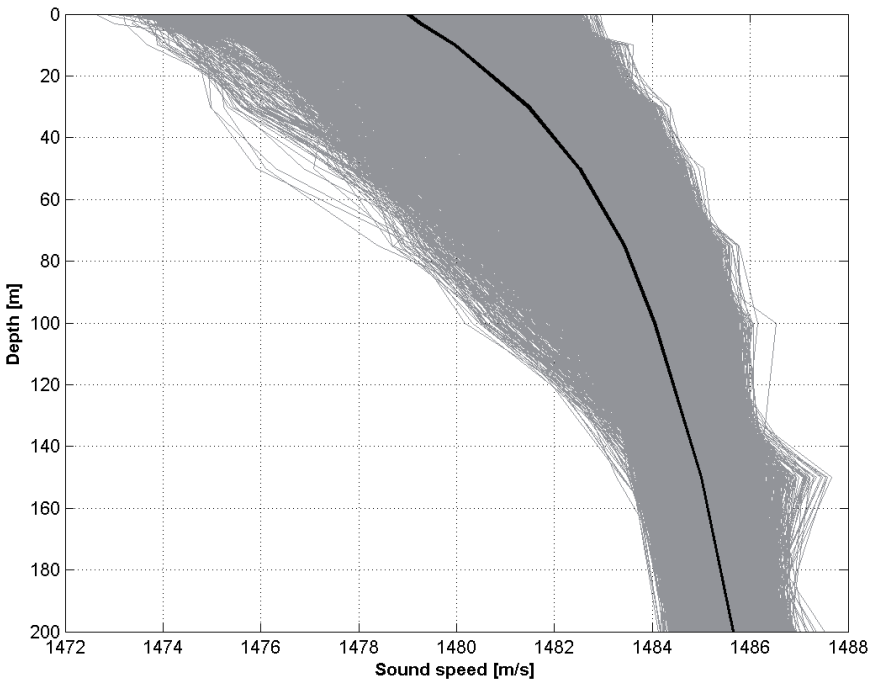

Fig. 3. Sound speed profiles from the March 2007 data set (grey) and the mean sound speed profile based on all the other sound speed profiles (black).

B. Oceanographic analysis

The study area is in the Norwegian Trench, close to the western coast of Norway. This part of the Norwegian Trench is relatively flat, with a depth around 300 meters, with a steep rise at the Norwegian Coast to the east. Further west, adjacent to the study area, is the slope leading up to the Norwegian Sea plateau, with a depth of about 100-150 meters. Circulation in the area is dominated by inflow and recirculation of saline Atlantic water (AW) which enters the North Sea from the north and the low salinity coastal waters (CW) in the Norwegian Coastal Current (NCC). The NCC originates in Skagerrak as a mixture of very low salinity water from the Baltic and water masses of Atlantic origin that has been more or less diluted through their residence in the North Sea [24]–[26]. The NCC follows the Norwegian coast, but with variable lateral extent which is mainly controlled by wind forcing and meander/eddy formation processes. The usual arsenals of frontal dynamics (frontal structures, filaments, meanders and eddies) are found at the transition between NCC and AW water masses [25], [27], [28].

In general water masses with salinity greater than 35 psu are referred to as AW and below 35 psu as CW, but

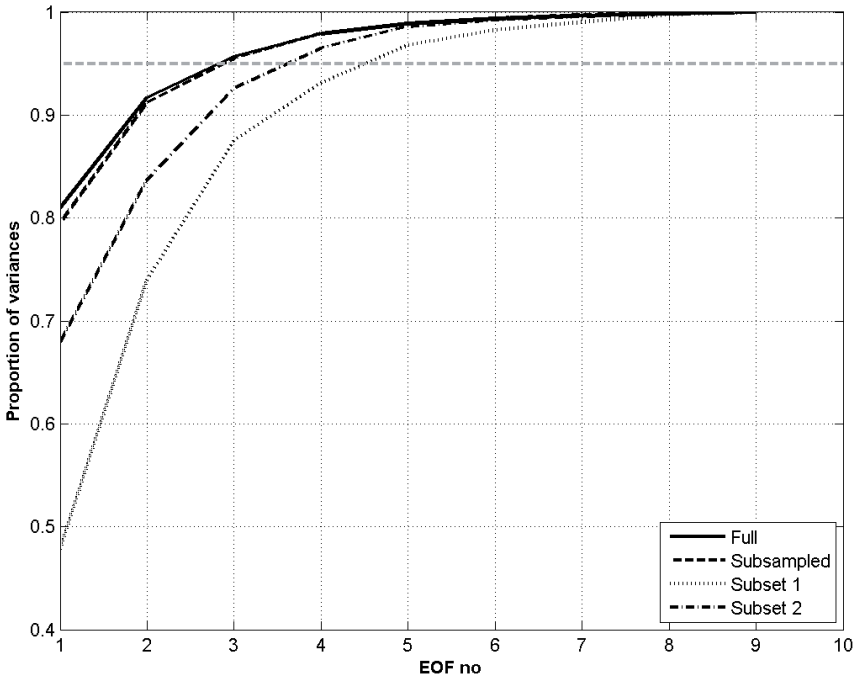

Fig. 4. The proportion of variances for the March 2007 full data set and each of the three subsets. The dashed line indicates the required threshold of 0.95.

34.5 psu is a better separation along most of the Norwegian coast [29]. In March, there is a strong correlation between water temperature and salinity, with CW being cold and fresh and AW being higher in temperature and salinity. Both our own observations as well as temperature and salinity values from the literature indicate that the typical difference in sound speed between the AW and CW water masses for March is on the order of 10 m/s. The typical distribution of the two water masses is that the CW is wedged between the Norwegian coast and the adjacent AW, the deepest part of CW being close to the coast. The upper layer salinity values is therefore a good indicator of the geographical distribution of the different water masses [29]. Fig. 7 shows surface salinity contours and the first EOF coefficient plotted geographically. Observe that most AW areas is associated with negative values of the first coefficient and most of the positive values correspond to CW. Since 80% of the variance is contained in the first coefficient, see Fig. 4, most of the oceanographic structure is expected to be seen in the first coefficient.

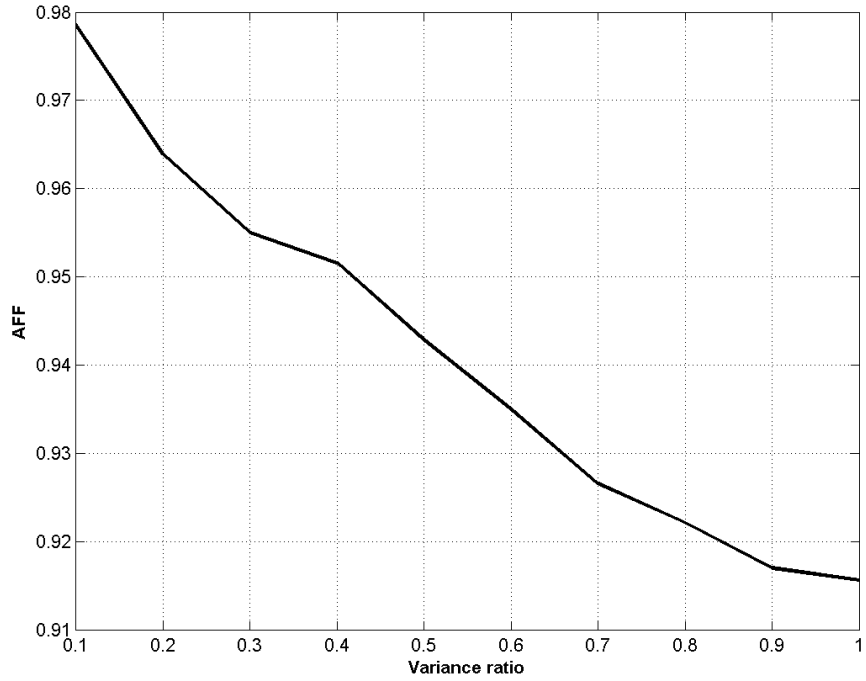

Fig. 5. The acoustic fitness function, $P(T_{\Delta SE})$, is computed for ten different groups of 1000 SSPs using a threshold $T_{\Delta SE} = 6dB$. The SSPs are generated using (8) with the EOFs and eigenvalues estimated from the data set presented in section III, with one minor exception: The last group utilizes the actual eigenvalues as the variances in (8), but in the remaining groups the variances are lowered in 10% steps. E g the first group uses a variance 90% lower than the last group.

C. Results

The described method for determining acoustic stability is applied on the data sets described in section III. The acoustic model Lybin [30] is used to model the signal excess. A towed array sonar at 50 m depth and working at frequencies around 1.5 kHz is used in the acoustic modelling. The bottom is assumed flat and 300 m deep. A group of SSPs is deemed acoustically stable if AFF is greater than 90%. The threshold on signal excess variations, $T_{\Delta SE}$, see (12), is set to 5 dB. The stability analysis is limited to ranges between 2 km and 10 km, and depths between 20 m and 200 m. All locations within the area are considered equally probable target locations. Signal excess levels greater than 0 dB are required, see (15).

Figs. 8 and 10 show the geographical distribution of acoustically stable groups for the full and subsampled data set and subset 1. Table I lists statistical data for each combination of data set and subdivision algorithm. Due to

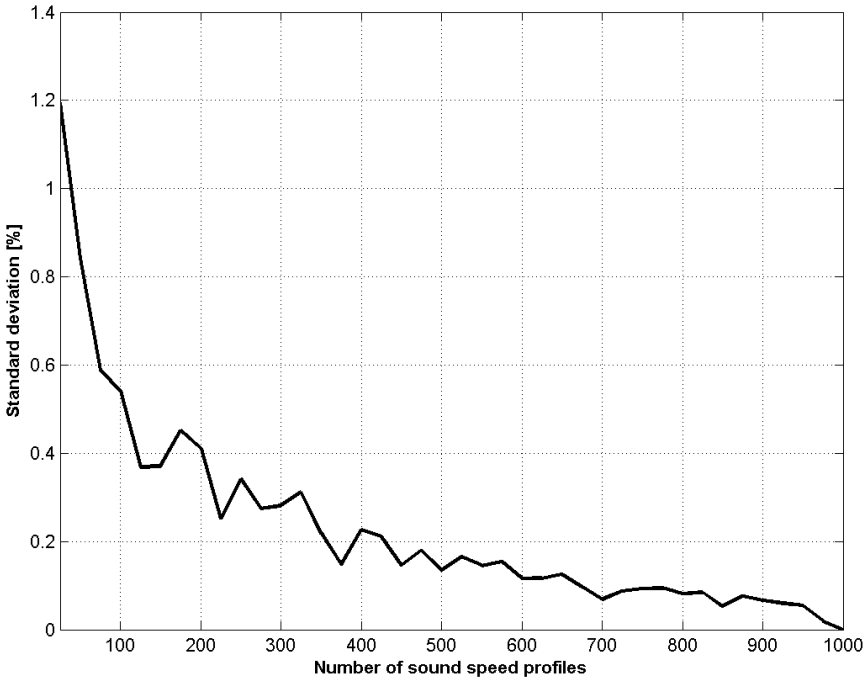

Fig. 6. The estimated standard deviation of the probability $P(T_{\Delta SE})$ in percent as a function of the number of SSPs used to estimate $P(T_{\Delta SE})$. A group of 1000 SSPs are generated using (8), where κ_k are modelled as zero–mean Gaussian random functions with variances given by λ_k. The standard deviations are estimated from random subsets of this group. Twenty subsets per subset size are used. The subset size is the number of SSPs used to estimate $P(T_{\Delta SE})$.

computing power limitations on the number of SSPs, the CC method was not used on the full data set. The entire subset 2 data set was in fact judged to be acoustically stable, with AFF exceeding 90% for all SSPs in that area.

We compare the distribution of groups for the full (Fig. 8 a) and subsampled (Fig. 8 b) data sets when using the OCM subdivision algorithm. The similarities for the largest groups (yellow, red, pink, light green and dark green colors) are obvious, both in area distribution and shape similarities. As for the smaller groups, their speckled, non-contiguous distribution indicate areas of high acoustic variability. It is expected that these small speckled groups are highly sensitive to the resolution of the data set, and detailed study of these discrepancies does not reveal much of interest. However, it is interesting to note that unclassified areas – the white areas in Fig. 8 a) and b) – are much smaller in the subsampled data set. These areas contain SSPs in groups that fail to meet the minimum size criteria after subdivision (section II).

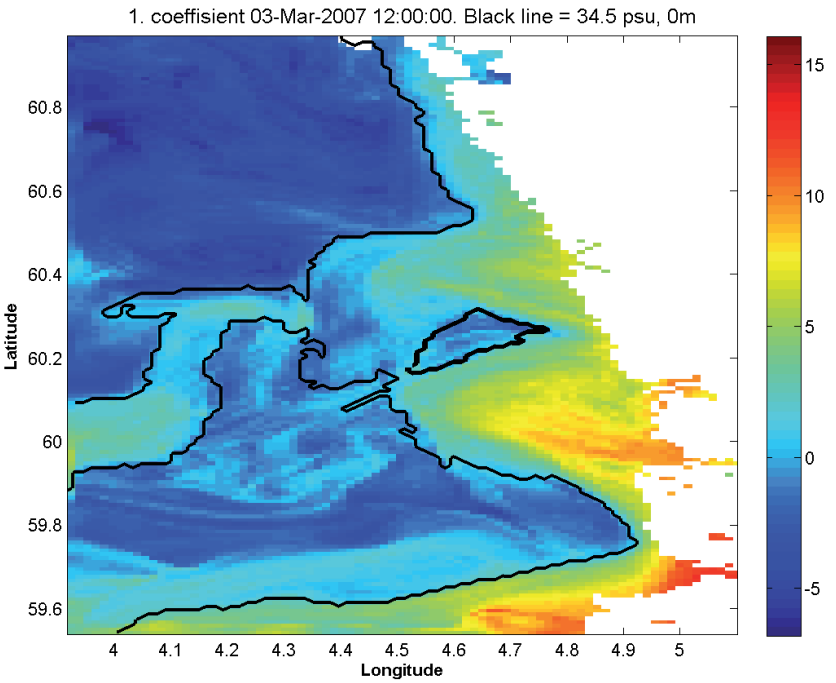

Fig. 7. The first EOF coefficient is plotted with surface salinity contours on top. The value of the surface salinity contour is 34.5 psu. Areas with surface salinity values above 34.5 psu are assumed AW, and the remaining areas are considered CW.

The most distinct differences between the OCM (Fig. 8 b) and CC results (Fig. 8 c) is that fewer, more contiguous, and larger groups are generated when using the CC method. There are no longer any voids due to groups that fail to meet the minimum size criteria. The CC method on the subsampled data set (Fig. 8 c) divides the whole area into four groups, much less than OCM subsampled (15 groups) and OCM full data set (10 groups). The shape and area of the largest OCM groups are comparable to the CC groups: The yellow areas are strikingly similar and the light green area of the CC method corresponds to the light green and red areas of the OCM full and subsampled data set. The pink CC area is composed of the pink, brown and dark green areas of the OCM method. There are some nuances in the exact boundaries, particular in the OCM areas of high variability, but the similarities in shape and extent are striking. OCM generates more groups because acoustically unstable groups are split into several groups, depending on the number of coefficients used. The CC subdivision algorithm, on the other hand, splits an acoustically unstable group in two.

Fig. 9 shows the sound speed as a function of depth along the east–west cross–section at 60.5 N (upper panel) together with the group distribution from the OCM and CC method along this line (lower panel). The classical

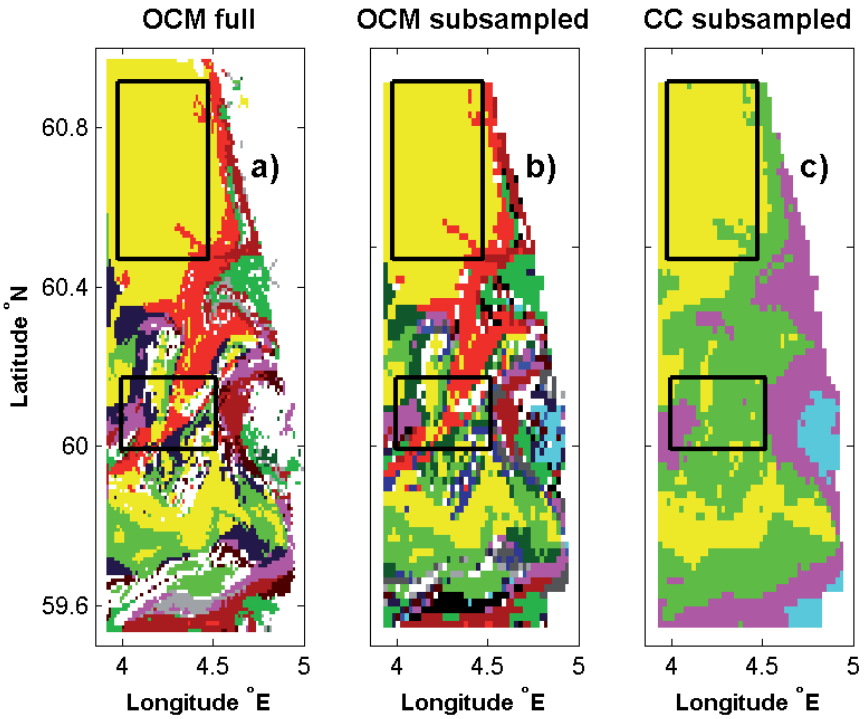

Fig. 8. The group distributions for the large area data sets. **(a)** Full resolution, OCM method. **(b)** Reduced resolution, OCM method. **(c)** Reduced resolution, CC method. Each colour represents a different group of SSPs. The black rectangles show the location of subset 1 (60-60.17 N) and subset 2 (60.47-60.92 N).

wedge–like structure of CW close to the coast can be seen, corresponding to systematic lower sound speed values in the upper right part of the cross section. The associated changes in vertical sound speed gradient and how that affects the sonar performance is distilled in the distribution of groups. The yellow group is clearly AW, with moderate vertical sound speed gradients. Further east, the green group of the CC method and the red group of the OCM method is associated with a slab of CW (low sound speed) above AW, and with a stronger vertical sound speed gradient at the transition between those two water masses. The interface is tilted downwards to the east. Closest to the coast, the pink (CC) and brown (OCM) group classifies a set of vertical SSPs where the interface between CW and AW is deeper, the gradient is stronger and the location of the strongest gradients are shifted downwards. The fact that the CC method produces fewer and more contiguous groups than the OCM method is also apparent in this cross section.

Subsets 1 and 2 are subsets of the full data set. Subset 1 is placed in an area with high concentration of groups when processing the full and subsampled data set, see Fig. 8 and 10. The high concentration of groups indicates

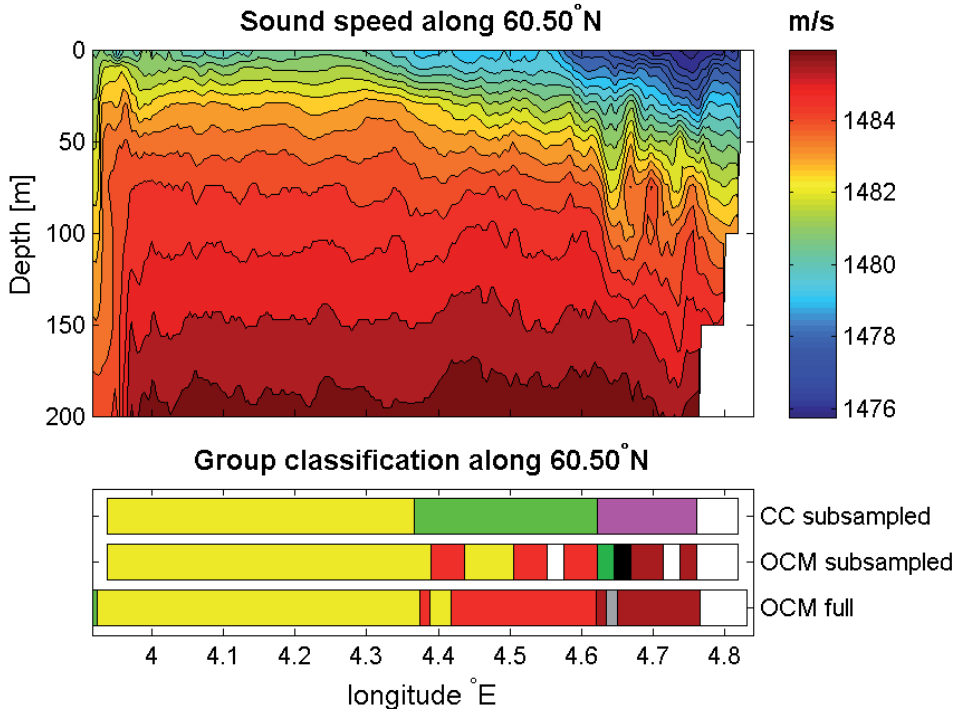

Fig. 9. East–West cross section of sound speed along 60.5 N (upper panel) compared with the results of the OCM and CC method.

that this area is acoustically unstable, see table IV-C.

Subset 2 is placed in an area with low concentration of groups when processing the full and downsampled data set. Processing the SSPs contained in subset 2 resulted in a single group with an AFF of 93% and therefore well above the threshold. This shows that groups initially classified as stable areas, see Fig. 8, are classified as stable also when applying the full method on SSPs from that area only. Note that when applying the method on the full data set, there is a second group also in the area containing subset 2, this group is not present when applying the method on data from subset 2 only because the group is too small to reduce the AFF below the 90% threshold.

Figs. 8 and 10 may serve as stability maps for sonar and rapid environmental assessment operations. A sonar platform operating in the presented area is advised to measure the SSP more frequently in areas with small, non–contiguous groups, e. g. subset 1. In contrast, less frequent measurements are required in areas like subset 2, where all profiles are contained in a single acoustically stable group. Similarly, in rapid environmental assessment missions more resources must be allocated to unstable regions than stable regions. Maps such as these may therefore provide valuable assistance in estimating how often new SSP measurements should be undertaken.

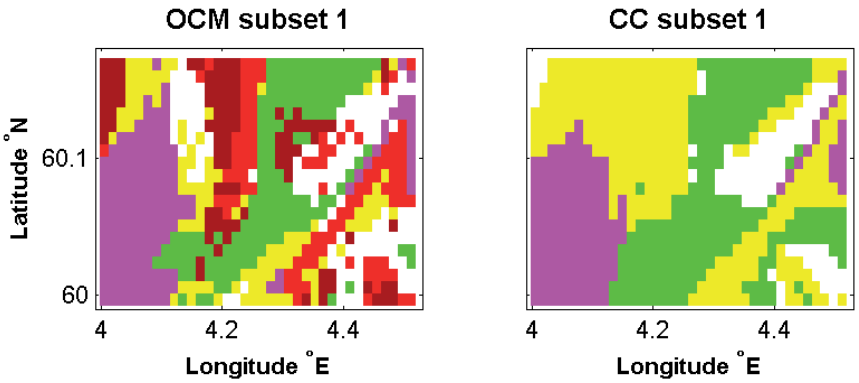

Fig. 10. The group distributions for sub area 1 using the OCM (left) and CC method (right).

Another useful application is for sonar operation planning. Detection ranges, based on representative SSPs from each group, may be estimated. The representative SSPs are generated by inputting the groups median coefficients in (8). Since the acoustic model is run only once per group, different sets of sonar parameters may be tested in order to maximise the detection range in each group at minimum computational cost. Note that the initial grouping is based on a single set of sonar parameters. Changes in the sonar parameters influence the groups acoustic stability, but studies made in connection to the presented work have shown that the group distribution remains almost the same for small changes in the sonar parameters. The considered sonar parameters were source level and sonar depth. This study is not considered within the scope of this work and therefore not presented here. If entirely different sonar systems are considered, for instance sonars working on different frequencies, then the method must be repeated for the specific sonar system. Furthermore, the method can easily be extended to other sonar applications not involving sonar performance prediction, but in that case the acoustic fitness function should be reconsidered.

V. Summary

A set of modelled sound speed profiles (SSP) is represented by empirical orthogonal functions (EOF). An approach based on EOF coefficients is shown equally efficient in classifying different water masses as traditional approaches based on salinity values. The EOF based approach is refined into two different automatic algorithms for separating groups of SSPs into several lesser and more homogeneous groups of SSPs; clustering of coefficients (CC) and ordering of coefficient magnitudes (OCM). The algorithms are combined with an acoustic fitness function, which is used for evaluating the acoustic stability within a group of SSPs. The combined method efficiently splits a large set of SSPs into several smaller acoustically stable groups.

The proposed method outputs a map of the group structure. Such maps may be used as decision aids for how often SSPs should be measured in a given area. Stable regions typically consist of large and geographically contiguous groups. Regions containing many small and non–contiguous groups are typically acoustically unstable, meaning that

the acoustic field is sensitive to the present oceanographic variations. For instance, during a rapid environmental assessment mission using gliders, the concentration of gliders should be higher in unstable regions than in stable regions. Likewise, during sonar operations, SSPs should be measured more frequently in unstable regions, than in stable regions.

Another possible application, useful for planning sonar operations, is to present maps of detection ranges based on a representative SSP from each group. A single representative SSP for an entire stable area also allows efficient optimisation of sonar performance. Sonar performance is modelled for the representative SSP. The optimisation is performed by tuning the sonar parameters for maximum sonar performance.

The method may be tuned to a specific type of operation by varying a set of parameters. The parameters include a priori knowledge of target behavior, for instance the maximum and minimum target depth. Other parameters allows the user to tune the requirements for a group of profiles to be classified as acoustically stable.

REFERENCES

[1] K. R. James and D. R. Dowling, "A method for approximating acoustic–field–amplitude uncertainty caused by environmental uncertainties," *the Journal of the Acoustic Society of America*, vol. 124, pp. 1465–76, 2008.

[2] S. E. Dosso, "Environmental uncertainty in ocean acoustic source localization," *Inverse Problems*, vol. 2, pp. 419–432, 2003.

[3] S. E. Dosso, P. M. Giles, G. H. Brooke, D. F. McCammon, S. Pecknold, and P. C. Hines, "Linear and nonlinear measures of ocean acoustic environmental sensitivity," *the Journal of the Acoustic Society of America*, vol. 121, no. 1, pp. 42–45, 2007.

[4] K. LePage, "Estimation of acoustic propagation uncertainty through polynomial chaos expansions," in *9th International Conference on Information Fusion*, 2006.

[5] ——, "Propagation and reverberation sensitivity to oceanographic and seabed variability," *IEEE Journal of Oceanic Engineering*, vol. 31, no. 2, pp. 402–412, 2006.

[6] S. Finette, "A stochastic representation of environmental uncertainty and its coupling to acoustic wave propagation in ocean waveguides," *the Journal of the Acoustic Society of America*, vol. 120, no. 5, pp. 2567–2579, 2006.

[7] K. LePage, "Modeling propagation and reverberation sensitivity to oceanographic and seabed variability," *IEEE Journal of Oceanic Engineering*, vol. 31, pp. 402–412, 2006.

[8] R. Davis, "Predictability of sea surface temperature and sea level pressure anomalies over the north pacific ocean," *Journal of Physical Oceanography*, vol. 6, no. 3, pp. 249–266, 1976.

[9] E. Fogelquist, J. Blindheim, T. Tanhua, S. sterhus, E. Buch, and F. Rey, "Greenland–Scotland overflow studied by hydro-chemical multivariate analysis," *Deep Sea Research Part I: Oceanographic Research Papers*, vol. 50, no. 1, pp. 73–102, 2003.

[10] A. Tolstoy, O. Diachok, and L. N. Frazer, "Acoustic tomography via matched field processing," *the Journal of the Acoustic Society of America*, vol. 89, pp. 1119–1127, 1991.

[11] M. D. Collins and W. A. Kuperman, "Focalization: Environmental focusing and source localization," *the Journal of the Acoustic Society of America*, vol. 90, pp. 1410–1422, 1991.

[12] K. Kim, K. Kim, T. Rhee, H. Rho, R. Limeburner, and R. Beardsley, "Identification of water masses in the Yellow Sea and the East China Sea by cluster analysis," in *Oceanography of Asian Marginal Seas*, K. Takano, Ed. Elsevier Oceanography Series, 1991, vol. 54, pp. 253–267.

[13] H. B. Hur, G. A. Jacobs, and W. J. Teague, "Monthly Variations of Water Masses in the Yellow and East China Seas," *Journal of Oceanography*, vol. 55, no. 2, pp. 171–184, 1999.

[14] A. Warn-Varnas, A. Gangopadhyay, and J. Hawkins, "Water masses in the monterey bay during the summer of 2000," *Continental Shelf Research*, vol. 27, pp. 1379–1398, 2007.

[15] A. R. Amiri-Simkooei, M. Snellen, and D. G. Simons, "Seafloor classification using multifrequency single-beam echo-sounder echo shape parameters," in *Proceedings of European Conference in Underwater Acoustics*, 2010.

[16] W. L. J. Fox, M. U. Hazen, C. J. Eggen, R. J. M. II, and M. A. El-Sharkawi, "Environmentally adaptive sonar control in a tactical setting," in *Impact of Littoral Environmental Variability on Acoustic Predictions and Sonar Performance*, N. G. Pace and F. B. Jensen, Eds. Kluwer Academic Publishers, 2002, pp. 595–602.

[17] H. A. Engedahl, "Implementation of the princeton ocean model (pom/ecom3d) at the Norwegian Meterological Institute," Norwegian Meteorological Institute, Oslo, Norway, Research Report 5, 1995.

[18] R. J. Urick, *Principles of underwater sound*, 3rd ed. Peninsula Publishing, 1983.

[19] C. W. Therrien, *Discrete Random Signals and Statistical Signal Processing*. Prentice Hall, 1992.

[20] A. K. Jain and R. C. Dubes, *Algorithms for Clustering Data*, ser. Prentice Hall Advanced Reference Series. Prentice Hall, 1988.

[21] J. H. Ward, "Hierarchical grouping to optimize an objective function," *Journal of the American Statistical Association*, vol. 58, no. 301, pp. 236–244, March 1963.

[22] S. Milligan, L. LeBlanc, and F. Middleton, "Statistical grouping of acoustic reflection profiles," *the Journal of the Acoustic Society of America*, vol. 64, no. 3, pp. 795–807, 1978.

[23] A. Ommundsen, J. K. Jensen, K. H. Midtbø, and H. Engedahl, "Operational metoc models at the Norwegian Meteorological Institute," Norwegian Defense Research Establishment (FFI), Kjeller, Norway, FFI Report 02369, 2008.

[24] E. Svendsen, R. Sætre, and M. Mork, "Features of the northern North Sea circulation," *Continental Shelf Research*, vol. 11, pp. 493–508, 1991.

[25] L. Otto, J. T. F. Zimmerman, G. K. Furnes, M. Mork, R. Sætre, and G. Becker, "Review of the physical oceanography of the North Sea," *Netherlands Journal of Sea Research*, vol. 26, pp. 161–238, 1990.

[26] G. K. Furnes, B. Hackett, and R. Sætre, "Retroflection of Atlantic water in the Norwegian Trench," *Deep Sea Research*, vol. 33, no. 2, pp. 247–265, 1986.

[27] R. Sætre, J. Aure, and R. Ljøen, "Wind effects on the lateral extension of the Norwegian coastal water," *Continental Shelf Research*, vol. 8, pp. 239–253, 1988.

[28] M. Mork, "Circulation phenomena and frontal dynamics of the Norwegian coastal current," *Phil. Trans. R. Soc. London*, vol. A 302, pp. 635–647, 1981.

[29] R. Sætre, *The Norwegian Coastal Current - Oceanography and Climate*. Tapir Academic Press, 2007.

[30] K. T. Hjelmervik, E. M. Dombestein, S. Mjølsnes, T. S. Såstad, and J. Wegge, "The acoustic raytrace model lybin – description and application," in *Proceedings from Underwater Defence Technology Conference and Exhibition, Glasgow 2008*, 2008.

TABLE I

RESULTS FROM ALL COMBINATIONS OF DATA SETS AND SUBDIVISION ALGORITHMS.

Data set	**Method**	**No groups**	**No profiles**	**Mean AFF**
Full data set	OCM	10	8816 (88%)	94%
Subsampled data set	OCM	15	2715 (95%)	94
	CC	4	2873 (100%)	93%
Subset 1	OCM	5	600 (83%)	94
	CC	3	640 (89%)	94%
Subset 2	Both	1	All	93%

Paper 7

In ocean evaluation of low frequency active sonar systems

In ocean evaluation of low frequency active sonar systems

Karl Thomas Hjelmervik
Geir Helge Sandsmark

Sonar performance measurements in the sea are always affected by uncontrollable and/or uncertain environmental conditions as sound speed variations, bottom topography or the acoustic properties of the sea floor. This paper presents a method to determine a sonar – target geometry which minimizes the uncertainty in target signal excess due to environmental variability.
An acoustic model is used to estimate the signal excess for a large number of sound speed profiles measured in the relevant area. The results are compared while searching for a target range and depth where the estimated signal excess is robust with respect to the expected variability of the sound speed profile in the actual area.
Results from sea trials will be presented, as well as simulated examples used to demonstrate the achieved robustness or sensitivity of the signal excess to environmental changes, at different test geometries.

1 Introduction

In general there is a need for quantifiable sonar performance tests carried out at sea under conditions resembling the normal working conditions for the equipment. The accuracy and reliability of such tests are frequently questioned. The limited confidence in such tests is due to acknowledged uncertainty in the environmental parameters and experienced inaccuracy of meso-scale ocean acoustic experiments. However experimental verification of propagation models may often show good agreement for some measurements while under different conditions there is virtually no resemblance between model and reality. Also a closer look at some modelling results indicates that the sensitivity of the received signal level, to for instance the target location, may vary significantly over an actual area in the ocean. In some cases the signal excess may remain near constant over a significant depth and range interval, while only a few meters displacement may cause large deviations of the signal or reverberation levels. Similarly a small deviation in the sound speed profile may cause entirely different propagation patterns for some cases and experiment geometries while other choices of target and sonar locations may provide more robust conditions.

With this background we have developed a method of conducting experiments at sea where the uncertainty of the results are limited, quantifiable and assessable. The method is based on running an acoustic model repeatedly. Each run uses a single sampled realisation of the environment as input. This paper focuses on variations in sound speed profile. Therefore a sample sound speed profile represents a realisation of the environment. The computations are based on a selection of sound speed profiles measured within the actual area as close to the test schedule as possible. The results are then analyzed to find favourable positions for the sonar and the target.

Overall considerations and aspects of underwater sensor testing is presented in ref (1). The current paper goes into more detail on how to handle the acoustic sensitivity issues due to varying oceanography.

Section 2 presents the tools used in the analysis. Section 3 shows an example of how the method can be used to find good locations for the sonar and the target during a test. Section 5 concludes the paper.

2 Numerical tools

Two different numerical tools are used in the method of finding stable conditions for testing acoustic equipment. The main tool is Lybin, an acoustic ray trace model that estimates the signal excess in a single vertical cross-section for a given environment and sonar. The second tool is a method of presenting the sensitivity of the signal excess to environmental variation. The results are presented graphically, denoted “stability plots”.

Lybin

Lybin is an acoustic ray trace model developed by Svein Mjølsnes, Norwegian Defence Logistic Organization. Ref (2) gives an overview of ray tracing and the underlying theory. The model is two-dimensional, covering depth and range. It estimates the *transmission loss*, the *reverberation level and the noise level* based on sonar data and environmental data. These data are applied to the sonar equations for estimation of *signal excess*. Detection theory (5,6) is used to find the *probability of detection* and the corresponding *detection range*. In this paper the signal excess is used.

Lybins transmission loss module was verified by NURC[1], (3). The evaluation team conclude: *“The general conclusion of this test is that the range-dependent ray-trace model LYBIN, developed by the Norwegian Navy, is indeed a valid alternative to*

[1] NATO Underwater Research Centre

existing propagation models in the AESS[2]. The LYBIN model has prediction accuracy similar to the GRAB 'reference' model but is considerably faster."

Lybin was presented at the Underwater Defense Conference and Exhibition in Glasgow 2008, ref (4).

Stability plots

The idea of stability plots is to compare the signal excess results from several different Lybin-runs, and find ranges and depths where the signal excess remains nearly constant from run to run.

For the purpose of finding stable acoustic conditions in an area of both spatially and temporally varying oceanography, Lybin is run using several different sound speed profiles measured in the actual area. The results from these runs are then compiled into the stability plots. One of these sound speed profiles is selected as a representative sound speed profile for the entire set of sound speed profiles. This could either be a mean of all the other sound speed profiles, or presumably better, a single measured sound speed profile, possessing some characteristics judged as *typical* for that set of sound speed profiles. In the latter case, the representative sound speed profile should be smoothed to remove measurement artifacts.

The stability plot shows the *stability parameter*, SP,given by:

$$SP(r,z) = \frac{1}{N}\sum_{i=1}^{N} step(T - |SE_r(r,z) - SE_i(r,z)|)$$

$SE_r(r,z)$ is the modelled signal excess at range r and depth z, measured in dB, using the representative sound speed profile. $SE_i(r,z)$ is the modelled signal excess for the i-th sound speed profile in the set. N denotes the size of the set. T is a set threshold, for example 3dB as used in this work. *step()* denotes the unit step function taking the value 1 for positive arguments and 0 elsewhere. $SP(r,z)$ is therefore a two-dimensional matrix of values between 0 and 1. The value of a single element is simply the fraction of cases that has a signal excess deviation from the typical case, lower than the selected threshold. Thus, an element takes the value 1 if the complete set of sound speed profiles results in a signal excess difference less than the selected threshold. The value 0.5 indicates that half the set of sound speed profiles results in a low signal excess difference. Figure 2 shows an example of the stability plot. The red areas represent areas where 100% of the runs resulted in signal excess values within a margin of T from the signal excess computed using the representative sound speed profile. Simply stated, red areas are stable, blue areas are unstable.

[2] Allied Environmental Support System

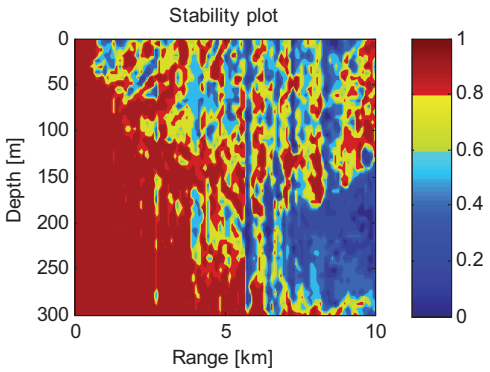

Figure 2 *Stability plot for a set of sound speed profiles. The sonar is at 25m depth.*

3 Results

The task of finding a stable environment for testing of the acoustic equipment is divided into two parts. First, a historically stable area must be found. Areas prone to oceanographic fronts or strong variations in terrain should be avoided. Second, just prior to the testing of the equipment, oceanographic measurements should be made to find the most stable region in that area *and* the relative positions of the equipment resulting in the most stable conditions. This paper is focused on the second part.

In the present example, a monostatic sonar is tested using a stationary, artificial test target (echo repeater). During the test, the distance between the sonar and the target is kept constant by letting the sonar vessel encircle the target. Three geometric parameters remain to be determined, in order to gain stable conditions for the test; sonar depth and target depth and range (distance from sonar vessel).

Sound speed measurements

The sound speed profiles used in this study was measured in November 2007, along lines using a towed CTD. The ten lines were approximately 27km long with 5km separation between the lines, see figure 3. Each star in figure 3 corresponds to a single sound speed profile. The red stars indicate positions suitable for performing the acoustic tests due to homogenous sound speed profiles. In the following analyses these seven sound speed profiles are used. The measurements resulted in a total of 170 sound speed profiles. Figure 4 presents all the measured sound speed profiles. Figure 5 shows a filled contour plot as a function of range and depth for line nr 5.

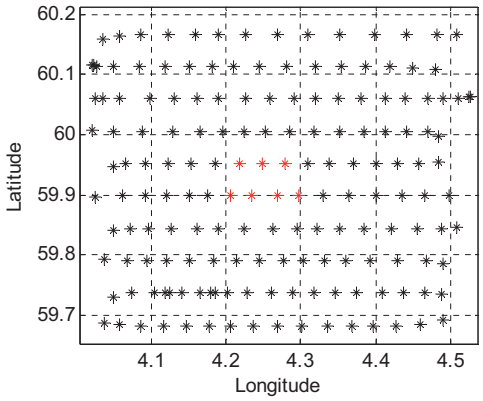

Figure 3 *Positions of the sound speed measurements made. The coordinates are presented in decimal degrees. The sound speed profiles were measured along east-west oriented lines.*

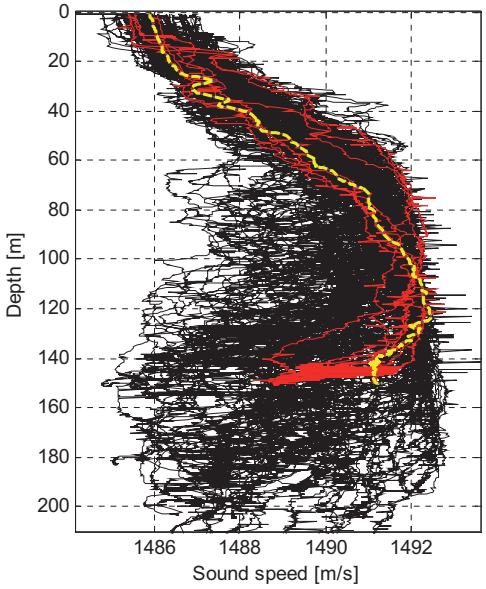

Figure 4 *170 sound speed profiles. Notice the strong variations below 60m depth compared to above 60m depth. The red curves are the sound speed profiles measured in the positions indicated by the red stars in figure 3. The yellow curve depicts the selected and smoothed representative sound speed profile.*

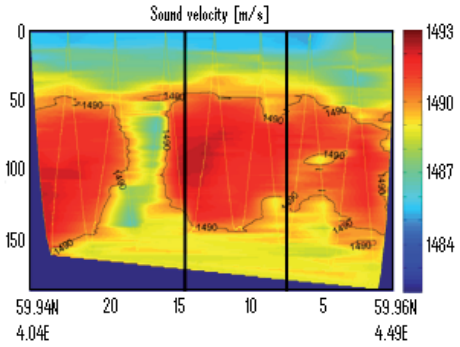

Figure 5 *Sound speed as a function of depth and range from west to east along line 5 (Line one in figure 3 is furthest to the north). The preferred area is between the two black vertical lines.*

Stability plot

The threshold, *T,* for determining the stability parameter was set to 3dB. Figure 6 shows a stability plot for the sonar at 50m depth. The red areas indicate range - depth pairs with stable signal excess, and therefore suitable positions for the target. Figure 7 shows the stability picture when the sonar is at 5m depth. Both cases show reasonably large areas for robust measurements. This is however not always the case. Figure 8 shows a stability plot using a set of sound speed profiles measured in April 2008. In this case the target should be deeper than 60m in order to ensure stability.

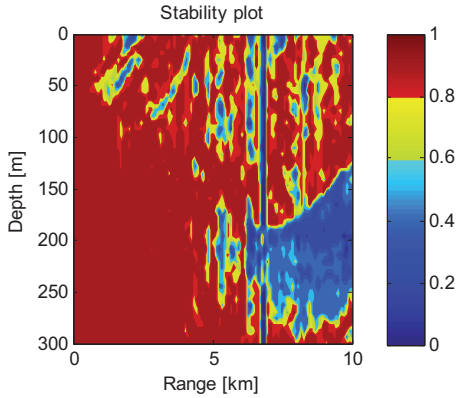

Figure 6 Stability plot for a sonar at 50m depth.

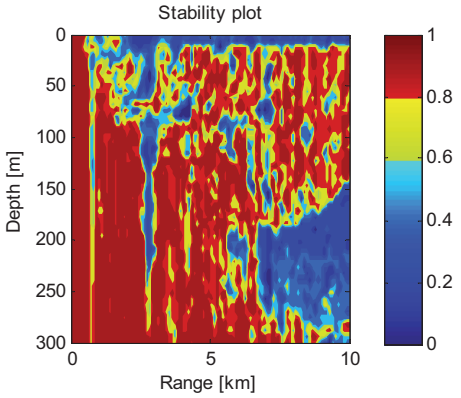

Figure 7 Stability plot for a sonar at 5m depth.

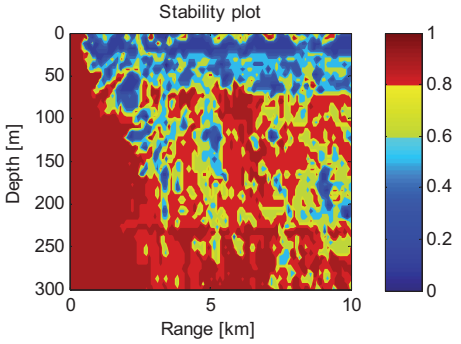

Figure 8 Stability plot for a sonar at 25m depth.

5 Conclusion

A mono-variable perturbation analysis is used to quantify the sensitivity of sonar performance measurements to temporal and spatial variations of environmental parameters with impact on the sonar performance. This analysis indicates that by a careful choice of sonar and target deployment, the sensitivity to unaccounted parameter variations may be kept within acceptable limits. Stability plots are introduced to quantify the stability of different sonar-target geometries.

Acknowledgments

We would like to direct our thanks to the crew on HU Sverdrup II for their help in gathering oceanographic data essential for this work. Furthermore we would like to add thanks to Jan Kristian Jensen and Petter Østenstad at FFI for presentation and interpretation of oceanographic data. Finally we would like to thank the Norwegian Navy for the use of their frigates in the studies and especially Svein Mjølsnes and Harald Tholo for their support and discussions.

References

[1] Sandsmark G H, Alsterberg S, Dombestein E M, Hjelmervik K T, Knudsen T, Mjolsnes S, Såstad T S, Tholo H, Wegge J: “Environmental impact and assessment: In ocean evaluation of sonar system performance, expectations and experience”, UDT 2007

[2] Jensen F B, Kuperman W A, Porter M B, Schmidt H: “Computational Ocean Acoustics”, Springer Verlag, 2000.

[3] Ferla, Isoppo, Martinelli and Jensen: “Performance assessment of the LYBIN-2.0 propagation loss module”, SACLANTCEN SM-384

[4] Hjelmervik K T, Mjølsnes S, Dombestein E M, Wegge J, Såstad T S: “The acoustic raytrace model Lybin – Description and applications”, UDT Glasgow 2008.

[5] van Trees, Harry L.: “Detection, Estimation and Modulation theory, parts I and III, John Wiley & Sons, 1968.

[6] Skolnik, Merrill Ivan: ”Radar Handbook”, New York: McGraw Hill, 1970.